



Journal of Soft Computing and Artificial Intelligence

ISSN: 2717-8226



Journal of Soft Computing and Artificial Intelligence

Journal homepage: <https://dergipark.org.tr/en/pub/jscai>

International
Open Access 

Volume 03
Issue 02

December, 2022

Journal of Soft Computing and Artificial Intelligence (JSCAI) is an international peer-reviewed journal that publishes integrated research articles in all areas of soft computing and artificial intelligence. The aim of the JSCAI journal is to provide a platform for researchers, professionals, and academicians around the world to combine and exchange new developments and their applications in various areas of soft computing and artificial intelligence. Journal of Soft Computing and Artificial Intelligence (JSCAI) is an international peer-reviewed journal that publishes integrated research articles in all areas of soft computing and artificial intelligence. The journal covers all branches of engineering, including mechanics, computer science, electronics, energy, aerospace engineering, materials science, nuclear engineering, systems analysis, alternative technologies, etc.

JSCAI publication, which is open access, is free of charge. There is no article submission and processing charges (APCs).

JSCAI is indexed & abstracted in:

Crossref (Doi beginning: 10.55195/jscai..xxxxxx)

Directory of Research Journals Indexing (DRJI)

Google Scholar

Index Copernicus (ICI Journal Master List)

OpenAIRE

Asos Index

Directory of Open Access scholarly Resources (ROAD)

Authors are responsible from the copyrights of the figures and the contents of the manuscripts, accuracy of the references, quotations and proposed ideas and the Publication Ethics (<https://dergipark.org.tr/en/pub/jscai/policy>)

Journal of Soft Computing and Artificial Intelligence (JSCAI) allows the author(s) to hold the copyright of own articles.









©
JSCAI
25 December 2022



This work is licensed under a Creative Commons Attribution 4.0 International License.

Table of Contents

Articles

	Classification of Unwanted SMS Data (Spam) with Text Mining Techniques Rasim ÇEKİK	Page: 41 – 50
	CREMA-D: Improving Accuracy with BPSO-Based Feature Selection for Emotion Recognition Using Speech Kenan DONUK	Page: 51 – 57
	Solving Multidimensional Knapsack Problem with Bayesian Multiploid Genetic Algorithm Emrullah GAZİOĞLU	Page: 58 – 64
	Real-time Iris Center Detection Based on Convolutional Neural Networks Kenan DONUK, Davut HANBAY	Page: 65 – 69
	Can Similarity Measures Techniques be Used to Model Face Recognition? Enes ALGÜL	Page: 70 – 75
	Generalized λ -Statistical Boundedness of Order β in Sequences of Fuzzy Numbers Mithat KASAP, Hifsi ALTINOK	Page: 76 – 82
	The Critical Significance of Boron Mine in Future Energy Technologies Fatih ARLI	Page: 83 – 92
	An Artificial Intelligence Regression Model for Prediction of NOx Emission from Flame Image Sedat GOLGİYZ, Mahmut DAŞKIN, Cem ONAT, Muhammed Fatih TALU	Page: 93 – 101



Journal of Soft Computing and Artificial Intelligence

Journal homepage: <https://dergipark.org.tr/en/pub/jscai>

International
Open Access 

Volume 03
Issue 02

December, 2022

Research Article

Classification of Unwanted SMS Data (Spam) with Text Mining Techniques

Rasim ÇEKİK¹ 

¹Department of Computer Engineering, Sirnak University, 7300, Sirnak, Türkiye

ARTICLE INFO

Article history:

Received November 26, 2022

Revised December 30, 2022

Accepted December 6, 2022

Keywords:

Feature Selection

Text Classification

Text Mining

Spam SMS

ABSTRACT

Text mining, which derives information from written sources such as websites, books, e-mails, articles, and online news, processes and structures data using advanced approaches. The vast majority of SMS (Short Message Service) messages are unwanted short text documents. Effectively classifying these documents will aid in the detection of spam. The study attempted to identify the most effective techniques on SMS data at each stage of text mining. Four of the most well-known feature selection approaches were used, each of which is one of these parameters. As a result, the strategy that yielded the best results was chosen. In addition, another parameter that produces the best results with this approach, the classifier, was determined. The DFS feature selection approach produced the best results with the SVM classifier, according to the experimental results. In Average Results, DFS showed the best result of 93.5361 for accuracy criterion, while it reached the highest result of 93.4953 for Macro-F1. This study establishes a general framework for future research in this area that will employ text mining techniques.

1. Introduction

With the rapid development of technology, the use of the Internet has increased tremendously. The influence of people on the internet has created a large amount of text documents. In this process, tools and techniques were needed to process text documents and provide access to information. The most effective method in this regard is text mining techniques, also called text analytics. Text Mining is the process of extracting previously unknown, potentially useful, structured and organized data from unstructured and disordered chunks of electronic text. Text mining, which infers from written sources such as websites, books, e-mails, articles, online news, processes the languages used in daily life and structures the data with the help of advanced approaches. Text mining

tasks include text classification and clustering in general, concept or entity extraction, granular taxonomy modelling, sentiment analysis, entity relationship modeling, document abstraction, etc. transactions can be sorted.

In this study, the classification technique of text mining is used. Text classification is a process that includes preprocessing operations such as root finding, letter transformation, and techniques such as feature weighting and feature selection. Classification is the activity of categorizing unlabeled data according to the model created with the help of labeled texts. The most important problems encountered in the text classification stage are high dimensionality and space structure. Various techniques and approaches have been proposed to

¹ Corresponding author

e-mail: rasimcekik@sirnak.edu.tr

DOI: 10.55195/jscai.1210559

overcome these problems. Examples of this are the use of dimension reduction techniques against the high dimensionality problem or the use of feature selection approaches to select the sub-feature set that best expresses the entire feature space. Parlak B. and Uysal A. [1] proposed a new statistical feature selection approach as a solution to high dimensionality. The model utilized corpus-based and class-based probabilities for statistical calculations. Again, A. Uysal and S. Günel [2] presented the distinguishing feature selector (DFS), an effective and successful feature selection approach.

In its simplest definition, SMS (Short message service) can be defined as a short text message service used on phones. It is a popular application because it is a service used around the world. That's why it is used by so many people. This service, which is so widely used, may have some disadvantages. Just like in e-mails, the most annoying situation in the field of SMS is that unwanted SMS messages (spam) (eg credit announcements of banks, promotional messages of stores, discount announcements of e-commerce sites, tariff messages of mobile communication providers) fall into the message box of the mobile phone. This situation causes people to waste their precious time and fill the message box unnecessarily. Finding a solution to this problem or minimizing the effect of the problem is an important step for mobile users to prevent unnecessary use of both phone resources and time. The simplest method in this regard is the use of a black/white list, known as the banned list, where the phone numbers of the people who send the spam messages are added. This method is used in many commercial applications [3]. However, this method requires the intervention of the phone user and will block spam as well as regular messages from blacklisted phone numbers. This may result in missing important messages or loss of information, which may be beneficial to the phone user. For example, discount messages, coupons from a legitimate e-commerce platform, or favorable loan deals from a bank may be viewed as spam. More effective and efficient methods are needed to avoid similar situations. Therefore, it would be a more accurate approach to filter the texts according to the content of the incoming message rather than the phone number. Classifying texts according to their content is one of the main tasks of text mining. In this

study, with the help of text mining techniques, it has been tried to classify whether SMS data is spam or not according to its content. Within the scope of the study, the most efficient framework model for SMS classification is revealed by using different text mining techniques and methods. Although there are a number of studies in the literature on SMS spam filtering, few studies have analyzed the effectiveness of the attributes used in the filtering process. In this study, it is examined that the classifiers achieve higher success by choosing features with high efficiency to classify SMS messages.

2. Literature Review

Telephone use has become one of the basic needs today. The phone is used in almost every part of life and people never leave it with them. Undoubtedly, one of the most frequently used applications in the vehicle, which has such an important use in our lives, is SMS. However, the vast majority of SMS data consists of spam messages. Rao S. et al. [17] showed in Figure 1 the Google trend analysis of web searches related to fake news, Deepfake and misinformation between 2016-2021. In addition, the fact that there are many studies in the literature on filtering the data of the SMS service shows the importance of the SMS application. For example, Delany S.J et al. [4] conducted a study covering a large literature review on SMS spam. In the study, motivating points about SMS spam were mentioned and some experimental studies were included. Similar studies have been done by research communities and have contributed to the field of spam detection [5-8]. It is possible to group the studies conducted in this field according to their methods. Studies were divided into 4 groups according to the methods used [9].

- machine learning,
- deep learning,
- spam graphic display
- spam filtering and detection with android application

Machine learning methods categorize messages as spam and non-spam with the help of classification and prediction approaches in data mining [10]. It is divided into two as labeled and unlabeled learning. Deep learning methods, on the other hand, try to detect spam using advanced versions of artificial neural networks [11]. Graphical representation

methods perform classification tasks using graphics in the text [12]. In the spam filtering and detection method with the Android application, a real-time mobile application is implemented to be run on mobile phones with Android operating system by using the feature vector and classifier pair that provides the most successful result in the simulation study [13]. In addition, the existing studies in the literature can be grouped under three headings: content-based, non-content-based and hybrid, according to the working principle of the approaches

they use [14]. Content-based approaches [15] provide weighting of text documents using the bag of words (BoWs) method. With weighting, the frequency of occurrence of a word in the document can be determined. Non-content-based [16] approaches use message attributes or signature patterns as attributes to identify spam on the network. Hybrid approaches offer a model by combining the superior features of both content-based and non-content-based approaches.

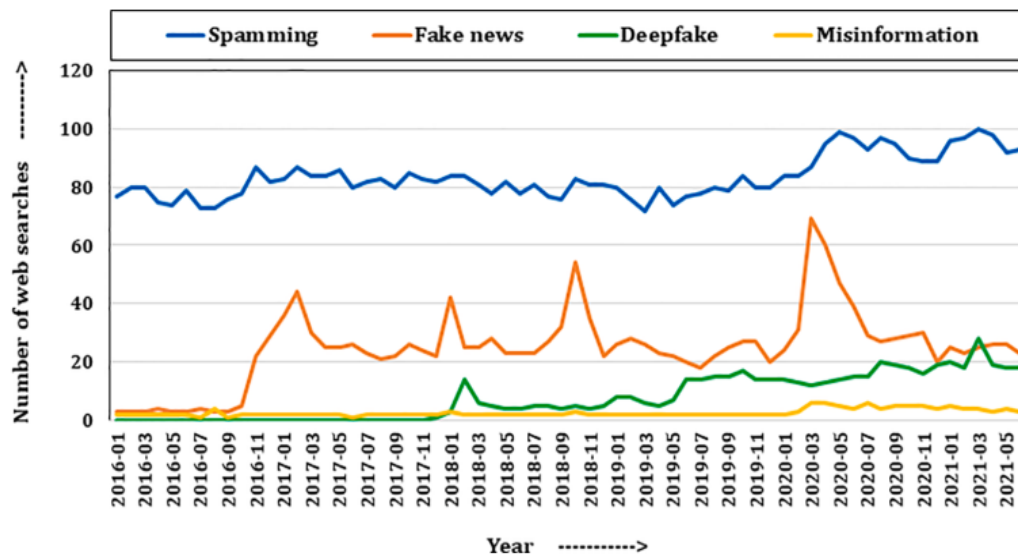


Figure 1 The Google trend analysis of web searches related to fake news, Deepfake and Misinformation

Existing SMS filtering approaches can be structurally divided into three groups [12]. These are shown in Figure 2.

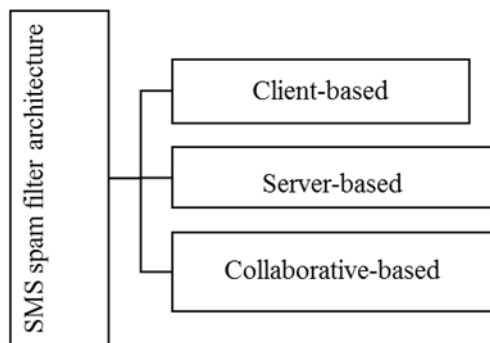


Figure 2 Structurally approach groups for SMS filtering

- *Client-based*: Approaches that offer solutions by filtering on mobile devices.
- *Server-based*: Approaches that offer solutions by filtering on network providers.
- *Collaborative-based*: These are approaches that

offer solutions by filtering on both network providers and mobile devices.

As the use of mobile devices in SMS filtering increases, the studies to be carried out in this area will remain up-to-date. Therefore, studies in this field continue without slowing down. Since this study is a content-based study, a summary of the studies on this subject is presented in Table 1.

Table 1: a summary of the content-based studies

ref	Used machine learning approach
[18], [23]	k-NN classifiers
[19]	SVMs and others
[20]	Winnow algorithm
[21]	Bayes
[22]	Naive Bayes

3. Text Mining and Techniques

Text Mining is also called Text Data Mining and Knowledge Discovery from Textual Databases. Although Text Mining is considered a sub-topic of

data mining, it is different from data mining. In Text Mining, it is the extraction of patterns from natural language texts rather than event-based databases. However, it offers knowledge discovery with stages similar to data mining. In summary, text mining is the process that aims structured data on unstructured text data. For example; It aims at studies such as classification of texts, clustering, extracting topics from texts, entity relationship modeling, sentiment analysis in texts, text summarization, author identification, and evaluation of customers' comments about the product. To achieve these goals, techniques such as text mining information extraction, information classification, syllable analysis, word frequency distribution, information extraction and visualization are used. The first of these methods is the text classification process.

Text classification offers a learning model by using available texts whose class is known beforehand. Then, the new incoming texts are classified according to this model. The biggest handicap in the classification process is the high dimensionality and the sparseness of the information system (IS). SMS the Information System is shown as $IS = (D, T)$. Where D stands for finite non-empty universal text document set, T stands for finite non-empty conditional and decision attribute set. $T = \{t, c\}$ specifies t conditional, c decision attributes. The processing order of the techniques used in the text classification process on the information system is

given in Figure 4.

3.1. Feature Selection Approaches

Since the size of the feature space is very large, it is necessary to select the most representative subset of the entire feature space in order to perform an efficient classification in text mining. The most effective method for this process is to use feature selection approaches. Feature selection approaches are grouped under three headings [28, 29]: filter, wrapper, and embedded. The feature selection taxonomy is given in Figure 3.

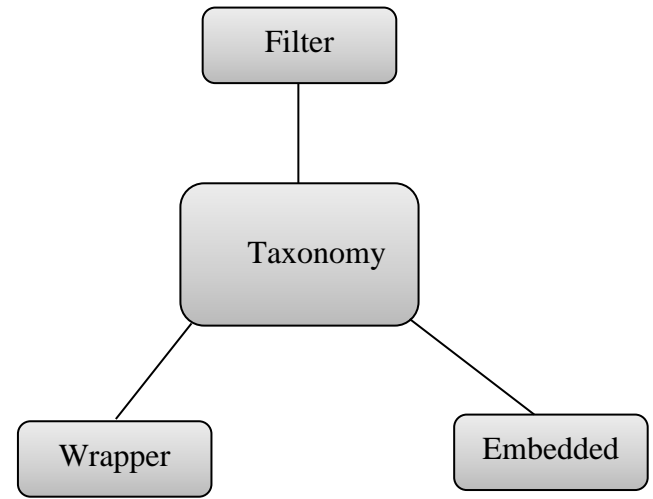


Figure 3 The feature selection taxonomy

Table 2 Brief information about used approaches

$$\begin{aligned}
 IG(t) &= - \sum_{i=1}^M P(C_i) \log P(C_i) \\
 &\quad + P(t) \sum_{i=1}^M P(t) \log P(t) \\
 &\quad + P(\underline{t}) \sum_{i=1}^M P(\underline{t}) \log P(\underline{t}) \\
 GI(t) &= \sum_{i=1}^M P(C_i)^2 P(t)^2 \\
 DFS(t) &= \sum_{i=1}^M \frac{P(C_i|t)}{P(\underline{t}|C_i) + P(t|\underline{C_i}) + 1}
 \end{aligned}$$

$P(C_i|t)$ and $P(C_i|\underline{t})$ show the conditional probability of class C_i given presence and absence of the term t , respectively. $P(t)$ and $P(\underline{t})$ are the probabilities of absence and presence of the term t .

The notation $P(C_i)$ in the formula indicates the probability that the t term will be in the C_i class. $P(t|C_i)$ and $P(C_i|\underline{t})$ show the conditional probability of the term t given classes other than C_i and absence of the term t given class C_i , respectively.

$$HI2(t, C) = \sum_{t \in \{0,1\}} \sum_{C \in \{0,1\}} \frac{(N_{t,C} - E_{t,C})^2}{E_{t,C}}$$

$$CHI2(t) = \sum_{i=1}^M P(C_i) * CHI2(t, C)$$

The N and E values represent the observed and expected frequency for each case of term t and class C, respectively.

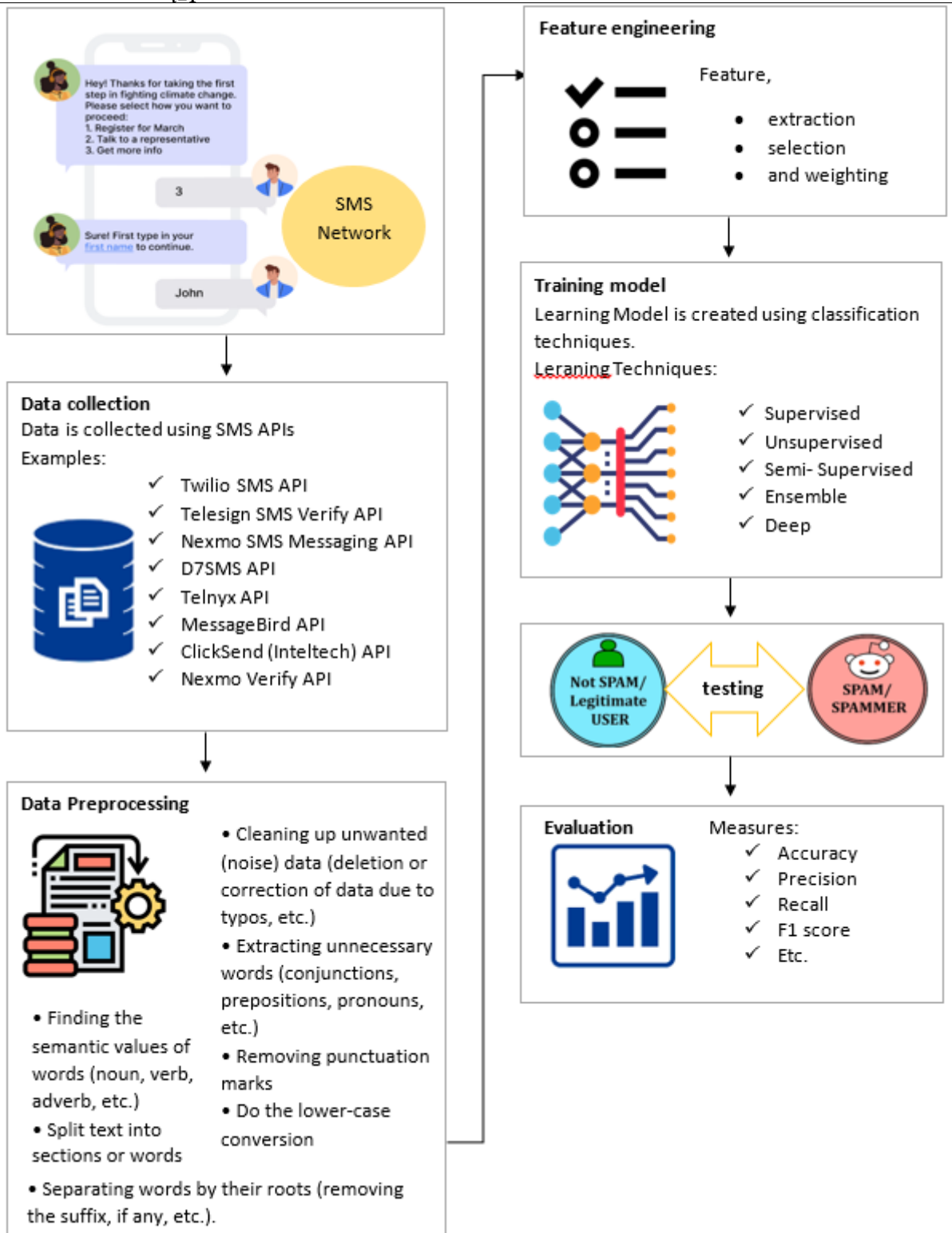


Figure 4 SMS Filtering process

Filter approaches evaluate each attribute independently. Calculates a score for each attribute

with a statistical function. It selects N attributes according to this score. Such approaches generally work faster. Wrapper approaches select a subset of features using a classifier. Such techniques are based on the analysis of the relationship between feature subset selection and relevance. Embedded approaches create a subset of features by taking advantage of the best aspects of the other two feature selection approaches. Embedded techniques are based on independent criteria. These criteria are used to select optimal feature subsets with known cardinalities. While wrapper and embedded techniques require frequent classifier interaction during the feature selection phase, filter techniques do not. Three of the best-known approaches to filters were used in this study: Information Gain (IG), Gini Index (GI), Distinguishing Feature Selector (DFS) and Max-Min Ratio (MMR). Brief information about these approaches is given in Table 2.

3.2. Classification Methods

There are classifiers designed in various models in the literature [30]. The purpose of classifiers is to label unlabeled data using labeled data. In this section, the classifiers used in the study are mentioned.

3.2.1. Support Vector Machines (SVM)

SVM, which is based on the concept of margin maximization, is regarded as an effective classifier in the literature. Depending on the type of core used, it also has linear and non-linear versions. In this study, the linear version of SVM was used. The margin concept is central to the SVM classifier [24]. Classifiers separate classes using hyperplanes. Each hyperplane is distinguished by its direction (w) and precise position in space (w_0).

3.2.2. K-Nearest Neighbors (KNN)

The k-nearest neighbors algorithm (KNN) is a non-parametric classification technique [25]. This technique is widely used in the field of text classification, as well as in many other fields. When a test document x is given, the approach finds k nearest neighbors of x among all documents in the training set and scores the category candidates based on the class of k candidates. The score of the category

of neighboring documents can be the similarity of document x and each neighbor. For neighbor calculation, it employs one of the distance calculation methods such as Euclidean (Euclidean), Manhattan, and Minkowski. The approach takes the k -highest-scoring neighbor score after calculating the document's neighbor scores.

3.2.3. Naive Bayes (NB)

In the field of text classification, the Naive Bayesian classifier has long been a popular method for categorizing texts. The theoretical foundation of the method is Thomas Bayes' theorem [26]. The independence of states in Bayes' theorem is the key to the naive Bayes classifier. As a result, the attributes are distinct. The classifier determines the probability of each situation and categorizes it based on the highest probability value.

4. Experimental Works

In this section, after giving information about the data set used in experimental studies, the success metrics used are introduced. Finally, the results obtained in the experimental studies are given and these results are analyzed.

4.1. Dataset

The SMS dataset is a collection of short text documents with free access on the Internet for detecting spam messages on phones. The dataset has been used in various studies to detect spam phone messages. First part of the collection consists of 450 manually retrieved messages on the Grumbletext Web site, where people in the UK are making public allegations about cell phone SMS spam messages. The second part of the collection is a subset of 3,375 SMS amateur messages randomly selected from the dataset of the NUS SMS Corpus (NSC), a dataset of approximately 10,000 legitimate messages collected for research at the Department of Computer Science at the National University of Singapore. The third part of the collection is a list of 450 SMS amateur messages collected from Caroline Tag's PhD Thesis. Finally, in SMS Spam Corpus v.0.1 Big, 1,002 SMS amateur messages and 322 spam messages were added to the collection, resulting in the dataset known

as the SMS Spam Collection [27].

A subset of the SMS Spam collection was used in this study. 612 messages of the subset were used as training data and 263 as test data.

4.2. Success Criteria

- **Accuracy:** It comes from the beginning of the most frequently used success criteria in the classification process in data mining. The accuracy score is obtained by dividing the results of correctly classified samples by the total number of samples.

$$CS = \text{size}(\text{Correctly Classified Samples})$$

$$Alls = \text{size}(\text{Number of All Samples})$$

$$\text{Accuracy} = \frac{CS}{Alls}$$

- **Macro-F1 Criterion:** Macro f1, one of the F criteria, is a frequently used criterion in the text classification field. In the macro-average, equal weight is given to each class regardless of class frequency, since the mean of all classes is taken after the F measure is calculated for each class in the data set. Therefore, it is necessary to specify the Precision and Recall metrics before giving the Macro-F1 mathematical background. Macro-F1 obtained using these two metrics is calculated as follows.:

$$p_i = \frac{1}{C} * \frac{\sum_{i=1}^C TP_i}{\sum_{i=1}^C TP_i + FP_i}$$

$$r_i = \frac{1}{C} * \frac{\sum_{i=1}^C TP_i}{\sum_{i=1}^C TP_i + FN_i}$$

$$F_i = 2 * \frac{p_i * r_i}{p_i + r_i}$$

$$\text{Macro-F1} = \frac{\sum_{i=1}^C F_i}{C}$$

In the formula, the pair (p_i, r_i) corresponds to precision and precision for class i , respectively.

4.3. Accuracy Analysis

In experimental studies, random feature sizes Top-60, 110, 250, 450, 650, and 950 were chosen. The achievements of DFS, IG, G1, and CHI2 feature selection approaches for SVM, KNN, and NB classifiers in these feature Tops are given in Figures 5, 6, and 7. Figure 5, Figure 6, and Figure 7 show the results of the feature selection approaches for the SVM, KNN, and NB classifiers, respectively, in the aforementioned feature dimensions. Moreover, each figure represents results for both Accuracy and Macro F1.

When Figure 5 is examined, it can be observed that DFS offers the best results for the Accuracy criterion. Likewise, DFS showed the best results for Macro F1. Also, it can be seen in Figure 6 that IG performs better for both metrics when the KNN classifier is used. For the NB classifier, CHI2 and GI performed better. This situation is the same for both metrics (See Figure 7). Results in Figures show that each feature performs well with a classifier.

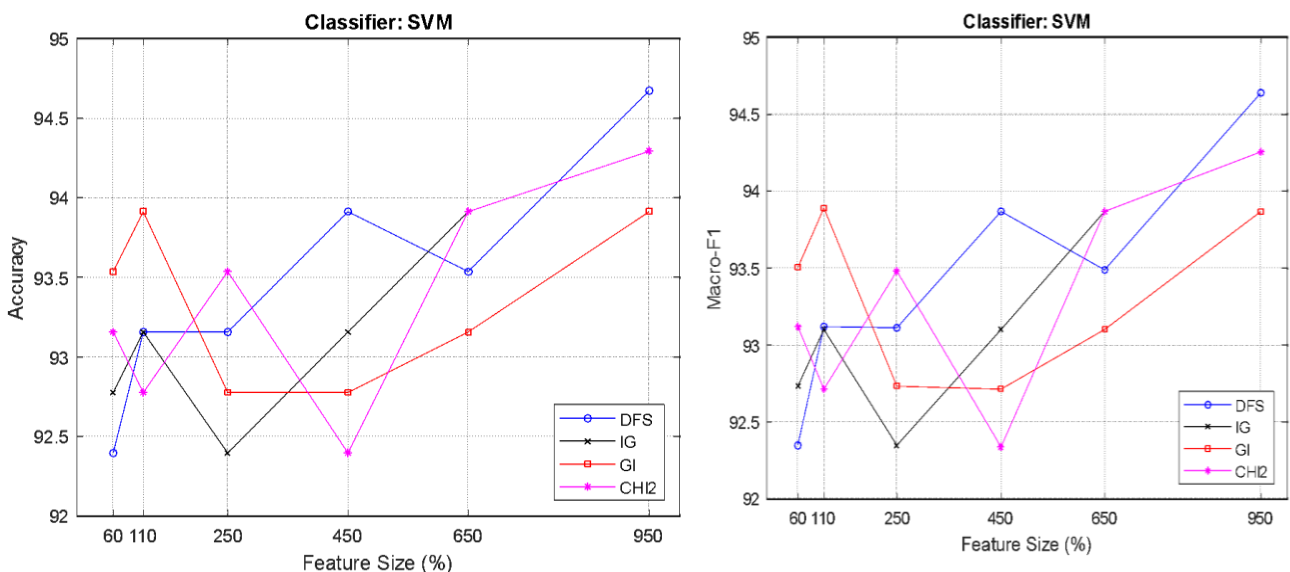


Figure 5 Accuracy and Macro- F1 Results for SVM Classifier

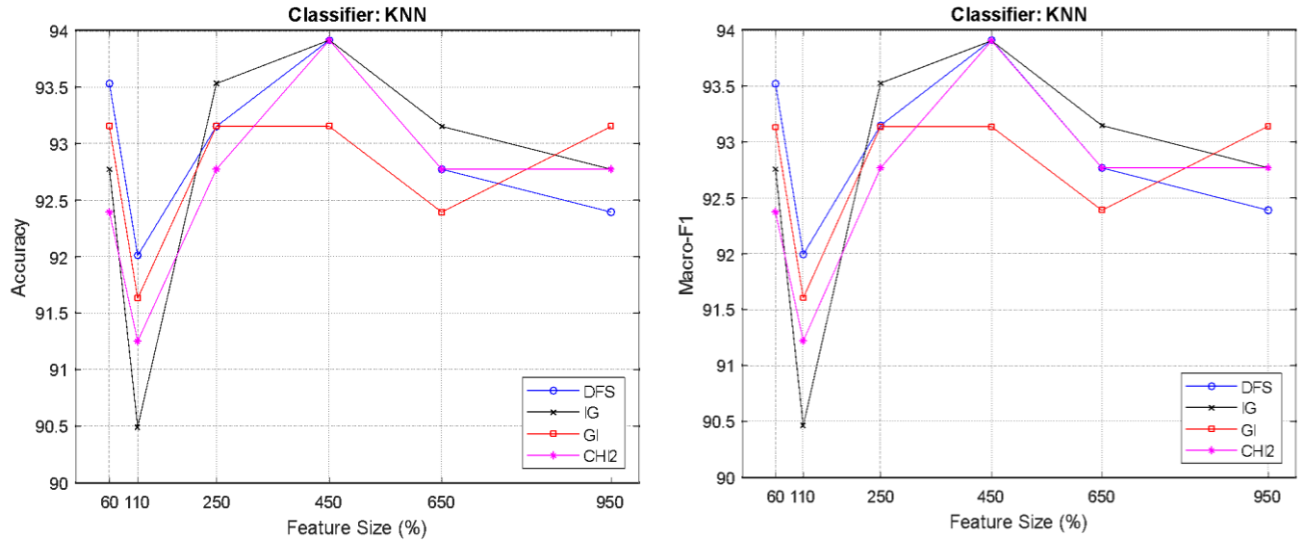


Figure 6 Accuracy and Macro- F1 Results for KNN Classifier

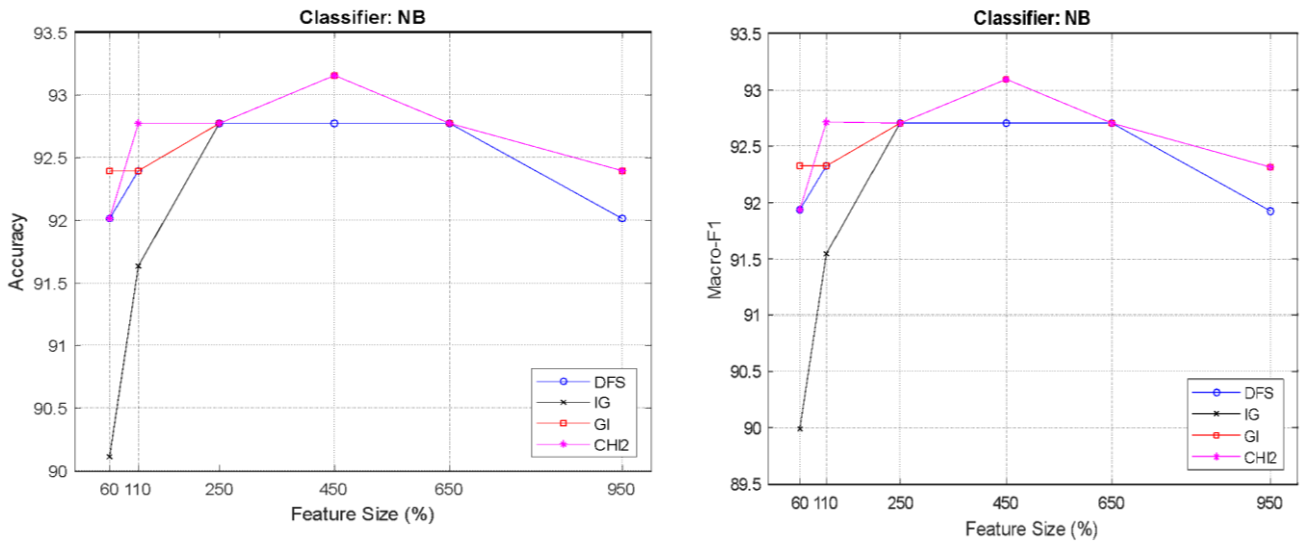


Figure 7 Accuracy and Macro- F1 Results for NB Classifier

In order to better interpret the results, it is necessary to look at the average of the performances of each feature for all classifiers. Table 3 and Table 4 was created for this process.

Table 3 Average Accuracy Results on all Classifiers

Feature Size	DFS	IG	GI	CHI2
60	92.6489	91.8885	93.0291	92.5222
110	92.5222	91.7617	92.6489	92.2687
250	93.0292	92.9024	92.9024	93.0292
450	93.5361	93.4094	93.0292	93.1559
650	93.0292	93.2826	92.7757	93.1559

950 93.0291 93.1559 93.1559 93.1559

Table 4 Average Macro-F1 Results on all Classifiers

Feature Size	DFS	IG	GI	CHI2
60	92.6019	91.8289	92.9885	92.4777
110	92.4816	91.7054	92.6082	92.2174
250	92.9891	92.8604	92.8590	92.9860
450	93.4953	93.3686	92.9825	93.1132
650	92.9890	93.2416	92.7334	93.1153
950	92.9863	93.1420	93.1093	93.1142

When the tables are examined, DFS in 450 dimensions achieves the best performance for all classifiers based on both criteria. These tables are useful for determining whether feature selection approaches exhibit statistically stable performance. It's also useful to see which feature sizes perform best. For example, IG performed poorly in small dimensions compared to other approaches, but better in larger dimensions. Furthermore, DFS and CHI2 performed similarly and produced more consistent results than other approaches. This demonstrates that DFS and CHI2 collaborate closely. In other words, it chooses features that are close to being distinctive. These characteristics do not have to be the same. Assume that feature *A* has a distinctness of 0.5689 and feature *B* has a distinctness of 0.5772. In this case, DFS may select attribute *A*, while CHI2 may select attribute *B*. However, the contributions of these two features to the classifier are nearly equal.

As a result, the DFS approach appears to be more stable and performs better at certain feature Top-N dimensions. Furthermore, the GI approach performed well with small feature sizes. In terms of classifiers, it is appropriate to say that SVM outperforms others. These results show that using DFS and SVM classifiers results in more accurate SMS spam detection.

5. Conclusion

In this study, text mining techniques were used to analyze the SMS dataset to determine the necessary parameters for an effective classification study. Four of the most well-known feature selection approaches, each of which is one of these parameters, were employed. As a result, the approach that produced the best results was chosen. In addition, the classifier, another parameter that produces the best results with this approach, was determined. According to the experimental results, the DFS feature selection approach produced the best results with the SVM classifier. This study provides a general framework for future studies in this field that will use text mining techniques.

References

- [1]. Parlak, B., & Uysal, A. K. (2021). A novel filter feature selection method for text classification: Extensive Feature Selector. *Journal of Information Science*, 0165551521991037.
- [2]. Uysal, A. K., & Gunal, S. (2012). A novel probabilistic feature selection method for text classification. *Knowledge-Based Systems*, 36, 226-235.
- [3]. Android Apps. (Accessed March 2012). Available: <https://play.google.com/store/apps>
- [4]. Delany, S. J., Buckley, M., & Greene, D. (2012). SMS spam filtering: Methods and data. *Expert Systems with Applications*, 39(10), 9899-9908.
- [5]. Xiang, Y., Chowdhury, M., & Ali, S. (2004). Filtering mobile spam by support vector machine. In N. Debnath (Ed.), *Proceedings of the third international conference on computer sciences, software engineering, information technology, E-business and applications* (pp. 1–4).
- [6]. Abayomi-Alli, O., Misra, S., Abayomi-Alli, A., & Odusami, M. (2019). A review of soft techniques for SMS spam classification: Methods, approaches and applications. *Engineering Applications of Artificial Intelligence*, 86, 197-212.
- [7]. Nagwani, N. K., & Sharaff, A. (2017). SMS spam filtering and thread identification using bi-level text classification and clustering techniques. *Journal of Information Science*, 43(1), 75-87.
- [8]. Nagwani, N. K. (2017). A Bi-Level Text Classification Approach for SMS Spam Filtering and Identifying Priority Messages. *International Arab Journal of Information Technology (IAJIT)*, 14(4).
- [9]. Hanif, K., & Ghous, H. Detection Of Sms Spam And Filtering By Using Data Mining Methods: Literature Review.
- [10]. Gupta, M., Bakliwal, A., Agarwal, S., & Mehndiratta, P. (2018). A Comparative Study of Spam SMS Detection Using Machine Learning Classifiers. 2018 11th Internationalfile:///E:/Sms Spamming/Sms Spamming 15.Pdf Conference on Contemporary Computing, IC3 2018, 1–7. <https://doi.org/10.1109/IC3.2018.8530469>
- [11]. Popovac, M., Karanovic, M., Sladojevic, S., Arsenovic, M., & Anderla, A. (2018). Convolutional Neural Network Based SMS Spam Detection. 2018 26th Telecommunications Forum, TELFOR 2018 - Proceedings, 1–4. <https://doi.org/10.1109/TELFOR.2018.8611916>
- [12]. Lu Zhang, Jiandong Ding, Yi Xu, Yingyao Liu, and Shuigeng Zhou. 2021. Weakly-supervised text classification based on keyword graph. In *Proceedings of the 2021 Conference on Empirical Methods in Natural Language Processing*, pages

- 2803–2813, Online and Punta Cana, Dominican Republic. Association for Computational Linguistics.
- [13]. Uysal, A. K., Günel, S., Ergin, S., & Günel, E. Ş. (2012, April). Detection of SMS spam messages on mobile phones. In 2012 20th Signal Processing and Communications Applications Conference (SIU) (pp. 1-4). Ieee.
- [14]. Abayomi-Alli, O., Misra, S., Abayomi-Alli, A., & Odusami, M. (2019). A review of soft techniques for SMS spam classification: Methods, approaches and applications. *Engineering Applications of Artificial Intelligence*, 86, 197-212.”
- [15]. Xiang, Y., Chowdhury, M., & Ali, S. (2004). Filtering mobile spam by support vector machine. In N. Debnath (Ed.), *Proceedings of the third international conference on computer sciences, software engineering, information technology, E-business and applications* (pp. 1–4).
- [16]. Boykin, P. O., & Roychowdhury, V. P. (2005). Leveraging social networks to fight spam. *IEEE Computer*, 38, 61–68.
- [17]. Rao, S., Verma, A. K., & Bhatia, T. (2021). A review on social spam detection: challenges, open issues, and future directions. *Expert Systems with Applications*, 186, 115742.
- [18]. Healy, M., Delany, S., & Zamolotskikh, A. (2005). An assessment of case-based reasoning for short text message classification. In N. Creaney (Ed.), *Proceedings of 16th Irish conference on artificial intelligence and cognitive science, (AICS-05)* (pp. 257–266).
- [19]. Gómez Hidalgo, J. M., Bringas, G. C., Sáenz, E. P., & García, F. C. (2006). Content based SMS spam filtering. In D. Bulterman, & D.F. Brailsford (Eds.), *Proceedings of the 2006 ACM symposium on document engineering DocEng '06* (pp. 107–114). New York, NY, USA: ACM.
- [20]. Cai, J., Tang, Y., & Hu, R. (2008). Spam filter for short messages using winnow. In *Proceedings of the international conference on advanced language processing and web information technology* (pp. 454–459). IEEE.
- [21]. Wu, N., Wu, M., & Chen, S. (2008). Real-time monitoring and filtering system for mobile SMS. In *Proceedings of 3rd IEEE conference on industrial electronics and applications* (pp. 1319–1324).
- [22]. Jie, H., Bei, H., & Wenjing, P. (2010). A Bayesian approach for text filter on 3G network. In *Proceedings of the 6th international conference on wireless communications networking and mobile computing* (pp. 1–5).
- [23]. Longzhen, D., An, L., & Longjun, H. (2009). A new spam short message classification. In *Proceedings of the first international workshop on education technology and computer science* (Vol. 2, pp. 168 –171).
- [24]. Joachims, T. (1998). Text categorization with support vector machines: Learning with many relevant features. In *European conference on machine learning* (s. (pp. 137-142).). Berlin, Heidelberg.: Springer, .
- [25]. Kowsari, K., Jafari Meimandi, K., Heidarysafa, M., Mendu, S., Barnes, L., & Brown, D. (2019). *Text classification algorithms: A survey*. Information.
- [26]. Pearson, E. (1925). Bayes’ theorem, examined in the light of experimental sampling. *Biometrika*.
- [27]. <https://archive.ics.uci.edu/ml/datasets/SMS+Spam+Collection>
- [28]. Çekik, R., & Uysal, A. K. (2020). A novel filter feature selection method using rough set for short text data. *Expert Systems with Applications*, 160, 113691.
- [29]. Çekik, R., & Uysal, A. K. (2022). A new metric for feature selection on short text datasets. *Concurrency and Computation: Practice and Experience*, e6909.
- [30]. Çekik, R., & Telceken, S. (2018). A new classification method based on rough sets theory. *Soft Computing*, 22(6), 1881-1889.
- [31]. Parlak, B., & Uysal, A. K. (2021). The effects of globalisation techniques on feature selection for text classification. *Journal of Information Science*, 47(6), 727-739.



Journal of Soft Computing and Artificial Intelligence

Journal homepage: <https://dergipark.org.tr/en/pub/jscai>

International
Open Access 

Volume 03
Issue 02

December, 2022

Research Article

CREMA-D: Improving Accuracy with BPSO-Based Feature Selection for Emotion Recognition Using Speech

Kenan DONUK¹ 

¹ Cizre Vocational School, Computer Programming Department. Sirnak University, 73200, Sirnak, Türkiye

ARTICLE INFO

Article history:

Received December 4, 2022

Revised December 15, 2022

Accepted December 21, 2022

Keywords:

BPSO Algorithm

Crema-D

CNN

SVM Algorithm

Speech Emotion

ABSTRACT

People mostly communicate through speech or facial expressions. People's feelings and thoughts are reflected in their faces and speech. This phenomenon is an important tool for people to empathize when communicating with each other. Today, human emotions can be recognized automatically with the help of artificial intelligence systems. Automatic recognition of emotions can increase productivity in all areas including virtual reality, psychology, behavior modeling, in short, human-computer interaction. In this study, we propose a method based on improving the accuracy of emotion recognition using speech data. In this method, new features are determined using convolutional neural networks from MFCC coefficient matrices of speech records in Crema-D dataset. By applying particle swarm optimization to the features obtained, the accuracy was increased by selecting the features that are important for speech emotion classification. In addition, 64 attributes used for each record were reduced to 33 attributes. In the test results, 62.86% accuracy was obtained with CNN, 63.93% accuracy with SVM and 66.01% accuracy with CNN+BPSO+SVM.

1. Introduction

Emotions are an important tool of human communication. People's cognitive and mental states manifest themselves by being reflected in their face, eyes, voice, or body with many different emotions such as surprise, disgust, fear, anger, sadness, happiness. By integrating interactive human-computer systems that continuously and automatically recognize people's emotional states with intelligent systems, these systems can be made more interactive. Emotion recognition using speech, the primary communication channel through which emotional states are conveyed, is an active area of research. Systems for speech emotion recognition (SER) are used in many different domains, e.g., call

centers [1], criminal case [2]. Some studies on SER methods in the literature are as follows. Zielonka et al. They used Crema-D, RAVDESS, SAVEE, TESS and IEMOCAP datasets in their study. In their study, the performance difference of spectrogram and mel-spectrogram features used to extract emotion-representing features was compared over Resnet-18 and a custom CNN model. As a result of the comparisons, it has been shown that mel-spectrograms are more suitable for classical CNN-based education. For the Crema-D dataset, they achieved an accuracy of 46.75% in the spectrogram feature use and 53.66% in the mel-spectrogram feature test results in the classical CNN architecture test results [3]. Shankar et al. conducted a study on

¹Corresponding author

e-mail: kenandonuk@sirnak.edu.tr

DOI: 10.55195/jscai.1214312

performance among model architectures of data augmentation. They used Gated-CNN, MLP-mixer, Bi-LSTM, Transformer architectures in their work. In the training of model architectures, the optimization hyper-parameters of the models were adjusted using the VESUS dataset. Then, the performances were evaluated by using 5-fold cross validation with IEMOCAP and Crema-D datasets, on which different data augmentation methods were applied on the models. It has been shown that speed perturbation, one of the data augmentation types, is a robust data augmentation strategy in increasing accuracy [4]. Donuk and Hanbay obtained the zcr, rmse and mfcc features of the audio signals of the Ravdess and Tess datasets. Considering the change of these features in an audio signal over time, they performed an LSTM-based classification [5]. In their study, Singh and Goel conducted a literature review on the databases used in speech emotion recognition studies between 2000-2021 and the motivations and limitations of deep learning used in speech emotion classification. Deep learning studies on speech emotion recognition were systematically summarized by examining 152 articles [6].

2. Material and Method

2.1. Crema-D Dataset

The Crowd-sourced Emotional Multi-modal Actors Dataset, Crema-D dataset contains 7442 clips created by theater directors for a total of 91 actors, 48 males and 43 females, ranging in age from 20 to 74 and of various ethnicities. Actors were asked to speak 12 specific phrases in one of six different emotions (Disgust, Fear, Sad, Anger, Neutral, Happy) and in three different intonations (Low, Medium, High). The recordings (auditory, visual, and audiovisual) were rated by 2,443 raters via crowdsourcing based on the intensity of the emotion and feeling. Human recognition of recordings made in three different modalities as auditory, visual, and audiovisual has a hit rate of 40.9%, 58.2%, and 63.6%, respectively [7]. The intensities of speech emotion labels belonging to the Crema-D data set used in our study are shown in the graph given in Figure 1.

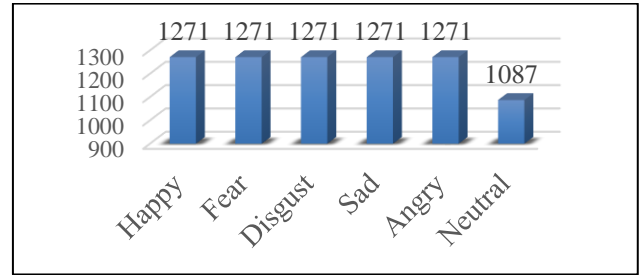


Figure 1 Crema-D dataset emotion distribution

Audio data of speech emotions are stored in digital media by analog-digital conversion. While performing this cycle, the quality of the signal is determined depending on the number of samples per second. In addition, a quantitative dimension of each sound sample of the signal is determined. In Figure 2, a digital representation of a sound with a sampling frequency of 22050 is given.

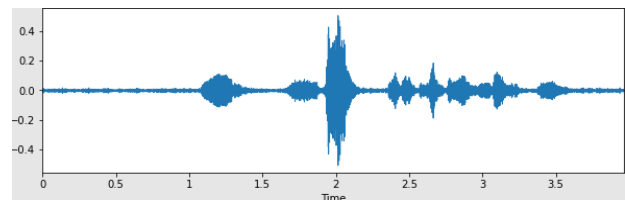


Figure 2 Audio signal

2.2. Data Preprocessing

It has been reported that the classification using the available sample values of the audio signals has little contribution to the performance of the model used [8]. For this reason, acoustic features that best represent emotions are needed. Some preprocessing steps are required to extract the appropriate features. These can be summarized as extracting the silent parts with low amplitude values from the audio signal, converting the obtained signals to the appropriate format for the model to be used in the classification, and finally extracting the features from the signals.

2.3. Data Cleaning and Editing

Before extracting the voice features from the speech recordings of the Crema-D dataset, the silent parts of the wave graphs that we think do not represent the current emotion were clipped using the librosa [9] library. With this process, emotions will be better represented while classifying from attributes. Figure 3 shows the original and clipped state of the signal to the "angry" sound sense.

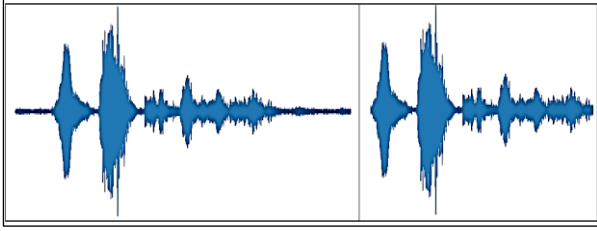


Figure 3 Cropped audio signal

To extract features with the same spatial dimensions from the audio signals obtained after clipping, all audio recordings were arranged to have the same sample size.

2.4. Feature Extraction

Acoustic sound features to represent speech emotions are needed to be used in classification from data set signals converted into a format suitable for feature extraction. There are different attributes representing sound in the literature. These can be listed as Zero Crossing Rate, Energy, Entropy of Energy, Spectral Centroid, Spectral Spread, Spectral Flux, Mel Frequency Cepstral Coefficients, Chroma Vector, Chroma Deviation. These attributes can be used together as well as alone. Mel Frequency Cepstral Coefficients (MFCCs), which are widely used among these attributes, were used in our study.

2.4.1. Mel-frequency Cepstral Coefficients

Mel-Frequency Cepstral Coefficients (MFCCs) are the most used features to represent the sound with a certain number of coefficients. To extract the MFCCs features, the audio signal needs to undergo a series of processing. First, the preprocessed audio signals are divided into frames with the same number of samples. With the division process, it is aimed to extract more consistent features from the audio signals. The number of frames to be obtained can be obtained with the formula given in Equation 1.

$$\left(\frac{\text{Number of samples} - \text{Frame length}}{\text{Hop length}} \right) + 1 \quad (1)$$

Hamming windowing is applied for each frame of the audio signals split into frames. With Hamming windowing, the frequency spectrum to be obtained from audio signals is improved. Thus, spectral leakage due to discrete frames of the audio signal is prevented. After this step, Fast Fourier Transform (FFT) is applied for each of the framed signals.

With FFT, the audio signal is passed from the time domain to the frequency domain. Thus, the amplitude and frequency values that make up the audio signal are extracted. FFT formula is given in Equation 2. In the equation, N represents the number of samples in the frame, n represents the relevant sample, $x(n)$ represents the value of the signal in the n sample, k the current frequency, $X(k)$ represents the amplitude and phase values of the k frequency in the audio signal [5].

$$X(k) = \sum_{n=0}^{N-1} x(n) e^{-i \frac{2\pi kn}{N}} \quad (2)$$

With the formula given in Equation 3, the powers of the frequencies are calculated by squaring the values obtained by FFT.

$$P_n = \frac{(HFD(x_n))^2}{N_{HFD}} \quad (3)$$

It has been reported that the human ear perceives sound frequencies linearly up to 1000 Hz and logarithmically for values after 1000 Hz [10]. With an empirical frequency scale called the Mel scale, sound frequencies are converted to frequency values suitable for the nature of the human ear. Calculation of sound frequency (f) from Mel scale type is given in Equation 4. After this stage, Mel spectrogram is obtained by applying Mel triangle filters (usually 12 filters) to the frequency spectrum. The powers of the Mel bands are obtained by multiplying the Mel filters in each different frequency range with the frequency values in the FFT applied frames [5].

Discrete Cosine Transform (DCT) is applied as the last step in MFCC feature extraction. In this step, commonly 13 MFCC coefficients are obtained for each signal frame. The number of coefficients in our study is 40. MFCC are feature coefficients that are often used in audio classification tasks. The coefficients obtained in each frame are added along the column to obtain the MFCC feature matrix. The MFCC coefficient extraction formula is given in Equation 5. $Ct(n)$ in the formula represents the n th MFCC coefficient of the t -frame. M indicates the number of MFCCs. The value of $X'n(m)$ shows the logarithmic energy of the m th mel filter [11].

$$Mel(f) = 2595 * (1 + \frac{f}{700}) \quad (4)$$

$$C_t(n) = \sum_{m=0}^{M-1} X'_n(m) \cos(\frac{\pi n(m-0.5)}{M}) \quad (5)$$

2.5. Particle Swarm Optimization

Particle Swarm Optimization (PSO) is a heuristic optimization technique developed by Kennedy and Eberhart [12] in 1995. This optimization was inspired by the movements of birds and fish in search of food, which move in flocks. For the herd to reach its goal, the communication of individuals in the herd with each other has been mathematically revealed. PSO is an algorithm used to solve nonlinear problems. In this algorithm, a population of candidate particles is created to find the best solution in the problem space. Each particle in the population tries to find the best solution. The particle that gives the best solution in the population becomes the leader (GBest) of the population, that is, it refers to the global best particle. The best solution obtained by the particles in the search space individually represents the individual best particle. The individual best particle is expressed by PBest. While the particles are searching for solutions in the search space, they update their velocities with every change of position by referencing the GBest and PBest solutions.

Velocity and position updates are given in Equations 6 and 7, respectively [13].

$$vn[t+1] = w[t]vn[t] + c1r1(xL,n[t] - xn[t]) + c2r2(xG,n[t] - xn[t]) \quad (6)$$

$$xn[t+1] = xn[t] + vn[t+1] \quad (7)$$

The expressions of the formulas given in Equations 6 and 7 are explained below [13].

$vn[t+1]$:The updated velocity of the particle

$w[t]$:Inertia coefficient

$vn[t]$:The previous velocity of the particle

$c1$:Coefficient of remembering own best position

$r1$:Random number between 0-1

$xL,n[t]$:The particle's best position ever

$xn[t]$:The previous position of the particle

$xG,n[t]$:Swarm leader's position

$r2$:Random number between 0-1

$c2$:Coefficient of remembering the position of the swarm leader

2.6. Proposed System

The proposed system is shown in Figure 4. The MFCCs feature coefficients obtained from the audio recordings in the Crema-D dataset were used in the training and testing stages of the CNN network.

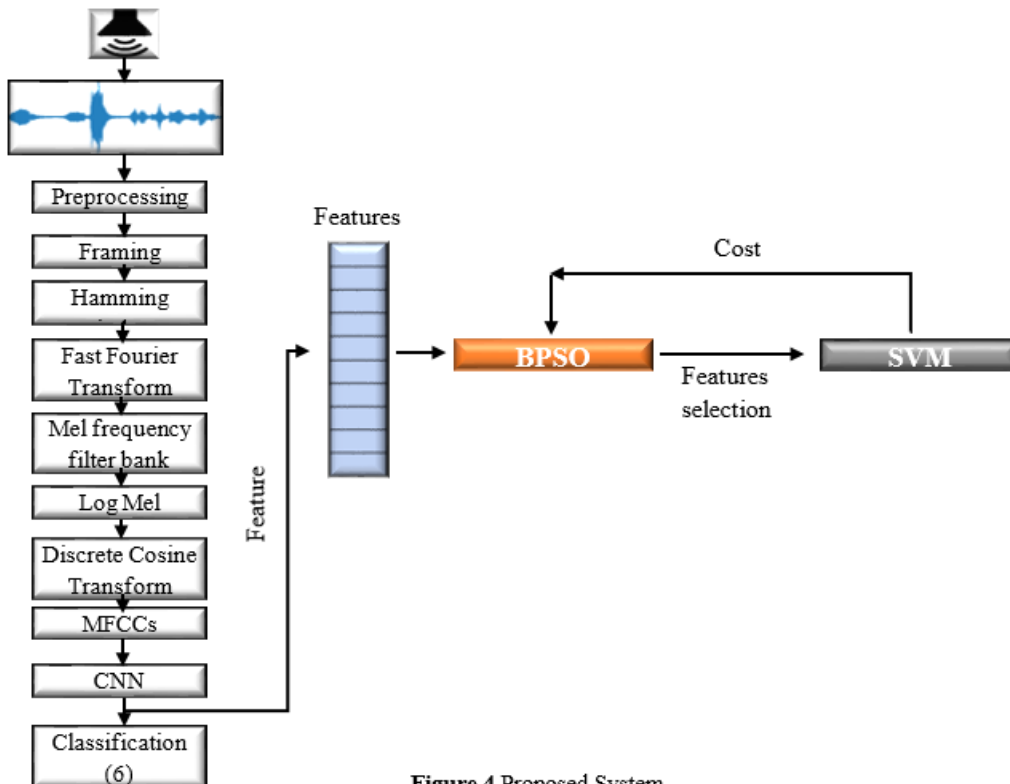


Figure 4 Proposed System

The MFCCs features obtained from the data set are divided into two as 80% training and 20% testing. Training and testing data are shown in Table 1.

Table 1 Crema-D dataset features

Number of clips	Frame feature count (MFCCs)	Number of frames
Training :5953	40	216
Test :1489	40	216

When Table 1 is examined, when the audio recording signals belonging to the equal sample number are divided into frames, 216 frames are obtained. For each frame, 40 MFCCs feature coefficients were extracted. The CNN structure of the proposed system is given in Table 2.

Table 2 CNN structure

Layer	Output Shape	Parameter
input_1 (InputLayer)	[(?, 40, 216, 1)]	0
conv2d (Conv2D)	(?, 40, 216, 64)	640
batch_normalization (BatchNormalization)	(?, 40, 216, 64)	256
activation (Activation)	(?, 40, 216, 64)	0
max_pooling2d (MaxPooling2D)	(?, 20, 108, 64)	0
dropout (Dropout)	(?, 20, 108, 64)	0
conv2d_1 (Conv2D)	(?, 20, 108, 64)	36928
batch_normalization_1 (BatchNormalization)	(?, 20, 108, 64)	256
activation_1 (Activation)	(?, 20, 108, 64)	0
max_pooling2d_1 (MaxPooling2D)	(?, 10, 54, 64)	0
dropout_1 (Dropout)	(?, 10, 54, 64)	0
conv2d_2 (Conv2D)	(?, 10, 54, 128)	73856
batch_normalization_2 (BatchNormalization)	(?, 10, 54, 128)	512
activation_2 (Activation)	(?, 10, 54, 128)	0
max_pooling2d_2 (MaxPooling2D)	(?, 5, 27, 128)	0
dropout_2 (Dropout)	(?, 5, 27, 128)	0
conv2d_3 (Conv2D)	(?, 5, 27, 128)	147584
batch_normalization_3 (BatchNormalization)	(?, 5, 27, 128)	512
activation_3 (Activation)	(?, 5, 27, 128)	0
max_pooling2d_3 (MaxPooling2D)	(?, 2, 13, 128)	0
dropout_3 (Dropout)	(?, 2, 13, 128)	0
flatten (Flatten)	(?, 3328)	0
dense (Dense)	(?, 64)	213056
batch_normalization_4 (BatchNormalization)	(?, 64)	256
activation_4 (Activation)	(?, 64)	0
dropout_4 (Dropout)	(?, 64)	0
dense_1 (Dense)	(?, 6)	390

3. Experimental Results

The CNN network is trained with training data. The error value of the network reached its minimum value at 45 epochs. Data normalization, maxpooling and dropout (0.3) were applied after all convolution operations except the last classification layer. "Adam" optimization algorithm is used to learn the network better. For the loss calculation, categorical_crossentropy was considered suitable as the loss function. While the classification layer is activated with the "softmax" activation function, the "ReLU" activation function is used in all other layers. The batch size of the network is 32.

After the training process, the performance of the model was tested in the testing phase. The test results were realized with an accuracy rate of 62.86%. Precision, recall, f1-score results of emotions were obtained via the sklearn library [14] in Table 3.

Table 3 Performance measurement metrics

Emotion	Precision	Recall	F1-score	Support
Angry	0.64	0.80	0.71	244
Digust	0.52	0.68	0.59	254
Fear	0.65	0.46	0.54	279
Happy	0.75	0.53	0.62	243
Neutral	0.71	0.77	0.73	235
Sad	0.59	0.56	0.57	234

CNN network trained with MFCCs features of speech sound recordings performs classification with 62.86% accuracy. At this stage, feature vectors of 5953x64 dimensions belonging to the fully connected layer of the trained CNN model before the classification layer are sent to the BPSO space for feature selection. In feature selection with BPSO, it creates swarm of solution snippets to find which features represent emotion better in 64-unit feature vectors. In BPSO, each particle, unlike PSO, consists of a 64-unit binary vector containing random "0" and "1" values. The new positions of the particles in motion in the search space must be determined at each iteration. For this, it is necessary to update the velocities of the particles. By applying the Sigmoidal function to the velocities of the particles, values between 0-1 are obtained. Then, the obtained values are compared with a randomly determined number between 0-1 and the new positions of the units of the

particle are updated as "0" or "1" [15]. Position calculation formulas in BPSO optimization are given in Equation 8 and Equation 9.

$$Sig(vn[t + 1]) = \frac{1}{1 + e^{-(vn[t+1])}} \quad (8)$$

$$xn[t + 1] = \begin{cases} 0, & \text{if } rand() \geq Sig(vn[t + 1]) \\ 1, & \text{if } rand() < Sig(vn[t + 1]) \end{cases} \quad (9)$$

Filtering is performed by comparing the particle swarm with the feature vectors obtained from the CNN. The index values of the units with the value "1" of the particle are marked and the features with these index values in the feature vector form the new vector representing the emotion. The resulting new feature vectors are classified by SVM and an error value is obtained [15]. This process ends with finding the solution candidate with the lowest error rate as a result of SVM classification. As a result of applying BPSO to 64 feature layers of each record obtained from the CNN network, features that better represent emotions were obtained from 64 features. Thus, the number of attributes has been reduced from 64 to 33. The accuracy obtained because of the SVM classification made with 33 feature vectors of each record increased by 3.15% and reached 66.01% accuracy. BPSO was performed with 40 iterations and 100 particles. The optimization graph of BPSO is given in Figure 5. In addition, the classification accuracy rates of CNN, SVM and CNN+BPSO+SVM, respectively, using the MFCCs attributes of the data set are given in Table 4.

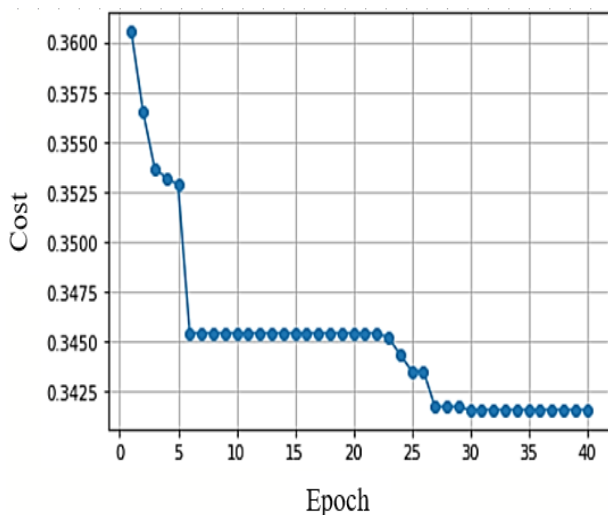


Figure 5 BPSO optimization graph

Table 4 Comparative accuracy rates

Method	Accuracy (%)
CNN	62.86
SVM	63.93
CNN+BPSO+SVM (Proposed method)	66.01

4. Conclusion

In our study, the effect of feature selection on classification accuracy was investigated. For this purpose, MFCCs features were extracted on the Crema-D speech dataset. The CNN architecture trained with these features achieved a test accuracy of 62.86%. By using the features in the last full connected layer of the CNN network, feature selection was performed with the help of BPSO. In the feature selection process, the error calculation was carried out with the help of the SVM algorithm. The number of features has been reduced by feature selection. In addition, the accuracy has been increased by 3.15%, reaching an accuracy rate of 66.01%.

References

- [1] M. Bojanić, V. DeliĆ, and A. Karpov, "Call Redistribution for a Call Center Based on Speech Emotion Recognition" *Applied Sciences* 2020, Vol. 10, Page 4653, vol. 10, no. 13, p. 4653, Jul. 2020, doi: 10.3390/AP10134653.
- [2] A. S. S. Kyi and K. Z. Lin, "Detecting Voice Features for Criminal Case" *2019 International Conference on Advanced Information Technologies, ICAIT 2019*, pp. 212–216, Nov. 2019, doi: 10.1109/AITC.2019.8921212.
- [3] M. Zielonka, A. Piastowski, A. Czyżewski, P. Nadachowski, M. Operlejn, and K. Kaczor, "Recognition of Emotions in Speech Using Convolutional Neural Networks on Different Datasets" *Electronics (Switzerland)*, vol. 11, no. 22, Nov. 2022.
- [4] R. Shankar, A. H. Kenfack, A. Somayazulu, and A. Venkataraman, "A Comparative Study of Data Augmentation Techniques for Deep Learning Based Emotion Recognition" Nov. 2022, doi: 10.48550/arxiv.2211.05047.
- [5] K. Donuk and D. Hanbay, "Konuşma Duygu Tanıma için Akustik Özelliklere Dayalı LSTM Tabanlı Bir Yaklaşım" *Computer Science*, vol. 7, no. 2, pp. 54–67, 2022, doi: 10.53070/bbd.1113379.

- [6] Y. B. Singh and S. Goel, "A systematic literature review of speech emotion recognition approaches" *Neurocomputing*, vol. 492, pp. 245–263, Jul. 2022, doi: 10.1016/J.NEUCOM.2022.04.028.
- [7] H. Cao, D. G. Cooper, M. K. Keutmann, R. C. Gur, A. Nenkova, and R. Verma, "CREMA-D: Crowd-sourced Emotional Multimodal Actors Dataset" *IEEE Trans Affect Comput*, vol. 5, no. 4, p. 377, Oct. 2014, doi: 10.1109/TAFFC.2014.2336244.
- [8] Ö. F. ÖZTÜRK and E. PASHAEİ, "Konuşmalardaki duygunun evrimsel LSTM modeli ile tespiti" *Dicle Üniversitesi Mühendislik Fakültesi Mühendislik Dergisi*, vol. 12, no. 4, pp. 581–589, Sep. 2021, doi: 10.24012/DUMF.1001914.
- [9] "librosa — librosa 0.9.2 documentation." <https://librosa.org/doc/latest/index.html> (accessed Dec. 01, 2022).
- [10] S. S. Stevens, J. Volkmann, and E. B. Newman, "A Scale for the Measurement of the Psychological Magnitude Pitch" *J Acoust Soc Am*, vol. 8, no. 3, pp. 185–190, Jan. 1937, doi: 10.1121/1.1915893.
- [11] Q. Chen and G. Huang, "A novel dual attention-based BLSTM with hybrid features in speech emotion recognition" *Eng Appl Artif Intell*, vol. 102, p. 104277, Jun. 2021, doi: 10.1016/J.ENGAPPAI.2021.104277.
- [12] J. Kennedy and R. Eberhart, "Particle swarm optimization" *Proceedings of ICNN'95 - International Conference on Neural Networks*, vol. 4, pp. 1942–1948, doi: 10.1109/ICNN.1995.488968.
- [13] K. Donuk, N. Özbey, M. Inan, C. Yeroğlu, and D. Hanbay, "Investigation of PIDA Controller Parameters via PSO Algorithm" *2018 International Conference on Artificial Intelligence and Data Processing, IDAP 2018*, Jan. 2019, doi: 10.1109/IDAP.2018.8620871.
- [14] F. Pedregosa FABIANPEDREGOSA *et al.*, "Scikit-learn: Machine Learning in Python" *Journal of Machine Learning Research*, vol. 12, no. 85, pp. 2825–2830, 2011, Accessed: Dec. 02, 2022. <http://jmlr.org/papers/v12/pedregosa11a.html>
- [15] K. Donuk *et al.*, "Deep Feature Selection for Facial Emotion Recognition Based on BPSO and SVM" *Politeknik Dergisi*, Dec. 2022, doi: 10.2339/POLITEKNIK.992720.



Journal of Soft Computing and Artificial Intelligence

Journal homepage: <https://dergipark.org.tr/en/pub/jscai>

International
Open Access

Volume 03
Issue 02

December, 2022

Research Article

Solving Multidimensional Knapsack Problem with Bayesian Multiploid Genetic Algorithm

Emrullah Gazioğlu¹ 

¹Computer Engineering Department, Engineering Faculty, Sirnak University, 73000, Sirnak, Türkiye

ARTICLE INFO	ABSTRACT
<p><i>Article history:</i></p> <p>Received</p> <p>Revised</p> <p>Accepted</p> <p><i>Keywords:</i></p> <p>Bayesian Optimization Algorithm</p> <p>MKP</p> <p>Genetic Algorithm Optimization</p>	<p>Solving optimization problems is still a big challenge in the area of optimization algorithms. Many proposed algorithms in the literature don't consider the relations between the variables of the nature of the problem. However, a recently published algorithm, called "Bayesian Multiploid Genetic Algorithm" exploits the relations between the variables and then solves the given problem. It also uses more than one genotype unlike the simple Genetic Algorithm (GA) and it acts like an implicit memory in order to remember the old but good solutions. In this work, the well-known Multidimensional Knapsack Problem (MKP) is solved by the Bayesian Multiploid Genetic Algorithm. And the results show that exploiting relations between the variables gets a huge advantage in solving the given problem.</p>

1. Introduction

Constraint Optimization Problems (COP) are still a big challenge in the area of computer science. One of them is the Multidimensional Knapsack Problem (MKP). The MKP is an extended version of the standard 0-1 Knapsack Problem (KP). While standard KP has only one resource, the MKP can has more than one resource. MKP is actually can be considered a real-world problem. Many real-world problems can be solved by MKP, such as cutting stock[1], loading problems [2], resource allocation for distributed computing[3], project selection[4], etc. MKP is still a current benchmark problem that continues to be solved with different approaches in recent years[5]–[8].

In the past ten years, many metaheuristic (MH) techniques are applied to solve different NP-Hard global optimization problems. Some of them are the following: Estimation of Distribution Algorithms (EDA)[9], Artificial Bee Colony (ABC)[10], Harmony Search (HS)[11], Ant Colony Optimization

(ACO)[12], Whale Optimization Algorithm (WOA)[13], Bat Algorithm (BA)[14], etc. However, all of them mentioned before don't consider the interactions between the problem's variables. In an ecosystem, all the objects have connected some way and they affect each other.

For this reason, it is important to exploit interactions between the variables and then use them to solve the problem effectively.

In this work, the Bayesian Multiploid Genetic Algorithm (BMGA)[15] is used, which has both an implicit memory scheme (to remember old solutions) and a Bayesian Network (to exploit interactions between variables) in order to solve the well-known Multidimensional Knapsack Problem (MKP) considering as a real-world benchmark problem.

To evaluate the BMGA's performance, six algorithms are selected as comparative algorithms. Note that, the results for the six algorithms listed below are already taken from the [16] and compared

¹ Corresponding author
e-mail: gazioglu@sirnak.edu.tr
DOI: 10.55195/jscai.1216193

to the BMGA's results.

- **Moth Search Algorithm (MS)**[17, s.]: A new optimization algorithm that is inspired by the Levy flights and the phototaxis of the moths. In this method, the fittest individual is considered the light source. The moths close to the fittest one fly in the form of Levy flights. On the other hand, because of the phototaxis, the moths far from the fittest one fly to the fittest one with big steps. These two different behaviors are the exploration and the exploitation of any other optimization method.
- **Self-Learning MS (SLMS)**[16]: In regular MS, each individual update their positions according to the fittest one. But it may cause it to fall into the local optimum. Authors, introduce a new self-learning strategy to enable individuals to update their positions not only according to the fittest one but also the closer individuals which have fitter than themselves.
- **Modified multi-verse optimization algorithm (MMVO)**[18]: In this algorithm, authors are inspired by the popular multi-verse theory which is based on three concepts: the wormhole, the black hole, and the white hole. In the algorithm, each universe is considered a solution candidate. If an individual gets close to the white hole, means it is getting better fitness values, and vice-versa (closing to the black hole), it is getting worse fitness values. And the wormholes are used as a diversification operator in the algorithm to maintain the diversity in the population.
- **Binary Gravitational Search Algorithm (BGS)**[19]: This is the binary version of GSA which is based on Newton's laws of gravity and motion: The gravitational force affects the objects and makes them attract each other. In the algorithm, each object is considered an agent, and each one of them has its mass. And their masses define their fitness values. As time passes, objects are attracted by the fitter masses which leads them to get a better fitness value.
- **Binary Hybrid Topology Particle Swarm Optimization (BHTPSO)**[19]: In the simple PSO[20], the particles may fall into local optimum if their velocities are zero. Because zero velocity means the particle's fitness value is good and shouldn't be changed. To overcome this, a small value is added to their velocities for

Algorithm 1 Pseudocode of BMGA

```

g ← number of genotypes
pop ← init(popSize, g)
randomly generate a probVec[ ]
while a termination condition not met do
    genotype2phenotype(pop, probVec[ ])
    best ← evaluate(pop)
    BN ← constructBN(pop)
    auxPop ← sampleBN(BN)
    probVec[ ] ← constructProbVec(auxPop)
    pop ← tournamentSelection(pop)
    pop ← uniformCrossover(pop)
    pop ← bitwiseMutation(pop)
return best
  
```

acceleration and enables them to escape from the local optimum.

- **Binary Hybrid Topology Particle Swarm Optimization Quadratic Interpolation (BHTPSO-QI)**[19]: This is the form of BHTPSO which is incorporated with a quadratic crossover operator.

This paper continues as follows: In Section 2, the BMGA is explained. In Section 3, MKP and its datasets are explained. In Section 4, the results are shown and finally, Section 5 concludes the paper.

2. Bayesian Multiploid Genetic Algorithm

The BMGA is constructed on the simple GA. However, it differs from simple GA in many ways.

First, the individuals in the simple GA have only one chromosome to represent a candidate solution. Both genetic operators and fitness calculations are done over this chromosome for each individual. However, in BMGA, each individual has two different structures: The genotypes and a phenotype. As we know, in nature, all living things have genotypes and phenotypes. Genotypes are inherited from the parents. However, the phenotype is the one that decides a living thing will look like to what.

The number of genotypes in an individual can be more than one. This feature provides an implicit memory scheme to the algorithm. Because all the genetic operators (crossover – mutation) are executed on the genotypes and the fitness calculations are executed on the phenotype of the individual. In this way, genotypes act like a memory. On the other hand, each individual has only one phenotype and its fitness value is calculated using that phenotype. That is, no matter how many genotypes an individual has, only one phenotype determines its fitness value. The structure of an individual is illustrated in Figure 1.

Second, BMGA uses a well-known Bayesian

Optimization Algorithm (BOA)[21] in it, in order to exploit the interactions between the variables. The BOA starts with a randomly generated population and creates a Bayesian Network (BN) by using this population. Since there is no prior information, BOA uses a greedy algorithm to form different BNs and then measure their quality using a special metric. After the algorithm finds the most suitable BN, then samples new individuals using that final BN. This procedure continues until a termination condition is met.

	0	1	2	3	4	5
genotype #1	1	1	0	1	1	0
genotype #2	0	0	0	1	0	0
genotype
genotype #k	1	1	0	1	0	0
Prob. Vector	0.5	0.3	0.7	0.1	0.8	0.9
phenotype	?	?	0	1	?	0

Figure 1 Illustration of an individual

In BMGA, the BOA is used in order to form a probability vector to determine the phenotypes of the individuals in the population. This works like this: First, the GA part of the BMGA randomly generates a population. In this generating part, only the genotypes of the individuals are generated. For instance, if an individual has four genotypes, and the size of the population is 100, then 400 genotypes are generated. Next, a probability vector is randomly formed to determine the phenotypes of the individuals for the first iteration. The probability vector is formed via genotypes of the best k% individuals of the population by calculating the probability of being 1 for each gene using Equation 1. After the probability of being 1 is calculated the Equation 1, for each gene in the phenotype, a random real number is generated between 0 and 1. This generated value is then compared to the corresponding value in the probability vector to determine the value of the phenotype. Assuming that number of genotypes is g , this comparison is held by using Equation 2 and Equation 3.

$$ProbVector_i = \frac{\text{number of ones for the } i^{th} \text{ gene}}{\text{size of the given population}} \quad (1)$$

$$val = (rand() < ProbVector_i) ? 1 : 0 \quad (2)$$

$$pheno_i = \begin{cases} 0, & \sum^g geno_i = 0 \\ 1, & \sum^g geno_i = g \\ val, & \text{other} \end{cases} \quad (3)$$

Once the phenotypes are determined, the fitness values of all individuals are calculated. After this first iteration, for the latter iterations, a new BN is constructed by using the same rule, and then a second population is sampled via BN. This second population is named auxiliary population, in short, “aux-pop”. The aux-pop has only one chromosome like in the simple GA. For the latter iterations, the probability vector is formed by the aux-pop, again, using Equation 1.

After explaining the key points of the BMGA, now we can explain it in general. The general pseudocode of the BMGA is given in Algorithm 1. After the BOA parts of the BMGA are executed, next, the GA part of the BMGA starts to run.

The standard tournament selection (size of n) is applied in the BMGA’s selection phase: Randomly chosen n solution candidates are compared and the fittest one is passed on to the next generation. This operation is performed until the size of the next generation is satisfied. Without recalculating its fitness value, the elite solution candidate from the last iteration is passed on to the current generation (elitism).

The uniform crossover approach is employed for crossover operation. It begins by randomly generating a mask vector in binary and then selecting two individuals, say i_1 , and i_2 , at each iteration. For each variable j (genes in chromosome), if the mask vector’s corresponding value is 1, i_1 ’s 1st genotype’s j^{th} variable is swapped with i_2 ’s 2nd genotype’s j^{th} variable with a probability of p_c . This procedure is performed on each pair of genotypes in each solution candidate separately.

The simple bitwise mutation is employed as a mutation tool. The genotypes of each solution candidate are inverted with a probability of p_m in the bitwise mutation process.

3. Preparing Test Environment

3.1. Multidimensional Knapsack Problem

MKP is a well-known benchmark problem for optimization algorithms. The goal of the problem finding a subset of given a number of items that obtain the optimal profit value while satisfying the given constraints. In this problem, there are n items, m resources, and $n \times m$ constraints. The formulation of the problem is given in Equation 4 and Equation 5.

$$\max \quad \sum_{j=1}^n p_j \times x_j \quad (4)$$

$$\text{subject to } \sum_{j=1}^n r_{ij} \times x_j \leq c_i, \quad \forall i \in \{1, 2, \dots, m\} \quad (5)$$

where n is the number of items, m is the number of resources (knapsacks), x_j denotes the whether the item j is collected, p_j is the profit of the item j , r_{ij} is the consumption of the j^{th} item at the i^{th} resource and finally c_i is the capacity of the i^{th} resource.

In order to test BMGA for MKPs, the first five problems are taken from the six different datasets which are provided on the well-known OR-LIB[22]. There are 30 different problems in that dataset and each has a different problem size. All problems have a tightness ratio of 0.25, however, their number of items and number of resources is changing. Also, they are encoded as “cbX-Y” in the result table, which means “Chu-Beasley, dataset X, problem Y”. All the necessary information is given in Table 2.

In this work, all 30 datasets are solved by BMGA. Then, the results are compared to the results obtained from [16]

3.2. Experimental Studies

For the experimental tests, first, some parameters of BMGA are set. These settings can be seen in Table 1.

Table 1 Parameter settings

Parameter	Value
number of generations	1000
Size of the population	100
Probability of crossover	1.0
Probability of mutation	0.03
Tournament size	4
number of genotypes	4
Population rate to form BN	0.1

Note that, each value in Table 1 is obtained by conducting a number of preliminary sensitivity tests[15].

For each test, with the same set of seeds, 30 independent runs were performed. For each run, best-of-generation (BOG) is saved and the overall performance is calculated as shown in Equation 6.

$$\bar{F}_{BOG} = \frac{1}{G} \sum_{i=1}^G \left(\frac{1}{N} \sum_{j=1}^N F_{BOG_{ij}} \right) \quad (6)$$

where G is the number of generations, N is the number of runs, $F_{BOG_{ij}}$ is the BOG of the j^{th} run's i^{th} generation. Last, \bar{F}_{BOG} is the overall offline performance.

4. Results

After setting the parameters in Table 1, the BMGA is tested for 30 different MKP datasets. For each

problem, 30 independent runs are executed. The results can be seen in Table 2. Also, the charts of the first problems of each group can be seen in Figure 2.

In the table, “Optimum” is the best-known optimum value so far provided in [22], “Best” is the best solution found during each test, and “Mean” is the average performance for the particular problem. In the “Prob. size” column, the size of the problem is given. For example, “5x100-0.25” means that the problem has 5 resources, 100 items, and a tightness ratio of 0.25.

Results show that BMGA is capable to solve MKP, is competitive, and obtains better solutions in terms of #Mean and #Best for most of the problem instances because of its Bayesian probability vector. More clearly, both in terms of #Best and #Mean, BMGA has got better results in 20 of 30 problems.

Although BMGA performs better than the other algorithms, for the test instances with 500 items, it performs slightly worse than the other test instances. That is because having more items means a bigger BN. And since BOA's BN is constructed with a 1-incoming edge rule, it is getting hard to exploit relations between the variables.

5. Conclusion

In this paper, the well-known optimization problem, the MKP, is solved by a recently proposed algorithm, the BMGA.

BMGA combines the powers of EDA and MS. By saying EDA, we mean BOA and by saying MS, we mean GA. While the MS part is responsible for the optimization process, the EDA part is responsible for exploiting relations between variables. Since it is a recently proposed algorithm, it has become mandatory to solve well-known optimization benchmark problems such as MKP.

For testing, BMGA is used to solve the most popular optimization dataset library's MKP instances. Then, the results are compared to the most recent paper. To get a fair comparison, the same number of fitness value calculations were done. The results showed that BMGA outperforms even the latest proposed algorithms.

This work tells us that exploiting the relations between the problem variables is important and useful while solving global optimization problems.

Table 2 Results for the test sets

Prob. size	Prob.	Optimum	Profit	BMGA	MS	SLMS	MMVO	BGSA	BHTPSO	BHTPSO-QI
5x100-0.25	cb1-1	24381	Best	24311	24253	24231	24192	24152	24169	24301
			Mean	24072	24004	24015	24050	23835	23822	23821
	cb1-2	24274	Best	24274	24258	24274	24274	23986	24109	23944
			Mean	24225	23934	24145	24274	23536	23657	23688
	cb1-3	23551	Best	23247	23538	23538	23538	23386	23435	23418
			Mean	23175	23272	23440	23520	23041	23072	23073
	cb1-4	23534	Best	23330	23256	23330	23288	23172	23253	23192
			Mean	23289	23024	23156	23120	22863	22928	22923
	cb1-5	23991	Best	23952	23845	23947	23947	23755	23815	23774
			Mean	23901	23567	23800	23900	23459	23473	23527
5x250-0.25	cb2-1	59312	Best	59203	58084	59107	58473	57565	57814	57800
			Mean	58980	57369	58736	58240	56554	56874	56685
	cb2-2	61472	Best	61227	60248	61280	60692	60057	59982	59767
			Mean	61185	59386	61041	60390	58613	58588	58680
	cb2-3	62130	Best	61831	61212	61787	61702	59936	60630	60524
			Mean	61684	59922	61476	61330	58975	59234	59186
	cb2-4	59463	Best	59167	58386	59101	58441	57970	57736	57884
			Mean	58777	57752	58787	58300	56744	56773	56584
	cb2-5	58951	Best	58753	57755	58485	58082	56959	57378	57550
			Mean	58566	56929	58097	58300	55961	56129	56361
5x500-0.25	cb3-1	120148	Best	119992	116296	119914	119978	111206	114493	114438
			Mean	119921	115444	119625	119900	108930	111017	111469
	cb3-2	117879	Best	116722	113732	117362	115634	108522	112821	112147
			Mean	115888	112257	116858	115400	106631	109276	109247
	cb3-3	121131	Best	117859	117666	120888	119156	111271	114774	116099
			Mean	117083	116367	120711	118900	109430	112035	112001
	cb3-4	120804	Best	120501	116454	120030	119124	111283	115828	114327
			Mean	119662	115396	119644	118900	109062	112200	111671
	cb3-5	122319	Best	119059	117900	121907	121141	112391	115889	117242
			Mean	118284	116767	121512	120800	110564	112253	113364
10x100-0.25	cb4-1	23064	Best	22917	22753	22835	22805	22836	22905	22876
			Mean	22694	22459	22604	22700	22334	22425	22449
	cb4-2	22801	Best	22836	22611	22650	22630	22441	22573	22408
			Mean	22541	22255	22432	22480	21991	22047	22017
	cb4-3	22131	Best	22012	21886	21962	22131	21849	21797	21949
			Mean	21662	21466	21632	21720	21313	21342	21461
	cb4-4	22772	Best	22420	22319	22463	22347	22325	22418	22376
			Mean	22391	21992	22233	22160	21961	22037	22029
	cb4-5	22751	Best	22312	22440	22619	22417	22168	22215	22254
			Mean	22182	22132	22279	22290	21840	21822	21903
10x250-0.25	cb5-1	59187	Best	58820	57757	58725	58476	56928	57530	57036
			Mean	58812	56708	58148	58310	55759	55854	55960
	cb5-2	58781	Best	58339	57363	58321	57937	56337	56568	56490
			Mean	58267	56793	58074	57790	55455	55443	55708
	cb5-3	58097	Best	57804	56690	57764	57062	55573	56426	55982
			Mean	57626	56024	57372	56960	54638	54793	54727
	cb5-4	61000	Best	60597	59930	60597	60326	58595	59030	59077
			Mean	60460	58934	60194	60030	57766	58057	57721
	cb5-5	58092	Best	57567	56863	57233	56276	56186	56217	56204
			Mean	57559	56066	56961	56060	54850	54941	54872
10x500-0.25	cb6-1	117821	Best	117371	113362	117287	–	108487	110996	111669
			Mean	116882	112541	116830	–	105760	107698	108367
	cb6-2	119249	Best	118730	115022	118737	–	109569	114262	113001
			Mean	118250	114250	118385	–	106775	108648	109197
	cb6-3	119215	Best	118905	115419	118488	–	109705	113987	112419
			Mean	118402	114372	118003	–	106853	108576	109004
	cb6-4	118829	Best	117354	115038	118116	–	108628	112476	112198
			Mean	116593	113444	117714	–	105679	107692	107796
	cb6-5	116530	Best	115334	112971	116530	–	106972	109567	109287
			Mean	114447	111707	115301	–	104509	106217	106212

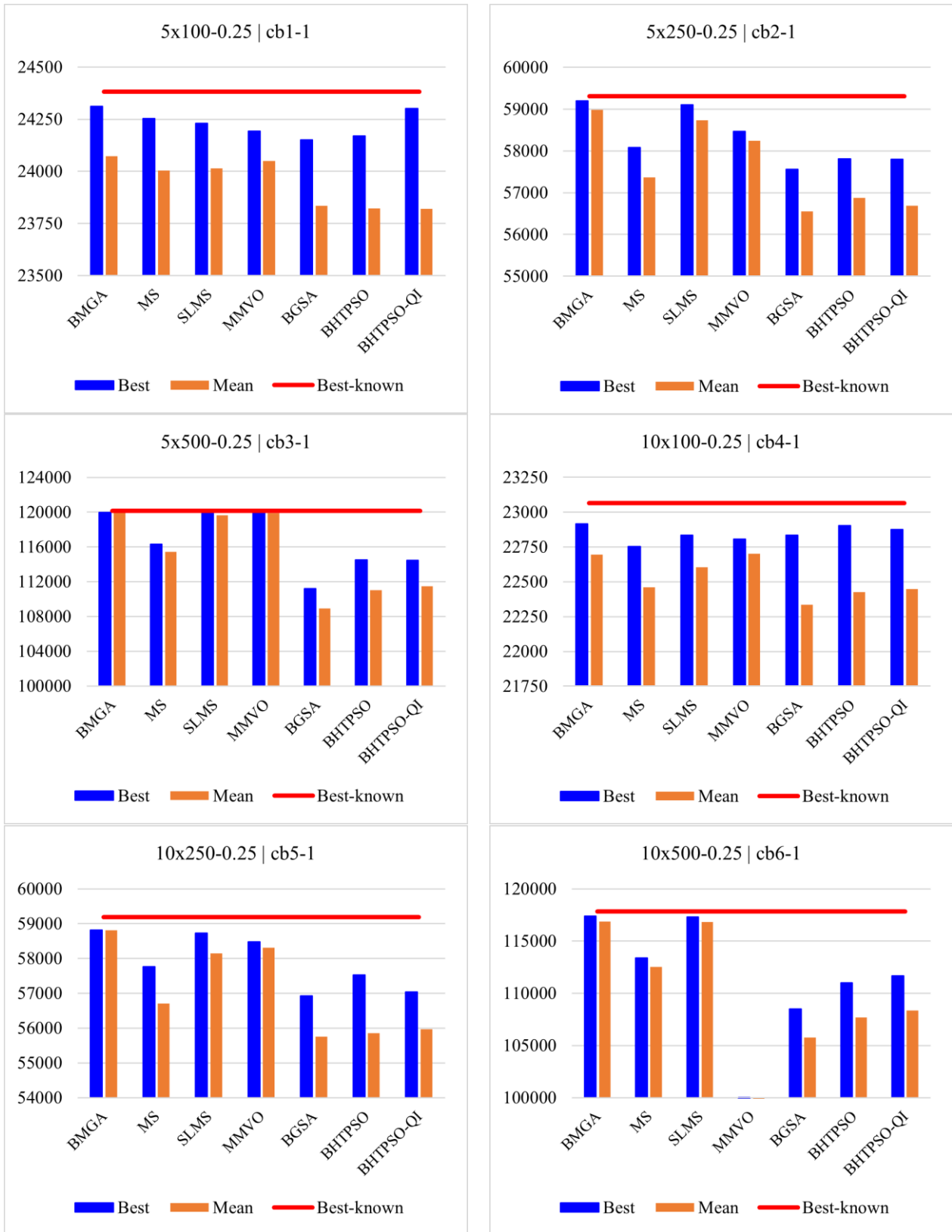


Figure 2 Results for the first dataset of each group of problem size

References

- [1] P. C. Gilmore and R. E. Gomory, "The Theory and Computation of Knapsack Functions", *Operations Research*, c. 14, sy 6, ss. 1045-1074, Ara. 1966, doi: 10.1287/opre.14.6.1045.
- [2] Y. Li, Y. Tao, and F. Wang, "A compromised large-scale neighborhood search heuristic for capacitated air cargo loading planning", *European Journal of Operational Research*, c. 199, sy 2, ss. 553-560, Ara. 2009, doi: 10.1016/j.ejor.2008.11.033.
- [3] G. B., "Allocation of Databases and Processors in a Distributed Computing System", *Management of Distributed Data Processing*, ss. 215-231, 1982.
- [4] M. Engwall and A. Jerbrant, "The resource allocation syndrome: the prime challenge of multi-project management?", *International Journal of Project Management*, c. 21, sy 6, ss. 403-409, Ağu. 2003, doi: 10.1016/S0263-7863(02)00113-8.
- [5] M. Abdel-Basset, R. Mohamed, K. M. Sallam, R. K. Chakraborty, and M. J. Ryan, "BSMA: A novel metaheuristic algorithm for multi-dimensional knapsack problems: Method and comprehensive analysis", *Computers & Industrial Engineering*, c. 159, s. 107469, Eyl. 2021, doi: 10.1016/j.cie.2021.107469.
- [6] V. Cacchiani, M. Iori, A. Locatelli, and S. Martello, "Knapsack problems — An overview of recent advances. Part II: Multiple, multidimensional, and quadratic knapsack problems", *Computers & Operations Research*, c. 143, s. 105693, Tem. 2022, doi: 10.1016/j.cor.2021.105693.
- [7] S. Gupta, R. Su, and S. Singh, "Diversified sine-cosine algorithm based on differential evolution for multidimensional knapsack problem", *Applied Soft Computing*, c. 130, s. 109682, Kas. 2022, doi: 10.1016/j.asoc.2022.109682.
- [8] A. Rezoug, M. Bader-el-den, and D. Boughaci, "Application of Supervised Machine Learning Methods on the Multidimensional Knapsack Problem", *Neural Process Lett*, c. 54, sy 2, ss. 871-890, Nis. 2022, doi: 10.1007/s11063-021-10662-z.
- [9] F. Wang, Y. Li, A. Zhou, and K. Tang, "An Estimation of Distribution Algorithm for Mixed-Variable Newsvendor Problems", *IEEE Transactions on Evolutionary Computation*, c. 24, sy 3, ss. 479-493, Haz. 2020, doi: 10.1109/TEVC.2019.2932624.
- [10] L. Ma, K. Hu, Y. Zhu, and H. Chen, "Cooperative artificial bee colony algorithm for multi-objective RFID network planning", *Journal of Network and Computer Applications*, c. 42, ss. 143-162, Haz. 2014, doi: 10.1016/j.jnca.2014.02.012.
- [11] B. Zhang, Q.-K. Pan, X.-L. Zhang, and P.-Y. Duan, "An effective hybrid harmony search-based algorithm for solving multidimensional knapsack problems", *Applied Soft Computing*, c. 29, ss. 288-297, Nis. 2015, doi: 10.1016/j.asoc.2015.01.022.
- [12] M. Dorigo and T. Stützle, "Ant Colony Optimization: Overview and Recent Advances", içinde *Handbook of Metaheuristics*, M. Gendreau and J.-Y. Potvin, Ed. Cham: Springer International Publishing, 2019, ss. 311-351. doi: 10.1007/978-3-319-91086-4_10.
- [13] S. Mirjalili and A. Lewis, "The Whale Optimization Algorithm", *Advances in Engineering Software*, c. 95, ss. 51-67, May. 2016, doi: 10.1016/j.advengsoft.2016.01.008.
- [14] Y. Zhou, L. Li, and M. Ma, "A Complex-valued Encoding Bat Algorithm for Solving 0-1 Knapsack Problem", *Neural Process Lett*, c. 44, sy 2, ss. 407-430, Eki. 2016, doi: 10.1007/s11063-015-9465-y.
- [15] E. Gazioğlu and A. S. Etaner-Uyar, "Experimental analysis of a statistical multiploid genetic algorithm for dynamic environments", *Engineering Science and Technology, an International Journal*, c. 35, s. 101173, Kas. 2022, doi: 10.1016/j.jestch.2022.101173.
- [16] Y. Feng and G.-G. Wang, "A binary moth search algorithm based on self-learning for multidimensional knapsack problems", *Future Generation Computer Systems*, c. 126, ss. 48-64, Oca. 2022, doi: 10.1016/j.future.2021.07.033.
- [17] G.-G. Wang, "Moth search algorithm: a bio-inspired metaheuristic algorithm for global optimization problems", *Memetic Comp.*, c. 10, sy 2, ss. 151-164, Haz. 2018, doi: 10.1007/s12293-016-0212-3.
- [18] M. Abdel-Basset, D. El-Shahat, H. Faris, and S. Mirjalili, "A binary multi-verse optimizer for 0-1 multidimensional knapsack problems with application in interactive multimedia systems", *Computers & Industrial Engineering*, c. 132, ss. 187-206, Haz. 2019, doi: 10.1016/j.cie.2019.04.025.
- [19] Z. Beheshti, S. M. Shamsuddin, and S. Hasan, "Memetic binary particle swarm optimization for discrete optimization problems", *Information Sciences*, c. 299, ss. 58-84, Nis. 2015, doi: 10.1016/j.ins.2014.12.016.
- [20] R. Poli, J. Kennedy, and T. Blackwell, "Particle swarm optimization", *Swarm Intell*, c. 1, sy 1, ss. 33-57, Haz. 2007, doi: 10.1007/s11721-007-0002-0.
- [21] M. Pelikan, "Bayesian Optimization Algorithm", içinde *Hierarchical Bayesian Optimization Algorithm: Toward a new Generation of Evolutionary Algorithms*, M. Pelikan, Ed. Berlin, Heidelberg: Springer, 2005, ss. 31-48. doi: 10.1007/978-3-540-32373-0_3.
- [22] J. E. Beasley, "OR-LIB <http://people.brunel.ac.uk/~mastjjb/jeb/orlib/files/>", 2005.



Journal of Soft Computing and Artificial Intelligence

Journal homepage: <https://dergipark.org.tr/en/pub/jscai>

International
Open Access 

Volume 03
Issue 02

December, 2022

Research Article

Real-time Iris Center Detection Based on Convolutional Neural Networks

Kenan DONUK¹ , Davut HANBAY² 

¹ Cizre Vocational School, Computer Programming Department, Sirnak University, 73200, Sirnak, Türkiye

² Department of Computer Engineering, Inonu University, 44280, Malatya, Türkiye

ARTICLE INFO

Article history:

Received December 8, 2022

Revised December 15, 2022

Accepted December 21, 2022

Keywords:

GI4E

CNN

Pupil center detection

Iris center detection

ABSTRACT

It is an active field of study in studies where the iris center is referenced, such as iris center detection, gaze tracking, driver fatigue detection. In this study, an approach for real-time detection of iris centers based on convolutional neural networks is presented. The GI4E dataset was used as the dataset for the proposed approach. Experimental results estimated the test data of the proposed convolutional neural network model with an accuracy of 97.2% based on the 0.025 error corresponding to the closest position to the iris center according to the maximum normalized error criteria. The study was also tested in real time with a webcam built into the computer. While the test accuracy is satisfactory, real-time speed performance needs to be improved.

1. Introduction

The eyes, one of the complex organs of the human body, are an organ located in the eye socket, providing vision with its spherical structure. The visible part of the eye consists of three parts, the sclera, iris, and pupil. The sclera forms the white area of the eye. The iris acts as a diaphragm, which forms the middle layer of the eye, whose color varies from person to person, and which determines the size of the pupil in the middle. The muscle fibers, which are positioned in a circle around the iris, cause the pupil to contract when they contract, adjusting the amount of light entering the eye according to the changing environmental conditions. Vision occurs when light is refracted from the cornea and transmitted to the lens/pupil and from there to the retina (fovea).

Detection of the iris center or pupil is an important field of study in many different sectors such as gaze tracking [1], [2], driver fatigue [3], medical research [4]. To be able to detect the iris center, first of all,

face and eye detection should be done on the images. For face and eye detection, there are ready-made algorithms such as DLIB [5], [6], MTCNN [7], OpenCv [8] in the literature. Some studies in the literature for pupil/iris center detection after eye detection are as follows.

Yu et al. proposed a robust iris center detection method for eye gaze tracking in their study. The method they propose is based on the geometric relationship between the iris center and the eye corners. It also presents an algorithm that predicts iris edge points to overcome the occlusions in the iris region because of eye movements [1]. Donuk and Hanbay in their study, they proposed a pupil center detection method based on U-Net architecture. They trained the proposed Mini-Unet architecture with the GI4E dataset. The test performance of the architecture detected a position close to the center of the pupil with an accuracy of 98.40% based on an

¹Corresponding author

e-mail: kenandonuk@sirnak.edu.tr

DOI: 10.55195/jscai.1216384

error value of 0.025 [9]. Lee et al. presented a fast-acting method of pupil center detection in robust and real-time applications. They used non-local block and self-attention block mechanisms in their proposed method. Non-local block mechanisms have been applied to reduce the delay in face detection, and self-attention block mechanisms have been applied to provide good image quality for glasses removal in images with glasses. The test success of the method on the GI4E dataset is 99.84% [10].

2. Material and Method

2.1. Dataset: GI4E

GI4E is a publicly available dataset of 103 user images taken via webcam for Iris center detection. These images were obtained from 12 different images with a resolution of 800x600 pixels for each user and looking at different points on the screen. Alongside the users' images in the dataset, there is a

manually labeled guide containing the coordinates of the iris centers and eye corners of the eyes in the images in pixels [11].

2.2. Dataset preprocessing

All images of the GI4E dataset have been converted to gray format and normalized for ease of data manipulation and Convolutional Neural Network (CNN) training. The eyes in the images were separated from the rest of the image by using the eye corner coordinates in the data set. The new iris center coordinates (x, y) of the separated eye images were recalculated using the eye corner coordinates. A total of 2472 eye images, 2 of each image, and the new iris center coordinates of the eye images are divided into 80% training and 20% test data for the training of the CNN network. In Figure 1, the process on the image in the data set is visualized.

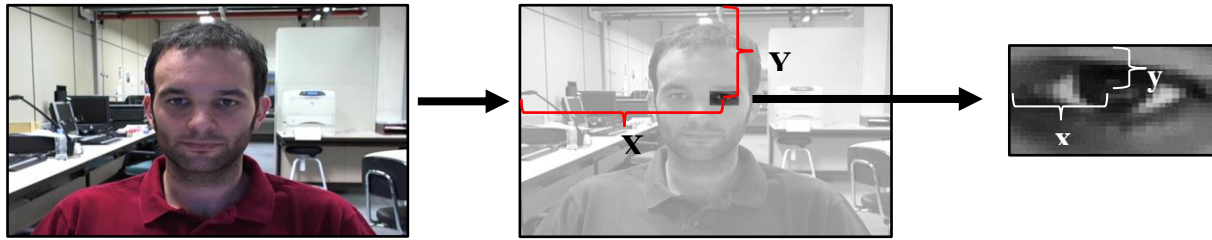


Figure 1 Dataset preprocessing

2.3. Proposed Method and Training

With data preprocessing, 2472 right and left eye images obtained from the GI4E data set were converted to 32x32 spatial dimensions in accordance with the input of the CNN model. In the CNN model, firstly, three convolutions (3x3) filters were applied to the input data, respectively. After the second and third convolution layers, the size is reduced by applying maxpooling. Then, the obtained features are flattened and transmitted to the full connected layer of the CNN model. The full connected layer consists of 128, 64 neurons and classification layers, respectively. It has been tried to increase the generalization ability of the network by applying 2 dropouts (0.4) in these layers, respectively. “BatchNormalization” and “ReLU” were applied as normalization and activation functions in all layers, respectively. Finally, as the learning optimization of

the network, the “Adam” optimization algorithm and for loss detection the euclidean_distance function, which expresses the distance between the real iris center coordinates and the iris center coordinate values estimated by the CNN network, are used. In this function, p and q represent the actual and estimated iris center coordinates, respectively. The distance between p and q is given by Equation 1.

$$d(p, q) = \sqrt{\sum_{i=1}^n (q_i - p_i)^2} \quad (1)$$

The proposed network reached the minimum error value in 400 iterations. The proposed CNN structure is shown in Figure 2. The accuracy and loss graphs of the proposed network are shown in Figures 3 and 4, respectively. When the loss and accuracy graphs are examined, we can see that the network is learning properly.

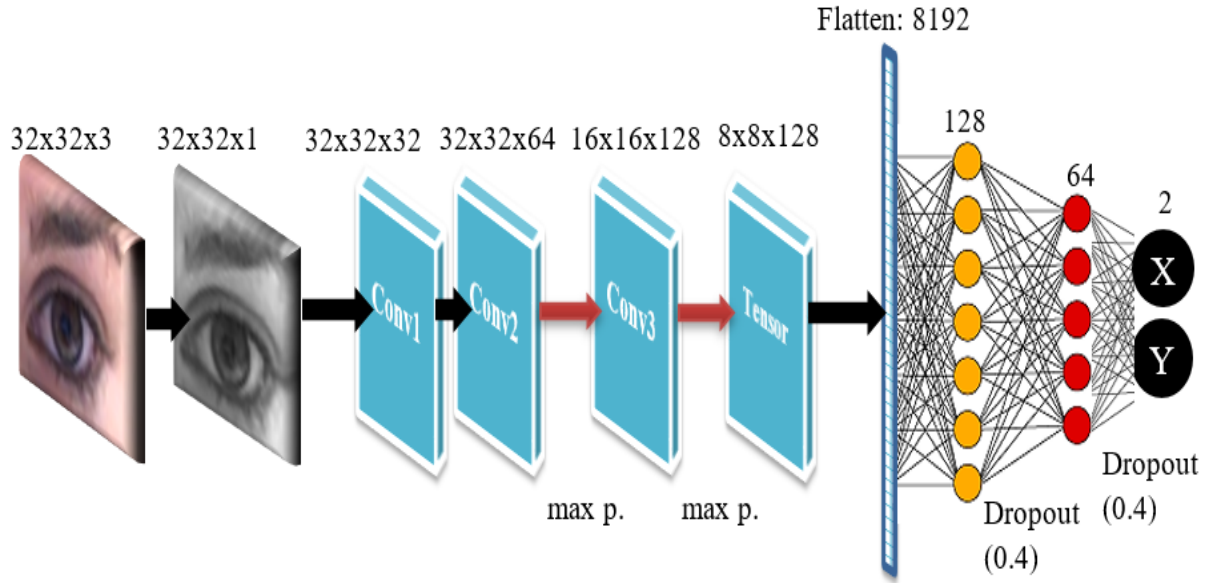


Figure 2 Proposed CNN structure

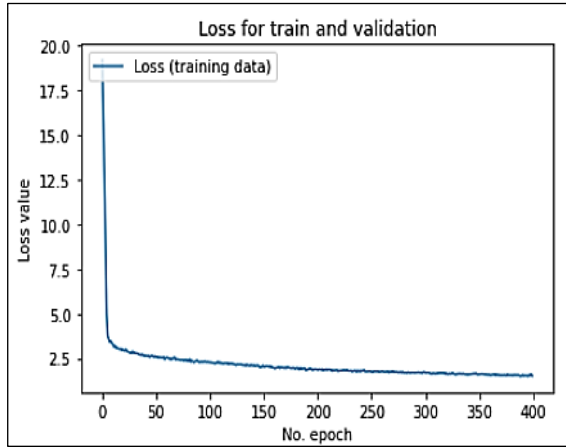


Figure 3 Loss graph

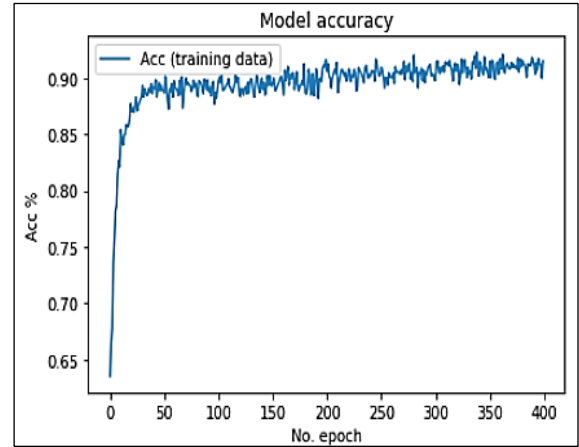


Figure 4 Accuracy graph

3. Experimental Results

To evaluate the performance of the trained network with the right and left eye images obtained from the data set and the coordinate labels corresponding to these images, an estimation was made with the 20% test data of the data set that was not used in the training. For the analysis of the estimation performance of the network, the maximum normalized error value criterion, which is widely used to measure the pupil center estimation performance, is used [12]. The formula for this error criterion is given in Equation 2.

$$d_{eye(error)} = \frac{\max(d_l, d_r)}{\|C_l - C_r\|} \quad (2)$$

Given in the equation, d_l is the distance between the true iris center of the left eye and the iris center predicted by the CNN model, and d_r is the distance between the true iris center of the right eye and the iris center predicted by the CNN model. Error detection is obtained by the ratio $\|C_l - C_r\|$ of the value greater than these two values to the actual distance between the iris centers of the right and left eyes. If the obtained $d_{eye(error)}$ value is less than 0.025 error value, the estimated iris center coordinate represents the closest value to the real iris center coordinate. If the error value is less than 0.05, the estimated iris center coordinate obtained represents a coordinate approximately within the actual

boundaries of the pupil [9], [13]. In Figure 5, the detected iris center detected manually in the data set

and the estimated iris center are marked on the eye image in white and red, respectively.

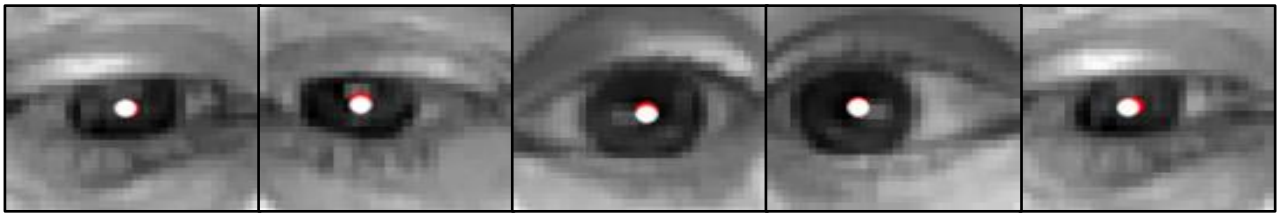


Figure 5 Actual and predicted iris center positions

The prediction results of the proposed CNN model on 500 test data obtained an accuracy of 97.2% according to 0.025 error and 99.8% according to 0.05 error from the maximum normalized error criterion. The proposed system has also been tested in real time with a webcam. In Figure 6, images of the real-time iris center detection application are given. For real-time application, first the face and then the eyes are detected from the webcam via OpenCv. After gray formatting and normalization, the dimensions of the eye regions are converted to 32x32 spatial

dimensions. The coordinates of the iris center are determined by giving the obtained instant eye images as input to the trained CNN model. However, these coordinates do not reflect the actual coordinate values because the spatial dimensions of the real eye image have been changed for CNN. Therefore, new iris center coordinate values are obtained by applying the inverse of the size change for the CNN input of the eye images to the detected coordinate values. The actual coordinate values obtained are marked on the face.



Figure 6 Real-time iris center detection

4. Conclusion

The proposed model revealed an accuracy of 97.2% for the GI4E dataset. Although the model gives good results in forward-facing eye positions, iris center detection results in higher errors in different face and eye poses (right, left, down and up). For more robust iris center detection, the generalization ability of the model can be increased by using datasets with different eye positions. Also, the proposed system is slow for real-time

applications. This is because the system first detects face and eye in real-time applications. The resulting eyes are then sent to the CNN model for iris center detection. This process causes the system to experience lag. Therefore, this delay can be overcome with face and eye detection algorithms that promise high speed in the literature and deep learning architectures that will reduce the cost for the CNN model.

References

- [1]. M. Yu *et al.*, “An easy iris center detection method for eye gaze tracking system,” *J Eye Mov Res*, vol. 8, no. 3, 2015, doi: 10.16910/JEMR.8.3.5.
- [2]. K. Donuk and D. Hanbay, “Video Based Real-Time Eye Tracking,” in *In: 28th IEEE Signal Processing and Communications Applications (SIU-2020)*, 2020, pp. 21–24.
- [3]. Q. Zhuang, Z. Kehua, J. Wang, and Q. Chen, “Driver fatigue detection method based on eye states with pupil and iris segmentation,” *IEEE Access*, vol. 8, pp. 173440–173449, 2020, doi: 10.1109/ACCESS.2020.3025818.
- [4]. H. Yan and Y. Zhang, “Detection of the pupil eigenvalues in medicine,” *Proceedings - 2010 International Conference on Computational and Information Sciences, ICCIS 2010*, pp. 989–992, 2010, doi: 10.1109/ICCIS.2010.244.
- [5]. “dlib C++ Library.” <http://dlib.net/> (accessed Dec. 08, 2022).
- [6]. V. Kazemi and J. Sullivan, “One millisecond face alignment with an ensemble of regression trees,” in *2014 IEEE Conference on Computer Vision and Pattern Recognition*, Jun. 2014, pp. 1867–1874. doi: 10.1109/CVPR.2014.241.
- [7]. K. Zhang, Z. Zhang, Z. Li, and Y. Qiao, “Joint Face Detection and Alignment Using Multitask Cascaded Convolutional Networks,” *IEEE Signal Process Lett*, vol. 23, no. 10, pp. 1499–1503, Oct. 2016, doi: 10.1109/LSP.2016.2603342.
- [8]. “Home - OpenCV.” <https://opencv.org/> (accessed Dec. 08, 2022).
- [9]. K. Donuk and D. Hanbay, “Pupil Center Localization Based on Mini U-Net,” *Computer Science*, pp. 185–191, Oct. 2022, doi: 10.53070/BBD.1173482.
- [10]. K. il Lee, J. H. Jeon, and B. C. Song, “Deep Learning-Based Pupil Center Detection for Fast and Accurate Eye Tracking System,” *Lecture Notes in Computer Science (including subseries Lecture Notes in Artificial Intelligence and Lecture Notes in Bioinformatics)*, vol. 12364 LNCS, pp. 36–52, 2020, doi: 10.1007/978-3-030-58529-7_3/COVER.
- [11]. A. Villanueva, V. Ponz, L. Sesma-Sanchez, M. Ariz, S. Porta, and R. Cabeza, “Hybrid method based on topography for robust detection of iris center and eye corners,” *ACM Transactions on Multimedia Computing, Communications, and Applications (TOMM)*, vol. 9, no. 4, Aug. 2013, doi: 10.1145/2501643.2501647.
- [12]. O. Jesorsky, K. J. Kirchberg, and R. W. Frischholz, “Robust Face Detection Using the Hausdorff Distance,” 2001, pp. 90–95. doi: 10.1007/3-540-45344-X_14.
- [13]. A. Larumbe-Bergera, G. Garde, S. Porta, R. Cabeza, and A. Villanueva, “Accurate Pupil Center Detection in Off-the-Shelf Eye Tracking Systems Using Convolutional Neural Networks,” *Sensors*, vol. 21, no. 20, p. 6847, Oct. 2021, doi: 10.3390/s21206847.



Journal of Soft Computing and Artificial Intelligence

Journal homepage: <https://dergipark.org.tr/en/pub/jscai>

International
Open Access

Volume 03
Issue 02

December, 2022

Research Article

Can Similarity Measures Techniques be Used to Model Face Recognition?

Enes Algül¹ 

¹Bingöl University, School of Engineering and Architecture, Department of Computer Science, Bingöl, Türkiye

ARTICLE INFO

Article history:

Received December 12, 2022

Revised December 14, 2022

Accepted December 16, 2022

Keywords:

Distance Methods

Classification

Eigenface

Facial Recognition

PCA

ABSTRACT

Facial recognition is used efficiently in human-computer interactions, passports, driver's licence, border controls, video surveillance and criminal identification, and is an important biometric's security option in many device-related security requirements. In this paper, we use Eigenface recognition based on the Principal Component Analysis (PCA) to develop the project. PCA aims to reduce the size of large image matrices and is used for feature extraction. Then, we use the euclidean distance method for classification. The dataset used in this project was obtained by AT&T Laboratories at Cambridge University [1]. The training dataset contains grayscale facial images of 40 people; each person has 10 different facial images taken from different angles and emotions.

This study aims to give researchers a hunch before they start to develop image recognition using deep learning methods. It also shows that face recognition can be done without deep learning.

1. Introduction

The combination of two Greek words, Bios (life) and Metron (measures) generate the term Biometrics [2]. Physical attributes and biometric features are unique to each person, and that separates each person apart from the others. These features include fingerprint [3], face, hand, iris [4], speech, smell, and gait. Biometric identity, in other words, the biometric signature cannot be easily stolen, forgotten and difficult to be copied by someone else. Therefore, it provides higher and more reliable security in identifying the person. Some biometric features, such as the iris [5], are stable over time and fingerprints never change from childhood to the end of life. In this work, face recognition has been researched in greater depth with a broader range of techniques.

This paper aims to investigate existing biometric security techniques and principles of facial recognition. The research question is: "Can similarity measurement techniques be used to model the face

authentication system?"

In this work, Face recognition was developed with Eigenface recognition based on PCA [6]. For this system, 400 images of 40 individuals have been trained. Then 40 known and 15 unknown facial images have been tested to check the accuracy. The project performance was measured by two standard rate methods: False Acceptance Rate (*FAR*) and False Rejection Rate (*FRR*).

The distance methods were researched for classification. Euclidean, Manhattan and Mahalanobis distance methods are the three methods examined in this study. The Euclidean distance method was chosen to measure the distances between facial images. Then, the threshold value was selected by multiplying the maximum value of the Euclidean Distance by 0.8. The threshold value was obtained as a result of many experiments. This multiplication process was inspired by Nasser Abouzakhar's work [7] and used in this project.

¹ Corresponding Author
e-mail: enes.algul12@gmail.com

2. Related Work

2.1. Principle Component Analysis (PCA)

PCA has been used in a variety of studies including computer science, meteorology, and neuroscience. PCA [8–10] was first used for facial recognition by Kirby and Sirovich in 1987. Later, Matthew A. Turk and Alex P. Pentland discovered a new facial recognition technique using Eigenface based on PCA in 1991 [11]. Their invention has been used for static and automatic real-time face recognition. This invention has helped to develop a face recognition system with fewer matrices multiplications. The purpose of using PCA is to reduce the size of large image sets (matrix). For example, suppose there are M grayscale images in a dataset for training, and the size of the images are $N \times N$. In order to build a matrix of images, $2D$ images need to be converted to $1D$. Therefore, each image is represented by $1D$ a column vector, and the size of this column is N^2 . There are M images, and if they are stored into one matrix, the size of this matrix will be $N^2 \times M$. Their covariance matrix needs to be calculated to find relationships between each column vector. Then, this covariance matrix will be used to extract eigenvectors and eigenvalues.

Let's represent the matrix of the dataset with A .

Covariance Matrix = $AA' = (N^2 \times M)(M \times N^2)$;

The size of the covariance matrix = $(N^2 \times N^2)$. This is too large to manage. For example, if the number of images is 400 and the size of each image is 256×256 , then the size of the covariance matrix = (65536×65536) . With the PCA technique, instead of Covariance = AA' , Covariance = $AA' = (M \times N^2)(N^2 \times M)$ is calculated. Consequently, the dimension of the Covariance matrix is = (400×400) and $(M \ll N^2)$. This size of the matrix is easier to manage.

2.2. Eigenface Technique

The eigenface technique [12,13] is a set of eigenvectors commonly used to recognize the human face [14]. The eigenvalues and eigenvectors are derived from the covariance matrix. The eigenface [15,16] can be obtained by multiplying the eigenvectors with the normalized matrix.

Eigenvectors can only be applied to square matrices. The covariance matrix in this work is square

(400×400) . The dominant eigenvectors in the covariance matrix correspond to the higher value and represent more characteristics and features. Eigenvectors were sorted by the eigenvalues. After the eigenvalues are sorted in descending order, the first eigenvectors have more characteristic features than the second one. The last eigenvector is showing the least characteristic features. Therefore, k number of eigenvectors were chosen heuristically to train the dataset. In this paper, 124 out of 400 eigenvectors were selected, and other eigenvectors were neglected. Then, the eigenfaces were calculated.

2.3. Threshold Value

Threshold [13] value is chosen heuristically. There is no specific method developed to find the threshold value. Commonly, it is chosen by multiplying 0.8 by the maximum values of minimum values of Euclidean distance.

In this article, the purpose of using threshold value is to decide whether the newly inputted image is a face image or not. If the distance between the inputted image and training images is less than the threshold value, the inputted images will have more facial features. Therefore, we can say that if it holds less than the threshold value it is identified as a face image. For this reason, choosing the threshold value affects the performance and result of the accuracy.

2.4. Distance Methods

To measure the distances between images for comparison purposes, three methods are commonly used. The equations of Euclidean, Manhattan, and Mahalanobis Distances are as follows:

Euclidean Distance:

$$d(X, Y) = \sqrt{\sum_{i=1}^M (X_i - Y_i)^2} = ||X - Y|| \quad (1)$$

Manhattan Distance:

$$d(X, Y) = \sum_{i=1}^M |X_i - Y_i| \quad (2)$$

Mahalanobis Distance:

$$d(X, Y) = \sqrt{(X_i - Y_i)^T C^{-1} (X_i - Y_i)} \quad (3)$$

where C refers to the covariance matrix.

3. Dataset

The dataset contains 40 individual persons' images,

and each person has 10 images, each one taken from different angles and emotions. The dataset was prepared by Cambridge University at AT&T laboratories. Each image has two dimensions and is a

grayscale image as seen in Figure 1. All images are in the same sizes. Each image has a width of 112 pixels and a height of 92 pixels



Figure 1 The first image of each person in the dataset.

4. Algorithm

Part 1:

Step 1: Prepare a data set for training (40 persons' 10 individual images, a total of 400 images).

Step 2: Resize whole images at the same size and convert them to grayscale images (2D).

Step 3: Convert each image in the dataset from 2D matrix (112 x 92) to 1D column vector (10304 x 1). Then build a new matrix (10304 x 400) where each column represents an images of the dataset. Here, I refers to 2D grayscale original images, Γ denotes 1D images.

$$\Gamma = (\Gamma_1, \Gamma_2, \Gamma_3, \dots, \Gamma_M)$$

where $M = 400$.

Step 4: Compute the average column Ψ .

$$\Psi = \frac{1}{M} \sum_{i=1}^M \Gamma_i \quad (4)$$

Step 5: Normalise the data set. Subtract the average column vector from each column of the dataset's matrix.

$$\Phi = \Gamma_i - \Psi \quad (5)$$

$$A = (\Phi_1, \Phi_2, \Phi_3, \dots, \Phi_M) \quad (6)$$

Here, Φ denotes adjusted columns, and $A(10304 \times 400)$ denotes the normalised matrix.

Step 6: Calculate the covariance (C) matrix. Use $C = A^t A$ instead of $C = A A^t$ to reduce the dimensional of the matrix (use PCA).

Step 7: Calculate eigenvalues (V) and eigenvectors (D).

$$[V \ D] = eig(C) \quad (7)$$

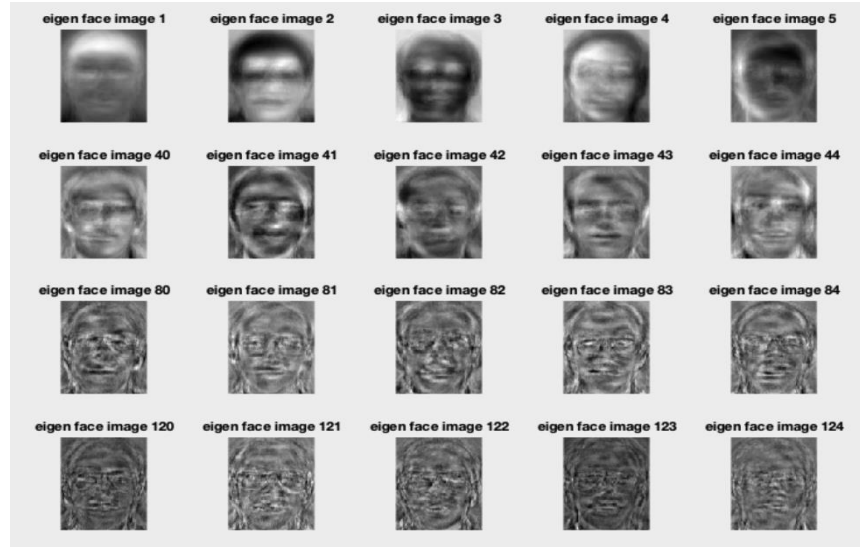


Figure 2 The Eigenfaces look like ghost image

Step 8: Sort the eigenvalues (D) in descending order, then find the corresponding eigenvectors (V). Calculate the eigenfaces (U) by multiplying the normalised images (A) and eigenvectors (V). Heuristically choose the most (more relevant) k (124) eigenfaces (U).

$$U = AV \quad (8)$$

Step 9: Multiply transpose of the $k(124)$ Eigenfaces and normalised images (A) to compute weights W

$$W = U^t A \quad (9)$$

Part 2:

Step 1: Input a new image.

Step 2: Convert inputted image to a grayscale image.

Step 3: Resize the inputted image.

Step 4: Convert 2D image to 1D column vector.

Step 5: Subtract the average column from the inputted column vector.

Step 6: Calculate the weights.

Step 7: Classify the images using Euclidean distance methods.

Step 8: Decide the threshold value by multiplying the max distance by 0.8.

Step 9: Compute the distance between inputted image and trained images for classification.

Step 9: Multiply transpose of the $k(124)$ Eigenfaces and normalised images (A) to compute weights W

$$W = U^t A \quad (9)$$

5. Experiments and Evaluations

The recognition performance was analyzed using two standard rate methods. These methods are False Acceptance Rate (FAR) and False Rejection Rate (FRR).

The distance between inputted image and the trained image in the dataset is calculated by the Euclidean Distance method. Then the calculated distances were compared by the Threshold value. If the distance is greater than the threshold, it is rejected, otherwise accepted. Then it matches with the image where the distance between them is minimum.

The distances between false images and trained images were calculated. The percentage of distances lesser than the threshold value represents the FAR . On the other hand, the distances of known images and trained images were calculated. The percentage of distances greater than the threshold value represents the FRR . 15 unknown faces were tested. 6 out of them did not match with any face image in the dataset. 9 images have been accepted even if they should not have had. So, the percentage of FAR is

%60. On the other hand, 40 known images have been tested. 1 out of them rejected though it should have been. That is, the percentage of *FRR* is %2.5. The threshold value is the same. This accuracy is not sufficient to use in real-time systems. Because even if the threshold value was very high the accuracy of unknown images tested was too low.

The *FRR* and *FAR* percentages are inversely proportional. The threshold value is affect their percentage. If the value of the threshold increased,

the *FAR* is decreased while *FRR* increased as shown in Table 1.

The experimental results on the Cambridge University, AT&T dataset using the eigenface-based on PCA for facial recognition represent that the classification accuracy on known images is %97.5. The dataset is small compared to other datasets used in deep learning applications. Despite this, very high result has been obtained.



Figure 3: The table of *FAR*, *FRR* and threshold value (the numbers in the brackets represent the number of tested images)

Table 1. The table of *FAR*, *FRR* and threshold value (the numbers in the brackets represent the number of tested image)

Threshold	% <i>FAR</i>	% <i>FRR</i>	<i>FAR</i> (15)	<i>FRR</i> (40)
0.2	0	77.5	0	31
0.4	20	27.5	3	11
0.6	40	15	6	6
0.8	60	2.5	9	1

In the use of deep learning methods, we can use mini-batches to train large datasets. Otherwise, it requires high memory, powerful CPU and GPU to train large image datasets. In the use of the Eigenface method, all data is combined into a single matrix. This method will produce an extremely large matrix for large datasets. Working on a large matrix is very risky because it requires a lot of memory to train. The Eigenface method is computationally very expensive.

6. Conclusion

In this work, we have developed a project to classify a facial image dataset. We have used the

eigenface method based on Principal Component Analysis (PCA) to recognise facial images. The dataset was obtained from AT & T laboratories at the University of Cambridge. PCA was used to reduce the dimension of the covariance matrix from the (10304 x 10304) to the (400 x 400). Then, 400 eigenvectors were derived from the covariance matrix used to find eigenfaces. The largest 124 out of 400 eigenfaces were used to recognise faces. The Euclidean Distance method was used to classify and find distances between tested images and trained images. In this work, 40 known and 15 unknown images were tested to obtain results.

References

- [1]. "The database of faces, [accessed 7 dec. 2022]." [Online]. Available: <https://cam.orl.co.uk/facedatabase.html>
- [2]. C. E. Bugge, J. Burkhardt, K. S. Dugstad, T. B. Enger, M. Kasprzycka, A. Kleinauskas, M. Myhre, K. Scheffler, S. Ström, and S. Vetlesen, "Biometric methods of animal identification," Course notes, Laboratory Animal Science at the Norwegian School of Veterinary Science, pp. 1–6, 2011.
- [3]. S. Prabhakar, A. K. Jain, and S. Pankanti, "Learning fingerprint minutiae location and type," *Pattern Recognition*, vol. 36, no. 8, pp. 1847–1857, 2003.
- [4]. H. Mehrotra, M. Vatsa, R. Singh, and B. M, "Does iris change over time?" *PloS one*, vol. 8, no. 11, p. e78333, 2013.
- [5]. H. Mehrotra, M. Vatsa, R. Singh, and B. Majhi, "Does iris change over time?" *PloS one*, vol. 8, no. 11, p. e78333, 2013.
- [6]. K. S. P. Reddy and D. K. N. Raju, "Design and implementation of an algorithm for face recognition by using principal component analysis (pca) in matlab," *International Journal of Advanced Research in Computer Science and Software Engineering*, vol. 6, no. 10, pp. 115–119, 2016.
- [7]. N. Abouzakhar and P. Enjamuri, "An enhanced eigenfaces-based biometric forensic model," in *Procs 4th International Conference on Cybercrime Forensics Education & Training*, 2010.
- [8]. S. Satonkar Suhas, B. Kurhe Ajay, and B. Prakash Khanale, "Face recognition using principal component analysis and linear discriminant analysis on holistic approach in facial images database," *Int Organ Sci Res*, vol. 2, no. 12, pp. 15–23, 2012.
- [9]. M. Karnan, "Face recognition using multiple eigenface subspaces," *Journal of Engineering and Technology Research*, vol. 2, no. 8, pp. 139–143, 2010.
- [10]. A. Kaur and T. Sarabjit Singh, "Face recognition using pca (principal component analysis) and lda (linear discriminant analysis) techniques," *International Journal of Advanced Research in Computer and Communication Engineering*, vol. 4, no. 3, pp. 308–310, 2015.
- [11]. M. Turk and A. Pentland, "Eigenfaces for recognition," *Journal of cognitive neuroscience*, vol. 3, no. 1, pp. 71–86, 1991.
- [12]. M. M. Ahsan, Y. Li, J. Zhang, M. T. Ahad, and K. D. Gupta, "Evaluating the performance of eigenface, fisherface, and local binary pattern histogram-based facial recognition methods under various weather conditions," *Technologies*, vol. 9, no. 2, p. 31, 2021.
- [13]. S. Gupta, O. Sahoo, A. Goel, and R. Gupta, "A new optimized approach to face recognition using eigenfaces," *Global Journal of Computer Science and Technology*, 2010.
- [14]. A. Ghosh, P. K. Kundu, and G. Sarkar, "Similarity detection of illuminance images using eigenface method," *Journal of The Institution of Engineers (India): Series B*, pp. 1–5, 2022.
- [15]. M. Slavković and D. Jevtić, "Face recognition using eigenface approach," *Serbian Journal of electrical engineering*, vol. 9, no. 1, pp. 121–130, 2012.
- [16]. M. Imran, M. Miah, H. Rahman, A. Bhowmik, and D. Karmaker, "Face recognition using eigenfaces," *International Journal of Computer Applications*, vol. 118, no. 5, 2015.



Journal of Soft Computing and Artificial Intelligence

Journal homepage: <https://dergipark.org.tr/en/pub/jscai>

International
Open Access

Volume 03
Issue 02

December, 2022

Research Article

Generalized λ –Statistical Boundedness of Order β in Sequences of Fuzzy Numbers

Mithat Kasap¹ , Hıfı Altınok² 

¹Department of Accounting, Sirnak University, 73000, Sirnak, Türkiye

²Department of Mathematics, Firat University 23119, Elazığ, Türkiye

ARTICLE INFO

Article history:

Received December 14, 2022

Revised December 20, 2022

Accepted December 23, 2022

Keywords:

Fuzzy number

Statistical boundedness

Statistical convergence

ABSTRACT

In this article, we investigate the idea of Δ_λ^m –statistical boundedness of order β for sequences of fuzzy numbers. Additionally, we provide different inclusion relations between Δ_λ^m –statistical boundedness of order β and Δ_λ^m –statistical convergence of order β .

1. Introduction

In the traditional approach to analysis of convergence, almost all of the terms of a sequence are required to belong to an arbitrarily small neighborhood of the limit. Fast [12] and Steinhaus [23] first proposed the idea of statistical convergence and later Schoenberg [21] gave a formal definition of that concept, independently. The essential tenet of statistical convergence is to loosen the restrictions of this condition and to insist that the convergence requirement be valid only for the vast majority of the elements. Later on, this concept and summability theory was associated by several mathematicians ([1],[5],[6],[9],[10],[13],[14],[18],[19],[22]). Recent years Gadjiev and Orhan [15] broaden the concept of statistical convergence into the ordered statistical convergence. Following this, Çolak [7] and Çolak and Bektaş [8] conducted research on the concept of statistical convergence. These investigations show that the principles of statistical convergence give a significant addition to the enhancement of classical analysis. In the foundational work that was authored

by Zadeh [24] the idea of fuzziness was first discovered and presented to the scientific world. In 1986, Matloka [17] provided the notion of fuzzy number sequence, and then in 1995, Nuray and Savaş [20] established the statistical convergence of these sequences.

The statistical boundedness in sequences of fuzzy numbers, was first described by Aytar and Pehlivan [4]. Altınok and Mursaleen [3] then used a difference operator to generalize the statistical boundedness. In their research, Altınok and Et [2] looked into the notion of “ λ –statistical boundedness of order β ” in relation to sequences of fuzzy numbers. In addition to this, they investigated the monotonicity, symmetricity and solidity of the sequence class $S_\lambda^\beta B(F)$.

Let $\lambda = (\lambda_n)$ be a non-decreasing sequence of positive real numbers that tends toward infinity such that $\lambda_1 = 1$, $\lambda_{n+1} \leq \lambda_n + 1$. We denote the set of all sequences (λ_n) defined in this way by Λ . We define λ_β –density of a subset E of \mathbb{N} by

¹ Corresponding author

e-mail: [added mithat@hotmail.com](mailto: added mithat@hotmail.com)

DOI: 10.55195/jscai.1218844

$$\delta_{\lambda}^{\beta}(\mathbb{E}) = \lim_n \frac{1}{\lambda_n^{\beta}} |\{k \in I_n : k \in \mathbb{E}\}| \text{ provided the limit exists,}$$

where $\beta \in (0,1]$ be any real number. Clearly, the λ_{β} –density of any finite subset of \mathbb{N} is 0 and the equality $\delta_{\lambda}^{\beta}(A^c) = 1 - \delta_{\lambda}^{\beta}(A)$ does not generally hold for values $\beta \in (0,1)$. The property $\delta_{\lambda}^{\beta}(A^c) = 1 - \delta_{\lambda}^{\beta}(A)$ holds only for $\lambda_n = n$ for all $n \in \mathbb{N}$ and for $\beta = 1$. In the case of $\lambda_n = n$ for all $n \in \mathbb{N}$, λ_{β} –density becomes equivalent to the β –density, in the case $\beta = 1$ reduces to the λ –density, in the special case $\beta = 1$ and $\lambda_n = n$ becomes equivalent to the natural density.

We say that x_k fulfills property $p(k)$ for λ –almost all k according to β and this is abbreviated as “*a. a. $k_{\lambda}(\beta)$* ” if $x = (x_k)$ is a sequence satisfying property $p(k)$ for every k other than a set of λ_{β} –density zero.

A fuzzy set consists of elements with degrees of membership. The idea of membership function is the most significant aspect of characterizing and defining a fuzzy set, and it is essential to the field of fuzzy sets. If a fuzzy set u on the set of real number \mathbb{R} possesses the criteria listed below, then we refer to that set as a fuzzy number:

- i) u is normal,
- ii) u is fuzzy convex,
- iii) u is upper semi-continuous,
- iv) $\text{supp } u = \text{cl}\{x \in \mathbb{R} : u(x) > 0\}$ is compact.

In this sense, a fuzzy number is a specific case of a normal, convex fuzzy set of the real numbers line and is an extension of real number. For a fuzzy number u , α –level set $[u]^{\alpha}$ is described by

$$[u]^{\alpha} = \begin{cases} \{x \in \mathbb{R} : u(x) \geq \alpha\}, & \text{if } \alpha \in [0,1] \\ \text{supp } u, & \text{if } \alpha = 0 \end{cases}$$

When $[u]^{\alpha}$ is a closed interval for each $\alpha \in [0,1]$ and $[u]^1 \neq \emptyset$, it is obvious that u is a fuzzy number.

Kizmaz [16] defined the difference spaces $\ell_{\infty}(\Delta)$, $c(\Delta)$ and $c_0(\Delta)$, which consist of any real-valued sequences $x = (x_k)$ such that $\Delta x = \Delta^1 x = (x_k - x_{k+1})$ in the sequence spaces ℓ_{∞} , c and c_0 . Et and Çolak [11] expanded the concept of difference sequences by making the difference m times such that $\Delta^m x_k = \Delta^{m-1} x_k - \Delta^{m-1} x_{k+1}$ for $(m = 1, 2, 3, \dots)$.

Within the scope of this investigation, we broaden the application of the concept of “ λ – statistical boundedness of order β ” to sequences of fuzzy numbers and present various inclusion relations by

making use of the generalized difference operator Δ^m . Moreover, in order to contribute to the field of the fuzzy numbers theory, we present certain relation theorems as a means of filling in the gaps that currently exist.

2. Main Results

In this part, we define and investigate the idea of Δ_{λ}^m –statistical boundedness of order β for fuzzy sequences, where β denotes any real integer such that $\beta \in (0,1]$.

Definition 1. Let $\lambda = (\lambda_n) \in \Lambda$, $\beta \in (0,1]$ and $X = (X_k)$ be a fuzzy sequence. A sequence $X = (X_k)$ is said to be a Δ_{λ}^m –statistically Cauchy sequence of order β if there exists a natural number $N(= N(\varepsilon))$ for every $\varepsilon > 0$ such that $d(X_k, X_N) < \varepsilon$ for *a. a. $k_{\lambda}(\beta)$* . i.e.

$$\lim_{n \rightarrow \infty} \frac{1}{\lambda_n^{\beta}} |\{k \in I_n : d(\Delta^m X_k, X_N) \geq \varepsilon\}| = 0.$$

Definition 2. Let $\lambda = (\lambda_n) \in \Lambda$, $\beta \in (0,1]$ and $X = (X_k)$ be a fuzzy sequence. It is said that a fuzzy sequence (X_k) is Δ_{λ}^m –statistically bounded above of order β if there is some value u satisfying

$$\lim_{n \rightarrow \infty} \frac{1}{\lambda_n^{\beta}} |\{k \in I_n : \Delta^m X_k > u\} \cup \{k \in I_n : \Delta^m X_k \sim u\}| = 0.$$

Similarly, if we can find a fuzzy number u satisfying

$$\lim_{n \rightarrow \infty} \frac{1}{\lambda_n^{\beta}} |\{k \in I_n : \Delta^m X_k < u\} \cup \{k \in I_n : \Delta^m X_k \sim u\}| = 0.$$

then a sequence (X_k) is said to be Δ_{λ}^m –statistically bounded below of order β . Here, we use the symbol \sim to show incomparable elements in $L(\mathbb{R})$.

A sequence $X = (X_k)$ of fuzzy numbers is Δ_{λ}^m –statistical bounded of order β if and only if (X_k) is both Δ_{λ}^m –statistical bounded above of order β and Δ_{λ}^m –statistical bounded below of order β . We will refer to the set of all Δ_{λ}^m –statistically bounded sequences of order of β fuzzy number sequences as $S^{\beta}B(\Delta_{\lambda}^m, F)$. On the other hand, $SB(\Delta_{\lambda}^m, F)$ will be used to designate the set of all Δ_{λ}^m –statistically bounded fuzzy sequences, $S^{\beta}B(\Delta^m, F)$ will be used to denote the set of all Δ^m –statistically bounded fuzzy sequences of order β , and $SB(\Delta^m, F)$ will be used to denote the set of all Δ^m –statistically bounded fuzzy sequences.

Theorem 3. Let β be a constant such that $\beta \in (0,1]$ and sequence $\lambda = (\lambda_n)$ belongs to space Λ . Then, if any sequence (X_k) is Δ^m -bounded, then it is Δ_λ^m -statistically bounded of order β , but the opposite is not always correct.

Proof. It is known that an empty set has zero β -density, so the first part of the proof is straightforward. To see the inverse, we take a sequence $X = (X_k)$ such that

$$X_k(x) = \begin{cases} \frac{1}{2}(x - k + 2), & \text{for } k - 2 \leq x \leq k \\ \frac{1}{2}(k + 2 - x), & \text{for } k \leq x \leq k + 2 \\ 0, & \text{otherwise} \end{cases} \quad \text{if } k = n^2 \\ (n = 1, 2, 3, \dots) \\ \begin{cases} \frac{1}{2}(x + 1), & \text{for } -1 \leq x \leq 1 \\ \frac{1}{2}(3 - x), & \text{for } 1 \leq x \leq 3 \\ 0, & \text{otherwise} \end{cases} := X_0 \quad \text{if } k \neq n^2.$$

and we obtain

$$[X_k]^\alpha = \begin{cases} [2\alpha + k - 2, k + 2 - 2\alpha] & \text{if } k = n^2 \\ [2\alpha - 1, 3 - 2\alpha] & \text{if } k \neq n^2. \end{cases}$$

After routine operations, α -level sets and membership functions of (ΔX_k) and $(\Delta^2 X_k)$ can be found as follows:

$$[\Delta X_k]^\alpha = \begin{cases} [4\alpha + k - 5, k - 4\alpha + 3] & \text{if } k = n^2 \\ [4\alpha - k - 4, 4 - 4\alpha - k] & \text{if } k + 1 = n^2 \\ [4\alpha - 4, 4 - 4\alpha] & \text{otherwise} \end{cases}$$

$$\Delta X_k(x) = \begin{cases} \frac{1}{4}(x - k + 5), & k - 5 \leq x \leq k - 1 \\ \frac{1}{4}(-x + k + 3), & k - 1 \leq x \leq k + 3 \\ 0, & \text{otherwise} \end{cases} \quad \text{if } k = n^2 \\ n = (1, 2, 3, \dots) \\ \begin{cases} \frac{1}{4}(x + k + 4), & -k - 4 \leq x \leq -k \\ \frac{1}{4}(-x - k + 4), & -k \leq x \leq k + 4 \\ 0, & \text{otherwise} \end{cases} \quad \text{if } k + 1 = n^2 \\ \begin{cases} \frac{1}{4}(x + 4), & -4 \leq x \leq 0 \\ \frac{1}{4}(-x + 4), & 0 \leq x \leq 4 \\ 0, & \text{otherwise} \end{cases} \quad \text{if } k \neq n^2$$

and

$$[\Delta^2 X_k]^\alpha = \begin{cases} [8\alpha + k - 9, k - 8\alpha + 7] & \text{if } k = n^2 \\ [8\alpha + k - 7, k - 8\alpha + 9] & \text{if } k + 1 = n^2 \\ [8\alpha - 2k - 8, -2k - 8\alpha + 8] & \text{if } k + 2 = n^2 \\ [8\alpha - 8, 8 - 8\alpha] & \text{otherwise} \end{cases}$$

$$\Delta^2 X_k(x) = \begin{cases} \frac{1}{8}(x - k + 9), & k - 9 \leq x \leq k - 1 \\ \frac{1}{8}(-x + k + 7), & k - 1 \leq x \leq k + 7 \\ 0, & \text{otherwise} \end{cases} \quad \text{if } k = n^2 \\ n = (1, 2, 3, \dots) \\ \begin{cases} \frac{1}{8}(x - k + 7), & k - 7 \leq x \leq k + 1 \\ \frac{1}{8}(-x + k + 9), & k + 1 \leq x \leq k + 9 \\ 0, & \text{otherwise} \end{cases} \quad \text{if } k + 1 = n^2 \\ \begin{cases} \frac{1}{8}(x + 2k + 8), & -2k - 8 \leq x \leq -2k \\ \frac{1}{8}(-x - 2k + 8), & -2k \leq x \leq -2k + 8 \\ 0, & \text{otherwise} \end{cases} \quad \text{if } k + 2 = n^2 \\ \begin{cases} \frac{1}{8}(x + 8), & -8 \leq x \leq 0 \\ \frac{1}{8}(-x + 8), & 0 \leq x \leq 8 \\ 0, & \text{otherwise} \end{cases} \quad \text{otherwise} \\ k \neq n^2$$

In the same manner, if we keep taking the difference m times for $m \in \mathbb{N}$, we can readily demonstrate that $X = (X_k) \in S^\beta B(\Delta_\lambda^m, F)$ for $\beta > \frac{1}{2}$, but it is (X_k) is not $SB(\Delta^m, F)$ since

$$\delta^\beta(\{k \in \mathbb{N}: \Delta_\lambda^m X_k > X_0\} \cup \{k \in \mathbb{N}: \Delta_\lambda^m X_k \prec X_0\}) = 0$$

and

$$\delta^\beta(\{k \in \mathbb{N}: \Delta_\lambda^m X_k < X_0\} \cup \{k \in \mathbb{N}: \Delta_\lambda^m X_k \succ X_0\}) = 0,$$

where $[X_0]^\alpha = [2^{m+1}(\alpha - 1), 2^{m+1}(1 - \alpha)]$, specifically, when $\beta = 1$ and $\lambda_n = n$ (See Fig. 1 for $m = 1$).

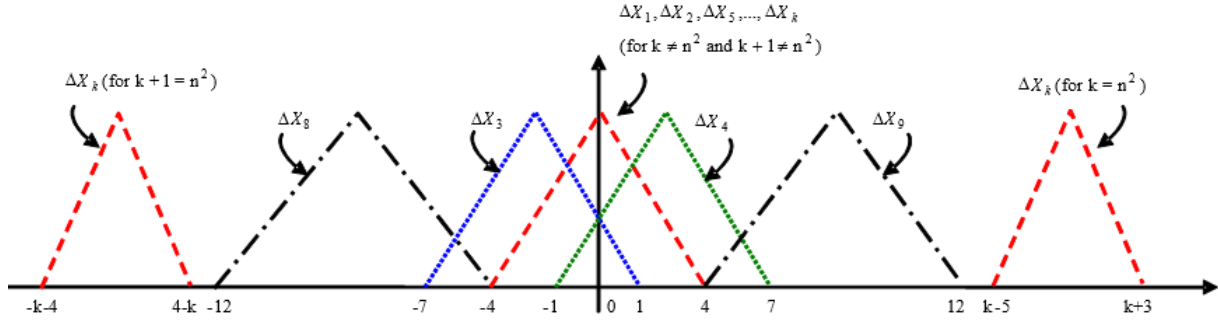


Figure 1. X_k is Δ^m – statistically bounded of order β , but not Δ^m – bounded for $m = 1$

Theorem 4. Let β be a constant such that $\beta \in (0,1]$ and sequence $\lambda = (\lambda_n)$ belongs to space Λ . For any fuzzy sequence (X_k) , if $(X_k) \in S^\beta(\Delta_\lambda^m, F)$, then $(X_k) \in S^\beta B(\Delta_\lambda^m, F)$, but the opposite is not correct.

Proof. Let fuzzy sequence $X = (X_k)$ belongs to sequence class $S^\beta(\Delta_\lambda^m, F)$. Then, we can talk about the existence of some number X_0 in fuzzy number space satisfying equality

$$\lim_{n \rightarrow \infty} \frac{1}{\lambda_n^\beta} |\{k \in I_n : d(\Delta^m X_k, X_0) \geq \varepsilon\}| = 0$$

for every $\varepsilon > 0$. Now we can write

$$\begin{aligned} & \lim_{n \rightarrow \infty} \frac{1}{\lambda_n^\beta} |\{k \in I_n : d(\Delta^m X_k, \bar{0}) \geq X_0 + \varepsilon\}| \\ & \leq \lim_{n \rightarrow \infty} \frac{1}{\lambda_n^\beta} |\{k \in I_n : d(\Delta^m X_k, X_0) \geq \varepsilon\}|. \end{aligned}$$

For the aforementioned inequality, since fuzzy sequence $(X_k) \in S^\beta(\Delta_\lambda^m, F)$, then it can be seen that the right side approaches 0.

To see the inverse, we take a sequence $X = (X_k)$ such that

$$X_k(x) = \begin{cases} \left\{ \begin{array}{ll} \frac{1}{2}(x-1), & \text{for } 1 \leq x \leq 3 \\ \frac{1}{2}(5-x), & \text{for } 3 \leq x \leq 5 \\ 0, & \text{otherwise} \end{array} \right\} := L_1 & \text{if } k \text{ is odd} \\ \left\{ \begin{array}{ll} \frac{1}{2}(x-7), & \text{for } 7 \leq x \leq 9 \\ \frac{1}{2}(11-x), & \text{for } 9 \leq x \leq 11 \\ 0, & \text{otherwise} \end{array} \right\} := L_2 & \text{if } k \text{ is even} \end{cases}$$

and we obtain

$$[X_k]^\alpha = \begin{cases} [2\alpha + 1, 5 - 2\alpha] & \text{if } k \text{ is odd} \\ [2\alpha + 7, 11 - 2\alpha] & \text{if } k \text{ is even} \end{cases}$$

After routine operations, α –level sets and membership functions of (ΔX_k) , $(\Delta^2 X_k)$ and $(\Delta^m X_k)$ can be found as follows:

$$[\Delta X_k]^\alpha = \begin{cases} [4\alpha - 10, -4\alpha - 2], & \text{if } k \text{ is odd} \\ [4\alpha + 2, -4\alpha + 10], & \text{if } k \text{ is even} \end{cases}$$

$$\Delta X_k(x) =$$

$$\begin{cases} \left\{ \begin{array}{ll} \frac{1}{4}(x+10), & -10 \leq x \leq -6 \\ \frac{1}{4}(-x-2), & -6 \leq x \leq -2 \\ 0, & \text{otherwise} \end{array} \right\} & \text{if } k \text{ is odd} \\ \left\{ \begin{array}{ll} \frac{1}{4}(x-2), & 2 \leq x \leq 6 \\ \frac{1}{4}(-x+10), & 6 \leq x \leq 10 \\ 0, & \text{otherwise} \end{array} \right\} & \text{if } k \text{ is even} \end{cases}$$

$$[\Delta^2 X_k]^\alpha = \begin{cases} [8\alpha - 20, -8\alpha - 4], & \text{if } k \text{ is odd} \\ [8\alpha + 4, -8\alpha + 20], & \text{if } k \text{ is even} \end{cases}$$

$$\Delta^2 X_k(x) =$$

$$\begin{cases} \left\{ \begin{array}{ll} \frac{1}{8}(x+20), & -20 \leq x \leq -12 \\ \frac{1}{8}(-x-4), & -12 \leq x \leq -4 \\ 0, & \text{otherwise} \end{array} \right\} & \text{if } k \text{ is odd} \\ \left\{ \begin{array}{ll} \frac{1}{8}(x-4), & 4 \leq x \leq 12 \\ \frac{1}{8}(-x+20), & 12 \leq x \leq 20 \\ 0, & \text{otherwise} \end{array} \right\} & \text{if } k \text{ is even} \end{cases}$$

and

$$[\Delta^m X_k]^\alpha = \begin{cases} [2^{m-1}(4\alpha - 10), 2^{m-1}(-4\alpha - 2)] & \text{if } k \text{ is odd} \\ [2^{m-1}(4\alpha + 2), 2^{m-1}(10 - 4\alpha)] & \text{if } k \text{ is even} \end{cases}$$

$$\Delta^m X_k(x) =$$

$$\begin{cases} \frac{1}{4}(2^{1-m}x + 10), & -10.2^{m-1} \leq x \leq -6.2^{m-1} \\ \frac{1}{4}(-2^{1-m}x - 2), & -6.2^{m-1} \leq x \leq -2.2^{m-1} \\ 0, & \text{otherwise} \end{cases} \quad \text{if } k \text{ is odd}$$

$$\begin{cases} \frac{1}{2}(2^{-m}x - 1), & 2^m \leq x \leq 3.2^m \\ \frac{1}{2}(-2^{-m}x + 5), & 3.2^m \leq x \leq 5.2^m \\ 0, & \text{otherwise} \end{cases} \quad \text{if } k \text{ is even}$$

Then, we conclude that $X = (X_k) \notin S^\beta(\Delta_\lambda^m, F)$, but it $(X_k) \in S^\beta B(\Delta_\lambda^m, F)$ in the special case $\lambda_n = n$, for all $n \in \mathbb{N}$ (See Fig. 2).

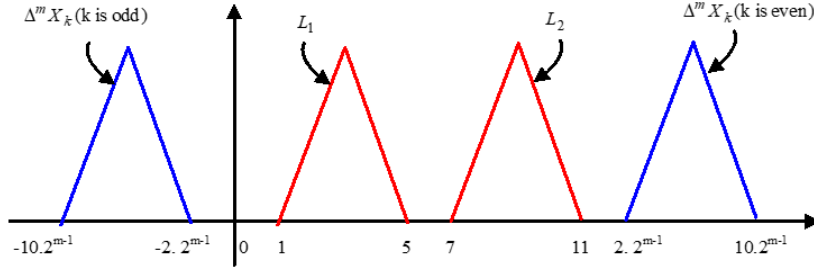


Figure 2. (X_k) is Δ_λ^m -statistically bounded of order β , but not Δ_λ^m -statistically convergent of order β for $\lambda_n = n$

Corollary 5. Let β be a constant such that $\beta \in (0, 1]$, $(X_k) \in L(\mathbb{R})$ and sequence $\lambda = (\lambda_n)$ belongs to space Λ .

- i) If $(X_k) \in S^\beta(\Delta_\lambda^m, F)$, then $(X_k) \in S^\beta B(\Delta_\lambda^m, F)$,
- ii) If $(X_k) \in S^\beta(\Delta_\lambda^m, F)$, then $(X_k) \in SB(\Delta_\lambda^m, F)$,
- iii) If $(X_k) \in S(\Delta_\lambda^m, F)$, then $(X_k) \in SB(\Delta_\lambda^m, F)$.

The opposite of above statements is not correct.

Theorem 6. Let the parameters β and γ are fixed real numbers such that $0 < \beta \leq \gamma \leq 1$, $(X_k) \in L(\mathbb{R})$ and $\lambda = (\lambda_n) \in \Lambda$. If $(X_k) \in S^\beta B(\Delta_\lambda^m, F)$, then $(X_k) \in S^\gamma B(\Delta_\lambda^m, F)$, but the opposite is not correct.

Proof. Let $0 < \beta \leq \gamma \leq 1$, then

$$\begin{aligned} & \delta^\gamma(\{k \in \mathbb{N}: \Delta_\lambda^m X_k > u\} \cup \{k \in \mathbb{N}: \Delta_\lambda^m X_k \sim u\}) \\ & \subseteq \delta^\beta(\{k \in \mathbb{N}: \Delta_\lambda^m X_k > u\} \cup \{k \in \mathbb{N}: \Delta_\lambda^m X_k \sim u\}) \end{aligned}$$

and similarly

$$\begin{aligned} & \delta^\gamma(\{k \in \mathbb{N}: \Delta_\lambda^m X_k < u\} \cup \{k \in \mathbb{N}: \Delta_\lambda^m X_k \sim u\}) \\ & \subseteq \delta^\gamma(\{k \in \mathbb{N}: \Delta_\lambda^m X_k < u\} \cup \{k \in \mathbb{N}: \Delta_\lambda^m X_k \sim u\}) \end{aligned}$$

This is the first part of the proof. Define the sequence (X_k) in the following way for the second half of the proof:

$$X_k(x) =$$

$$\begin{cases} \frac{1}{2}(x - k + 1), & k - 1 \leq x \leq k + 1 \\ \frac{1}{2}(-x + k + 3), & k + 1 \leq x \leq k + 3 \\ 0, & \text{otherwise} \end{cases} \quad \text{if } k = n^3$$

$$\begin{cases} \frac{x}{2}, & 0 \leq x \leq 2 \\ 2 - \frac{x}{2}, & 2 \leq x \leq 4 \\ 0, & \text{otherwise} \end{cases} := X_0 \quad \text{if } k \neq n^3$$

and we obtain

$$[X_k]^\alpha = \begin{cases} [2\alpha + k - 1, k + 3 - 2\alpha], & \text{if } k = n^3 \\ [2\alpha, 4 - 2\alpha], & \text{if } k \neq n^3 \end{cases}$$

After routine operations, α -level sets and membership functions of (ΔX_k) can be found as follows:

$$[\Delta X_k]^\alpha =$$

$$\begin{cases} [4\alpha + k - 5, k - 4\alpha + 3] & \text{if } k = n^3 \\ [4\alpha - k - 4, 4 - 4\alpha - k] & \text{if } k + 1 = n^3 \\ [4\alpha - 4, 4 - 4\alpha] & \text{otherwise} \end{cases}$$

$$\Delta X_k(x) =$$

$$\begin{cases} \left\{ \begin{array}{ll} \frac{1}{4}(x-k+5), & k-5 \leq x \leq k-1 \\ \frac{1}{4}(-x+k+3), & k-1 \leq x \leq k+3 \\ 0, & \text{otherwise} \end{array} \right\} & \text{if } k = n^3 \\ \left\{ \begin{array}{ll} \frac{1}{4}(x+k+4), & -k-4 \leq x \leq -k \\ \frac{1}{4}(-x-k+4), & -k \leq x \leq -k+4 \\ 0, & \text{otherwise} \end{array} \right\} & \text{if } k+1 = n^3 \\ \left\{ \begin{array}{ll} \frac{1}{4}(x+4), & -4 \leq x \leq 0 \\ \frac{1}{4}(-x+4), & 0 \leq x \leq 4 \\ 0, & \text{otherwise} \end{array} \right\} & \text{if } k \neq n^3 \end{cases}$$

Then, we can say that $(X_k) \notin S^\beta B(\Delta_\lambda^m, F)$ for $0 < \beta \leq \frac{1}{3}$, but $(X_k) \in S^\gamma B(\Delta_\lambda^m, F)$ for $\frac{1}{3} < \gamma \leq 1$ in the special case $\lambda_n = n$, then $(X_k) \in SB(\Delta_\lambda^m, F)$

Corollary 7.

i) The sequence classes $S^\beta B(\Delta_\lambda^m, F)$ and $S^\gamma B(\Delta_\lambda^m, F)$ are equivalent $\Leftrightarrow \beta = \gamma$.

ii) If $(X_k) \in S^\beta B(\Delta_\lambda^m, F)$, then $(X_k) \in SB(\Delta_\lambda^m, F)$ for $0 < \beta \leq 1$.

Since it's easy to show that each of the following results is true, we're just going to say them without giving proof.

Theorem 8. Let β be a constant such that $\beta \in (0,1]$, $(X_k) \in L(\mathbb{R})$ and $\lambda = (\lambda_n) \in \Lambda$. If $(X_k) \in S^\beta B(\Delta_\lambda^m, F)$, then it is Δ_λ^m -statistically Cauchy sequence of order β .

Theorem 9. Let β be a constant such that $\beta \in (0,1]$, $(X_k) \in L(\mathbb{R})$ and $\lambda = (\lambda_n) \in \Lambda$. Every Δ_λ^m -statistically Cauchy fuzzy sequence of order β is Δ_λ^m -statistical bounded of order β .

Theorem 10. Let β be a constant such that $\beta \in (0,1]$, $(X_k) \in L(\mathbb{R})$ and $\lambda = (\lambda_n) \in \Lambda$. Every Δ_λ^m -bounded sequence of fuzzy numbers is Δ_λ^m -statistically bounded of order β .

Proof. The first part of the proof is straightforward. Define the sequence (X_k) in the following way for the second half of the proof:

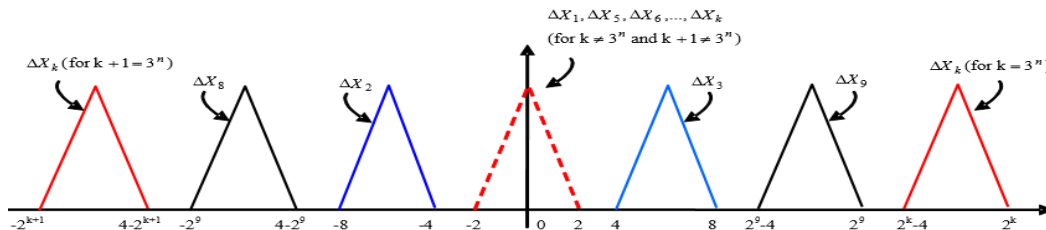


Figure 3. (X_k) is Δ_λ^m -statistically bounded of order β , but not Δ_λ^m -bounded for $m = 1$ and $\lambda_n = n$

$$X_k(x) =$$

$$\begin{cases} \left\{ \begin{array}{ll} x-2^k+1, & \text{for } 2^k-1 \leq x \leq 2^k \\ 2^k+1-x, & \text{for } 2^k \leq x \leq 2^k+1 \\ 0, & \text{otherwise} \end{array} \right\} & \text{if } k = 3^n \\ & (n = 1, 2, \dots) \\ \left\{ \begin{array}{ll} x-1, & \text{for } 1 \leq x \leq 2 \\ -x+3, & \text{for } 2 \leq x \leq 3 \\ 0, & \text{otherwise} \end{array} \right\} & \text{if } k \neq 3^n \end{cases}$$

and we obtain

$$[X_k]^\alpha = \begin{cases} [\alpha+2^k-1, -\alpha+2^k+1], & \text{if } k = 3^n \\ & (n = 1, 2, 3, \dots) \\ [\alpha+1, -\alpha+3], & \text{if } k \neq 3^n \end{cases}$$

After routine operations, α -level sets and membership functions of (ΔX_k) can be found as follows:

$$[\Delta X_k]^\alpha = \begin{cases} [2\alpha+2^k-4, 2^k-2\alpha] & \text{if } k = 3^n \\ [2\alpha-2^{k+1}, 4-2\alpha-2^{k+1}] & \text{if } k+1 = 3^n \\ [2\alpha-2, 2-2\alpha] & \text{otherwise} \end{cases}$$

$$\Delta X_k(x) =$$

$$\begin{cases} \left\{ \begin{array}{ll} \frac{1}{2}(x-2^k+4), & 2^k-4 \leq x \leq 2^k-2 \\ \frac{1}{2}(-x+2^k), & 2^k-2 \leq x \leq 2^k \\ 0, & \text{otherwise} \end{array} \right\} & \text{if } k = 3^n \\ \left\{ \begin{array}{ll} \frac{1}{2}(x+2^{k+1}), & -2^{k+1} \leq x \leq -2^{k+1}+2 \\ \frac{1}{2}(-x-2^{k+1}+4), & -2^{k+1}+2 \leq x \leq -2^{k+1}+4 \\ 0, & \text{otherwise} \end{array} \right\} & \text{if } k+1 = 3^n \\ \left\{ \begin{array}{ll} \frac{1}{2}(x+2), & -2 \leq x \leq 0 \\ \frac{1}{2}(-x+2), & 0 \leq x \leq 2 \\ 0, & \text{otherwise} \end{array} \right\} & \text{if } k \neq 3^n \end{cases}$$

In the same manner, if we keep taking the difference m times for $m \in \mathbb{N}$, we can readily demonstrate that $(X_k) \in S^\beta B(\Delta_\lambda^m, F)$, but it is not Δ_λ^m -bounded for $\lambda_n = n$, $\beta = 1$ and $m = 1$ (See Fig. 3).

3. Conclusion

After Matloka [17] gave the definition of fuzzy sequence, many studies were carried out on this subject and a relationship was established with the summability theory. Now in this paper, we defined the sequence class $S^\beta B(\Delta_\lambda^m, F)$ by making use of the generalized difference operator Δ^m and any sequence (λ_n) . Furthermore, we presented various inclusion relations between this sequence class and other ones as a means of filling in the gaps that currently exist.

References

- [1]. H. Altınok, Statistical convergence of order β for generalized difference sequences of fuzzy numbers, *J.Intell. Fuzzy Systems*, c.26, ss.847-856, 2014.
- [2]. H. Altınok and M. Et, On λ -Statistical boundedness of order β of sequences of fuzzy numbers, *Soft Computing*, c.19, s.8, ss. 2095-2100, 2015.
- [3]. H. Altınok and M. Mursaleen, Δ -Statistical boundedness for sequences of fuzzy numbers, *Taiwanese Journal of Mathematics*, c.15, s.5, ss. 2081-2093, 2011.
- [4]. S. Aytar and S. Pehlivan, statistically monotonic and statistically bounded sequences of fuzzy numbers, *Inform. Sci.*, c.176, s.6, ss. 734-744, 2006.
- [5]. V.K. Bhardwarj and I. Bala, On weak statistical convergence, *Int. J. Math. Sci. Art.* ID 38530, 9 pp., 2007.
- [6]. V.K. Bhardwaj and S. Gupta, On some generalizations of statistical boundedness, *J. Inequal.* c.2014, s.12, 2014.
- [7]. R. Çolak, Statistical convergence of order α , *Modern Methods in Analysis and Its Applications*, Yeni Delhi, India: Anamaya Pub, ss. 121-129, 2010.
- [8]. R. Çolak and Ç.A. Bektaş, λ -Statistical convergence of order α , *Acta Math. Sin. Engl. Ser.* c. 31, sy 3, ss. 953-959, 2011.
- [9]. J. S. Connor, The statistical and strong p- Cesaro convergence of sequences, *Analysis*, c. 8, ss. 47-63, 1988.
- [10]. M. Et, strongly almost summable difference sequences of order m defined by a modulus, *Studia Sci. Math. Hungar* c. 40, sy 4, ss. 463-476, 2003.
- [11]. M. Et and R. Çolak On some generalized difference sequence spaces, *Soochow J. Math.* c. 21, sy 4, ss. 377-386, 1995.
- [12]. H. Fast, Sur la convergence statistique, *Colloq. Math.*, sy 2, ss. 241-244, 1951.
- [13]. J. Fridy, On statistical convergence, *Analysis*, sy 5, ss. 301-313, 1985.
- [14]. J. A. Fridy and C. Orhan, Statistical limit superior and limit inferior, *Proc. Amer. Math. Soc.*, c. 125, sy 12, ss. 3625-3631, 1997.
- [15]. A. D. Gadjiev and C. Orhan, Some approximation theorems via statistical convergence, *Rocky Mountain J. Math.* c. 32, sy 1, ss. 129-138, 2002.
- [16]. H. Kızmaz, On certain sequences spaces, *Canadian Math. Bull.*, c. 24, ss. 169-176, 1981.
- [17]. M. Matloka, Sequences of fuzzy numbers, *BUSEFAL*, c. 28, ss. 28-37, 1986.
- [18]. S. A. Mohiuddine, A. Alotaibi and M. Mursaleen, Statistical convergence of double sequences in locally solid Riesz spaces, *Abstr. Appl. Anal.* ID 719729, 9 pp., 2012.
- [19]. M. Mursaleen, λ -Statistical convergence, *Math. Slovaca*, c. 50, sy 1, ss. 111-115, 2000.
- [20]. F. Nuray and E. Savaş, some new sequence spaces defined by a modulus function, *Indian J. Pure Appl. Math.* c. 24, sy 11, ss. 657-663, 1993.
- [21]. I. J. Schoenberg, The integrability of certain functions and related summability methods, *Amer. Math. Monthly*, c. 66, ss. 361-375, 1959.
- [22]. T. Salat, On statistically convergent sequences of real numbers, *Math. Slovaca*, c. 30, ss. 139-150, 1980.
- [23]. H. Steinhaus, Sur la convergence ordinaire et la convergence asymptotique, *Colloq. Math.* c. 2, ss. 73-74, 1951.
- [24]. L. A. Zadeh, Fuzzy sets, *Information and Control* c. 8, ss. 338-353, 1965.



Journal of Soft Computing and Artificial Intelligence

Journal homepage: <https://dergipark.org.tr/en/pub/jscai>

International
Open Access

Volume 03
Issue 02

December, 2022

Review Article

The Critical Significance of Boron Mine in Future Energy Technologies

Fatih ARLI¹ 

¹Faculty of Engineering, Department of Energy Systems Engineering, Sırnak University, 73000, Sırnak, Turkey

ARTICLE INFO

Article history:

Received December 9, 2022

Revised December 11, 2022

Accepted December 25, 2022

Keywords:

Boron

Fossil energy resources

Energy field

Ion batteries

ABSTRACT

The boron element forms more than 600 compounds with different element roots and shows very different properties. Boron compounds with these different properties deserve to be the most crucial strategic feature in the world as they meet the demands above the targeted standards in industries such as energy, structure, chemistry, weapons, and space. Today, the industries of developed countries have begun to take advantage of these energy sources due to the reduction of fossil energy resources, the inability of the industry to store enough electricity for an entire facility, and the limitations imposed on environmental policies. Developing countries continue to use fossil resources, but health and environmental costs are increasing. Whether they are developed or developing countries, they have attached importance to the research of energy systems that can replace fossil energy systems, which are environmentally friendly, sustainable, and high-performance. Boron has an essential role in the energy field for the isolation, high energy value retention, fuel and ion batteries, solar panels, and high-temperature transistors. In this study, the desired properties of boron compounds in energy studies were investigated by considering the positive effects of boron on the energy demand.

1. Introduction

Boron has an atomic weight of 10.81, an atomic diameter of 1.17 Å, a density of 2.84 gr/cm³, an electronegativity of 2, an ionization energy of 191 kcal/g atoms, a heat of fusion of 5.3 kcal/g atoms, a melting point of 2300 °C, and a boiling point of 4002 °C (Table 1 and 2). It is classified as a semi-metallic element. It is found in the earth with hydrogen, oxides, hydro-oxides (water), and alkaline metals (such as Mg, Na, and Ca). Boron has a wide range of uses, such as carbon and nitrogen. It demonstrates non-metal properties in the compounds to which it is attached. However, in the elemental state, it has the

property of electrical conductivity [1]–[4]. From this point of view, there is a need for a system that is both environmentally friendly and capable of meeting the demands of the industry. Therefore, it is thought that the compounds of boron with other elements remain within the framework of environmental awareness and high-performance issues [5]–[11]. Boron has played a leading role in the improvement of hydrogen scavengers, the improvement of ion batteries, the increase in the efficiency of solar panels, the reduction of energy losses in direct fuel processes, energy production (electricity) and transportation,

¹ Corresponding author

e-mail: fatiharli@sirnak.edu.tr

DOI: 10.55195/jscai.1216892

and the removal of greenhouse gases and heavy metals released as a result of combustion. Boron elements in nanoparticle form and boron compounds such as boric acid and sodium boron hydride are the most demanded in the energy sector. These are critical to ensure sensitivity (such as resistance to

oxidation and catalysis), control of energy reactions, and uniform distribution of reactions in primary cycles [12]–[14]. In this study, the use of boron in energy research was examined, and its effects on energy use performance and efficiency were investigated.

Table 1. Boron atom structure

Atomic diameter	1.17 Å
Atomic volume	4.63 cm ³ / mol
Electron array	1s ² 2s ² 2p ¹
Valence electrons	2s ² p ¹
Electron number (no load)	5
Ion diameter	0.23 Å
Proton units	5
Number of neutrons	6
Crystalline	Rhombohedral

Table 2. Boron physical properties

Atomic Mass	10,811
Appearance	Yellow-brown ametalic and crystal
Conductivity	Electrical: 1.0 E -12 106 / cm
Thermal Expansion coefficient	0.0000083 cm / °C (0°C)
Density	2,34 g/cc - 300K
Hardness	Mohs: 9,3 (Vickers: 49000M.N.m ⁻²)
Flexibility status	Bulk: 320/GPA
Enthalpy	573,2 kJ/mol (25°C)
Enthalpy (Fusion)	22,18 KJ/mol
Enthalpy (Evaporation)	480 kJ/mol
Heat (Evaporation)	489,7 KJ/mol
Pressure value (Steam)	0,348Pa – 2300 °C
Melting point	2573 °K - 2300°C – 4172 °F
Specific heat value	1,02 J/g.K
Boiling point	4275 gr°K – 4002 of – 7236 °F
Molar volume	4,68 cm ³ /mol
Physical form	20°C ve 1atm: Solid state

2. Investigation of the Effect of Boron Additives in Fuels

From the past to the present, there has been a decrease in fossil energy sources day by day. The emission of greenhouse gases such as C_xO_y and S_xO_y to the atmosphere by burning these sources reduces the air quality and causes an increase in global warming. In addition, studies have been started to obtain higher performance from this energy. There has been a focus on clean energy research that can improve these factors and reduce the environmental impact of fossil fuels. In these matters, using the boron element guides in

keeping the energy of hydrogen gas, which has a very high calorific value and does not give any gas other than water vapor to the atmosphere, and ensures that petroleum-based fuels are more efficient and less polluting [7], [9], [15], [16]. Hydrogen is an environmentally friendly energy source with a high combustion degree. However, keeping the reactive heat due to the combustion of this energy source element is a significant problem. Boron has a crucial role in solving this problem. Boron particle materials, loading speed, and base fuel type positively affect suspension quality and combustion behavior. The combustion behavior of dilute and dense suspensions

prevents the reduction of combustion efficiency due to the flocculation of the formed residues and boron particles [17]. The propulsion system's performance in combustion engines directly depends on the energy density and combustion behavior of the combustible material released. Metal particles (such as Al, Fe, and Pb) may be suspended in fuel binders with polymeric properties. The boron element in the fuel containing these particles is ideal due to its energy density. However, boron requires prolonged exposure to combustibles due to its high melting and boiling points. In this, Magnesium seems to be a natural complement to boron fuel. While it has a lower energy density, it burns with a high flame temperature and reacts quickly with a low melting point combustion. The combustion temperature in fuels with Fe content is proportional to the amount of Fe in them. The burning effects of iron can be controlled thanks to the boron element. Doped boron's effect on ferrous iron's burning times appears to be greater for larger particles. In this combustion process, a boron-rich boron-oxygen solution is formed in the first stage, and its temperature rises until saturation. The second stage begins when the solution becomes saturated. Particle temperature concentration decreases, and dissolved oxygen increases. During the second combustion stage, a vapor phase reaction zone is formed. Combustion ends when the composition of the combustion particle is formed. The iron selectively reacts with the surrounding gaseous oxygen, increasing the combustion rate of boron and then easily reducing by boron. Thus, a surface reaction of replacing the boron-containing gas oxidizer with a faster surface results in a rapid reduction in the volume of the iron by oxidation. The reaction complexes between the burning particles boron and oxidized iron occur in the dense phase, and B_xO_y products are rapidly formed in the composition [6], [18]. Silane-coated boron nanoparticles are highly dispersible in liquid. Hydrocarbon fuels such as decalin can thus increase the energy content of liquid fuels. Since Al and B particle additives are high energy and boron is a suitable catalyst, they increase usability and efficiency by increasing the stability and capability of combustion. It is observed that there is an upward shift at the highest decomposition temperature for B for Al. Adding heat-sensitive metals such as Al, Mg, and Fe is an effective method to overcome the energy release efficiency limitation of boron-based fuels. The duration of combustion of element B has a remarkable contribution.

B grains exhibit higher heat release than Al grains [11], [19]–[22]. Removing sulfur from the S_xO_y release is essential in clean fuel systems. Due to the textural catalyst feature of the boron element, it strengthens the particle dispersion. It improves the high catalytic activity, providing high rates of sulfur removal [23], [24]. Considering all these, it is clear that the element boron will play a vital role in the future of environmentally friendly fuel energy.

3. Investigation of the Use of Boron in Battery Systems

Boron is a raw material used in solar cells, fuel cells, and lithium-ion batteries. Battery mainly consists of four primary components: cathodes, anodes, electrolytes, and separators. Figure 1 demonstrates the schematics of these components in conventional Li-ion batteries (LIBs) and the movement of electrons, ions, and current flow during charging and discharging conditions [25]. Sodium boron hydride ($NaBH_4$) is a boron compound that can be preferred because of its advantages, such as hydrogen storage, easy control of reactions, and non-flammable and explosive properties. Boron-containing complex hydrides are also crucial because they are used in liquid conditions and are based on $NaBH_4$ containing 10.5% hydrogen by weight in solid form. $NaBH_4$ gives its hydrogen in reaction with water in a catalyst solution environment and turns into sodium metaborate ($NaBO_2$). This reaction makes it possible to store hydrogen gas. This reaction is cyclical. That is, the development of the catalyst suitable for the system and the product of $NaBO_2$ formed as a result of the reaction into $NaBH_4$ again emerges. This system can be applied in two primary ways in hydrogen production, other than fuel cells and directly as a fuel cell. Except for the fuel cell, the sodium borohydride solution with the catalyst is passed through the hydrogen production unit and converted to hydrogen. This hydrogen is used in fuel cells because of its low temperature. In this system, sodium borohydride catalytically releases hydrogen in aqueous media and is especially important in applications where hydrogen transport and storage are problematic such as weight, volume, and safety. In a direct sodium borohydride fuel cell, on the other hand, sodium borohydride is directly used as fuel without hydrogen production intermediate stage, and electrical energy is produced. The direct sodium borohydride fuel cell is portable, especially with low power requirements [26], [27]. Boron nitride

nanocomposite increases the hydrogen storage capacity in lithium-ion batteries due to the wide molecular surface area [28]. The decomposition

reactions of O_2 and H_2O at the cathode of fuel cells are essential for the cells to function well.

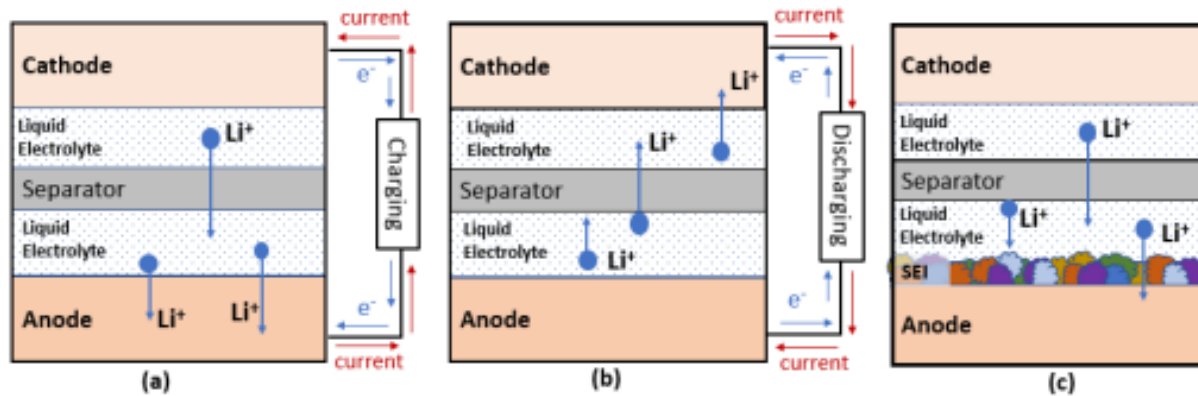


Figure 1 Schematic diagram of LIBs for (a) charging (b) discharging and, (c) formation of SEI.

Although it provides control of these reactions as a platinum catalyst, it is expensive in terms of cost. Here, with the use of boron nanostructures as a cheaper catalyst for reactions, the dissociation energy of O_2 and H_2O is lower than with the use of platinum [14].

4. The Importance of the Use of Boron Internal Combustion Engines

In using boron in internal combustion engines, the distilled boron enters the combustion chamber with the appropriate amount of pure oxygen gas (with a purity of 99-100%). After the pressure of the oxygen gas is increased to a specific value (approximately 100 bar) with the movement of the piston in the engine, it enters an exothermic reaction with the boron, and by this reaction, the explosion pushes the piston up with the air shock, thus starting the engine. Boron does not have flammable and explosive properties at room temperature. With this feature, it is a reliable and non-hazardous raw material. It releases the energy required for the operation of internal combustion engines by performing combustion or explosion only in certain weather conditions and when combined with certain oxygen. Pure boron can be easily recovered by heating the oxidized boron compound. On the other hand, pure oxygen can be obtained by filtering the oxygen present in the air at the rate of 21% by the silver filters to be placed in front of the vehicle while the vehicle is driving. The residue of boron-fueled engines is B_2O_3 , which has a crystalline liquid structure. This compound can now be stored as ingots by cooling or pressing, repurified, and used as fuel [26]. An improvement in energy performance can be achieved when boron minerals are compared as an additive to the primary

fuels of vehicles used in land and sea transportation (automobile, truck, locomotive, ship). Among the elements that release energy when burned, boron has a high density of 92.77 megajoules/Liter of combustion energy and comes after aluminum [29]–[31]. Boron fuel has a structure that does not burn easily, and its safety is higher than other fuels. There is no risk of spontaneous combustion. 2.2 units of boron can do the work of one unit of hydrogen. However, the weight of boron in the same unit volume is 11 times less than the weight of hydrogen. In other words, hydrogen there is no loss even if it is not used for years. Since boron is an environmentally friendly element, it does not cause environmental pollution. No harmful gas emission occurs as a result of combustion combustion [27], [32], [33].

5. Use of Boron as Rocket Fuel

The use of boron in the aircraft and aviation industry has become a trend. Investigations in this industry, mainly in the USA, Europe, Japan, and Russia are noteworthy. Research in Aerodynamics in Aviation and the desire to travel and study the universe paved the way for space travel operating in the new system and has guided progress on better fuel. For this purpose, it has been realized that the boron-energy issue has a crucial role. In the American air and naval forces, significant investments have been made in R&D studies and projects to use boron hydrogen compounds (Boranes), which can provide approximately 50% more energy than fossil-based hydrocarbon compounds in rockets and aircraft that can move above the atmosphere. As examples of these projects, applications such as HERMES and X-Files High

Energy Boron fuels are used in Ariane rockets. Boron can release high amounts of heat in its exothermic reactions per mass and volume.

When this heat released is analyzed per mass, it is approximately two times the heat released in the reactions of aluminum and 2.5 times that of magnesium. They can perform high-yield reactions with boron, fluorine, and its compounds. The heat energy released in fluorination reactions with exothermic fluorine compounds is about 1.8 times the heat energy released in oxidation reactions. Boron fuels are activated with high activation energy. It creates a working system with high chemical stability and controllable structures. The boron compound adsorbed occupies 11 times more volume than boron at the same weight. This weight provides a significant advantage in terms of storage. In addition, it is located on a reel with its structure in the form of a boron thread. For hydrogen, it should be stored in a thick and cooling tank. Boron fuels are not stored in a fuel tank but in a chain link structure on a reel. Since it does not have volatility, the outer surfaces of the fuels flocculate by forming an interaction network with the fuel. Then, the amorphous boron, which is absorbed by the Hydro-Carbon (H-C) chains in the fuels, can be effective in the combustion waves. Boron atoms undergo oxidation during the combustion of H-C structures, causing heat to emerge on the combustion surface. The effectiveness of the ignition and combustion rate increases depending on the thermal friction sensitivity of the fuel and the substances sensitive to oxidation, such as iron and aluminum in the fuel [16], [18], [20].

6. Use of Boron in Electric Motors

Electric motors using boron are associated with fuel cells, an electrochemical battery. It is also used alone in vehicles and can store energy chemically thanks to the anode, cathode, and electrolyte systems. Fuel cells do not decrease efficiency over time and do not need recharging. It continues to produce electricity as long as the fuel and the material that will enable it to oxidize are supplied. Electricity is generated by the interaction of the anode and the cathode and the reaction of hydrogen and oxygen. Pure gaseous water and heat are released as a reaction product. While the required oxygen is supplied from the air, hydrogen is supplied from the fuel used simultaneously. While the structure of fuel cells is similar to the battery, the working system is similar to internal combustion engines. Although it uses electrical energy, it receives from the anode and cathodes in its internal structure. It provides this energy from the energy it produces, not from the energy stored like a battery. This system's operation

depends on the presence of hydrogen; the most important factor of energy production is hydrogen. The purpose of cell use is to ensure energy continuity by preventing power interruption. The desired energy can be obtained if a suitable mass of sodium borohydride solution is created in a fuel cell. Although this energy is approximately equal to half of the energy obtained from the same amount of gasoline, the energy conversion efficiency of the electric motor is approximately three times higher than that of the internal combustion engine. The roads covered with the existing fuel tanks are still valid for sodium borohydride, and sodium borohydride is present in the fuel system. Here, sodium borohydride and water react thanks to the catalyst, and as a result of this reaction, hydrogen and sodium boron powder are released. The released hydrogen feeds the fuel cell and makes it possible to obtain direct current (DC) in the fuel cell. Direct current is stored in the cell, and energy is transferred to the electric motor. The vehicle moves when the electric motor transmits the power to the vehicle's wheels [34]–[39].

7. Effects of Boron on Magnetic Working Systems

For the motors to work, the magnets that will provide the magnetic feature must have high B-H characteristic data. Using ferroboration (Fe_xB_y) alloyed magnetic materials with large coherent force and permanent magnetization values are vital. The production of Fe_xO_y , boron oxide, boric acid, or boron ores (especially colemanite, boron oxide, and boric acid) as raw materials takes place in two stages. In the first stage, Ore + Fe Sawdust + Coke + Quartz mixture is used as a charge in the Electric Arc Furnace with Carbothermic Reduction (High-carbon Ferroboration), and in the second stage, Boron oxide + Hematite + Al, Powder + Igniter (BaO_2 or KClO_4 + Al) is used as a charge. It is produced using a mixture of the Aluminothermic Reduction method (Low carbon, high aluminum ferroboration). The essential components in Ferroboration Alloys (Fe_2B , FeB) are B, C, Si, and Al. According to the amount of B, which can vary between 12-21%, their densities are between about 6.3-7 g/cm³, and their hardness is between about 1600-1950 Vickers, their thermal conductivity is between about 0.1-0.3 W/cm K, their melting temperature is about 1389-1550 °C. Its Curie Temperatures vary between 1550 °C and approximately 598-1015 °K. In the quality of

applications, the behavior of the ferrobore against different chemicals depends on the purity ratio. While it can dissolve with Fe_2B and HCl under borane formation, Pure FeB has high chemical resistance against HCl and H_2SO_4 at all temperatures. Due to the presence of N molecules in HNO_3 , it is completely soluble. FeB and Fe_2B react with nitrogen gas at temperatures above 350°C , resulting in BN product.

It loses its bright silver color in humid weather and becomes pale gray. A reaction can be seen between pure hot water and ferrobore. In the Fe-B-containing material system, alloys containing approximately 0.04-4.2% B and steels with a thinly adsorbed FeB layer on the surface layer can withstand corrosive oxidation up to approximately $800\text{--}1000^\circ\text{C}$. One of the critical magnetic materials in which ferrobore is used is Nd-Fe-B (Neodymium Ferrobore) alloy magnets. Nd-Fe-B magnets commercially have the greatest strength and the most significant permanent flux density (12 Kg). This density is quite desirable when comparing the density of Sm-Co magnets (11.2 Kg) and the density of ferrites (11.5-4.4 Kg). Moreover, an 850 g Nd-Fe-B magnet works with 3 kg of ferrite. Due to the reasons mentioned above, boron magnets have an ideal structure thanks to their ability to meet the demands of the industry [40]–[49].

8. Use of Boron in Nuclear Energy Systems

Materials with boron elements can be used to prevent the damage of radiation emissions in nuclear energy reactors in nuclear energy systems. The boron material used here is boron carbide. Boron carbide is a material with a melting temperature of 2450°C , high hardness, and highly resistant to chemical reactions and radiation. Boron carbide is used for loading rods of advanced nuclear power plants. The absorption ability of high-energy neutrons that can create a boron carbide radiation effect is due to the high absorber cross-section of the boron isotope in its structure. As a protective shield material that does not leak neutrons, boron carbides are used in Phenix reactors, fast breeder reactors. The new generation stainless steel called Bor-304 is the material of the tanks used to transport nuclear waste fuels. In the nuclear energy sector, gadolinium and samarium can be used as they have neutron scavenging properties like boron, but it is below the system performance provided on the board. In the fusion reaction of the B11 atom by colliding with the proton, clean nuclear energy without radioactive

emission was released. During this reaction, the proton fuses with the ion, and as the reaction product, C^{12} is formed as an ion with atomic number 6 and mass number 12. Boron, which contains B10 and B11 isotopes in its compounds, these isotopes can absorb neutrons during nuclear reactions and slow down the reaction rate. Thanks to this, it is used in the control rods of nuclear reactors as well as in the construction of moderators since it prevents and slows the fission reaction of neutrons with the uranium-235 atom and turns into one of the compounds of boron oxide, boric acid and ferrobore improved with dimethyl ether and amorphous boron. They absorb neutrons in nuclear reactors and prevent or stop fission, which is a chain reaction with uranium-235. In this way, power control is provided in fission energy by terminating the reactor or by adjusting the amount of reacting neutrons [50]–[56]. To provide Nuclear Grade, powdered boron carbide is used as neutron shield components in nuclear reactor systems, boron steels, and boron alloys with titanium. Almost every boron atom can absorb a neutron.

For this reason, boron is used in the control systems of atomic reactors, cooling pools, and closing the reactor with an alarm. Boron emits only a very low-energy gamma ray and absorbs alpha particles smoothly. Neutrons with energies more significant than one mega electron volt ($1 < \text{MeV}$) form an inelastic molecular collision with the target atom. In inelastic collisions, the neutrons that come with the neutron-atom reaction transfer a particular part of their atomic energy to the target atom and excite this atom. This exciting target atom is unstable and then becomes stable by emitting gamma rays. At the beginning of the atomic motions of neutron capture, target atoms absorb neutrons. Then, it is observed that the atom, which becomes excited, transforms into its isotope or gets rid of this excited state by emitting gamma rays and takes its final state. Here, using a boron atom as the target atom leads to the desired results [57]–[62]. It has also been reported that after 2016, a neutron reaction with B11 in the magnetic field for the tri-alpha reaction took place, and a high amount of energy was produced with a nuclear reaction without the risk of radiation. The way to be used as a nuclear fuel has been opened.

9. Conclusion

Boron compounds are used in many critical areas in the energy sector. Innovative boron compounds are

needed in many fields, from nuclear energy to solar panels, from electric motors to internal combustion engines, and from rocket fuel technology to space technologies. Especially the development of a new nuclear engine using the B11 isotope in the tri-alpha reaction and its use by NASA for the journey to Mars are essential heralds that Boron will be an indispensable alternative fuel in future space technologies. However, the transition to fuel technologies that do not contain fossil fuels to compensate for the damages caused by the emissions caused by the use of fossil fuels in the last 100 years is a harbinger of the fact that boron compounds will be used very often in this field.

References

- [1] N. Kabay, E. Güler, and M. Bryjak, "Boron in seawater and methods for its separation - A review," *Desalination*, vol. 261, no. 3, pp. 212–217, 2010, doi: 10.1016/j.desal.2010.05.033.
- [2] E. MEYDAN, "Boron Compounds With Magnetic Properties and Their Application Areas in Industry," *J. Sci. Perspect.*, vol. 3, no. 1, pp. 11–20, Feb. 2019, doi: 10.26900/jsp.3.002.
- [3] K. M. Kadish, K. M. Smith, and R. Guilard, *The Porphyrin Handbook: Inorganic, organometallic and coordination chemistry*, vol. 7. 2000.
- [4] D. E. Garrett, "Borate Minerals and the Origin of Borate Deposits," in *Borates*, vol. 36, no. 05, Elsevier, 1998, pp. 1–50. doi: 10.1016/B978-012276060-0/50002-4.
- [5] H. Çelikkan, M. Şahin, M. L. Aksu, and T. Nejat Veziroğlu, "The investigation of the electrooxidation of sodium borohydride on various metal electrodes in aqueous basic solutions," *Int. J. Hydrogen Energy*, vol. 32, no. 5, pp. 588–593, Apr. 2007, doi: 10.1016/j.ijhydene.2006.06.065.
- [6] E. T. Sandall, J. Kalman, J. N. Quigley, S. Munro, and T. D. Hedman, "A study of solid ramjet fuel containing boron–magnesium mixtures," *Propuls. Power Res.*, vol. 6, no. 4, pp. 243–252, 2017, doi: 10.1016/j.jprr.2017.11.004.
- [7] E. Larsson, P. Olander, and S. Jacobson, "Boric acid as fuel additive – Friction experiments and reflections around its effect on fuel saving," *Tribol. Int.*, vol. 128, pp. 302–312, Dec. 2018, doi: 10.1016/j.triboint.2018.07.004.
- [8] A. Eslami, S. G. Hosseini, and S. M. Pourmortazavi, "Thermoanalytical investigation on some boron-fuelled binary pyrotechnic systems," *Fuel*, vol. 87, no. 15–16, pp. 3339–3343, Nov. 2008, doi: 10.1016/j.fuel.2008.05.020.
- [9] X. tian feng E *et al.*, "Jet fuel containing ligand-protecting energetic nanoparticles: A case study of boron in JP-10," *Chem. Eng. Sci.*, vol. 129, pp. 9–13, Jun. 2015, doi: 10.1016/j.ces.2015.02.018.
- [10] H. Ji *et al.*, "Silicotungstic acid immobilized on lamellar hexagonal boron nitride for oxidative desulfurization of fuel components," *Fuel*, vol. 213, pp. 12–21, Feb. 2018, doi: 10.1016/j.fuel.2017.08.076.
- [11] Y. Zhu, S. Gao, and N. S. Hosmane, "Boron-enriched advanced energy materials," *Inorganica Chimica Acta*, vol. 471. Elsevier S.A., pp. 577–586, Feb. 24, 2018. doi: 10.1016/j.ica.2017.11.037.
- [12] S. Z. Li and X. J. Liu, "Development of boron tracking and boron hideout (CRUD) model based on subchannel approach," *Nucl. Eng. Des.*, vol. 338, pp. 166–175, Nov. 2018, doi: 10.1016/j.nucengdes.2018.08.023.
- [13] W. D. Tennyson *et al.*, "Bottom up synthesis of boron-doped graphene for stable intermediate temperature fuel cell electrodes," *Carbon N. Y.*, vol. 123, pp. 605–615, Oct. 2017, doi: 10.1016/j.carbon.2017.08.002.
- [14] F. J. Owens, "Prediction of electrocatalytic activity of boron nanostructures," *Chem. Phys. Lett.*, vol. 691, pp. 131–134, Jan. 2018, doi: 10.1016/j.cplett.2017.11.007.
- [15] Y. Gan, Y. S. Lim, and L. Qiao, "Combustion of nanofluid fuels with the addition of boron and iron particles at dilute and dense concentrations," *Combust. Flame*, vol. 159, no. 4, pp. 1732–1740, Apr. 2012, doi: 10.1016/j.combustflame.2011.12.008.
- [16] S. A. Hashim, S. Karmakar, A. Roy, and S. K. Srivastava, "Regression rates and burning characteristics of boron-loaded paraffin-wax solid fuels in ducted rocket applications," *Combust. Flame*, vol. 191, pp. 287–297, May 2018, doi: 10.1016/j.combustflame.2018.01.018.
- [17] B. Pajot, A. Chari, M. Aucouturier, M. Astier, and A. Chantre, "Experimental evidence for boron-hydrogen interaction in boron-doped silicon passivated with hydrogen," *Solid State Commun.*, vol. 67, no. 9, pp. 855–858, Sep. 1988, doi: 10.1016/0038-1098(88)90117-2.
- [18] K. L. Chintersingh, M. Schoenitz, and E. L. Dreizin, "Boron doped with iron: Preparation and combustion in air," *Combust. Flame*, vol. 200, pp. 286–295, Feb. 2019, doi: 10.1016/j.combustflame.2018.11.031.
- [19] M. Du and G. Li, "Preparation of silane-capped boron nanoparticles with enhanced dispersibility in hydrocarbon fuels," *Fuel*, vol. 194, pp. 75–82, 2017, doi: 10.1016/j.fuel.2017.01.001.
- [20] Y. Pal and V. R. Kumar, "Thermal decomposition study of paraffin based hybrid rocket fuel containing Aluminum and Boron additives," *Thermochim. Acta*, vol. 655, pp. 63–75, Sep. 2017,

- doi: 10.1016/j.tca.2017.06.002.
- [21] O. V. Klimov *et al.*, “CoMoB/Al₂O₃ catalysts for hydrotreating of diesel fuel. The effect of the way of the boron addition to a support or an impregnating solution,” *Catal. Today*, vol. 305, pp. 192–202, May 2018, doi: 10.1016/j.cattod.2017.07.004.
- [22] P. K. Ojha and S. Karmakar, “Boron for liquid fuel Engines-A review on synthesis, dispersion stability in liquid fuel, and combustion aspects,” *Prog. Aerosp. Sci.*, vol. 100, pp. 18–45, 2018, doi: 10.1016/j.paerosci.2018.05.003.
- [23] D. Liang, R. Xiao, J. Liu, and Y. Wang, “Ignition and heterogeneous combustion of aluminum boride and boron–aluminum blend,” *Aerosp. Sci. Technol.*, vol. 84, pp. 1081–1091, Jan. 2019, doi: 10.1016/j.ast.2018.11.046.
- [24] T. A. Saleh, S. A. AL-Hammadi, and A. M. Al-Amer, “Effect of boron on the efficiency of MoCo catalysts supported on alumina for the hydrodesulfurization of liquid fuels,” *Process Saf. Environ. Prot.*, vol. 121, pp. 165–174, Jan. 2019, doi: 10.1016/j.psep.2018.10.019.
- [25] C. Zheng, “Examining the Benefits of Using Boron Compounds in Lithium Batteries: A Comprehensive Review of Literature,” *Batteries*, vol. 8, no. 10, MDPI, Oct. 01, 2022. doi: 10.3390/batteries8100187.
- [26] A. M. Alexander and J. S. J. Hargreaves, “Alternative catalytic materials: carbides, nitrides, phosphides and amorphous boron alloys,” *Chem. Soc. Rev.*, vol. 39, no. 11, pp. 4388–4401, 2010, doi: 10.1039/b916787k.
- [27] N. S. Hosmane, Ed., *Boron Science*. CRC Press, 2016. doi: 10.1201/b11199.
- [28] R. N. Muthu, S. Rajashabala, and R. Kannan, “Hydrogen storage performance of lithium borohydride decorated activated hexagonal boron nitride nanocomposite for fuel cell applications,” *Int. J. Hydrogen Energy*, vol. 42, no. 23, pp. 15586–15596, Jun. 2017, doi: 10.1016/j.ijhydene.2017.04.240.
- [29] L. Vinet and A. Zhedanov, *A “missing” family of classical orthogonal polynomials*, vol. 44, no. 8. Springer, 2011. doi: 10.1088/1751-8113/44/8/085201.
- [30] J. J. Croat, *Rapidly solidified neodymium-iron-boron permanent magnets*. Elsevier, 2017. doi: 10.1016/C2016-0-04355-3.
- [31] A. W. Thornton, A. Ahmed, M. Mainak, H. B. Park, and A. J. Hill, *Ultrafast transport in nanotubes and nanosheets*. CRC Press, 2015. doi: 10.1201/b18073.
- [32] Gerhart K. Gaulé, *Boron: Volume 2: Preparation, Properties, and Applications*. Springer, 2013. [Online]. Available: [https://books.google.com.tr/books?id=GHgECAAAQBAJ&dq=%5B33%5D.%09Gaulé,+G.+K.+\(2013\).+Boron:+Volume+2:+Preparation,+Properties,+and+Applications.+Springer.&lr=&hl=tr&source=gbs_navlinks_s](https://books.google.com.tr/books?id=GHgECAAAQBAJ&dq=%5B33%5D.%09Gaulé,+G.+K.+(2013).+Boron:+Volume+2:+Preparation,+Properties,+and+Applications.+Springer.&lr=&hl=tr&source=gbs_navlinks_s)
- [33] D. She, J. Zhang, B. Xia, C. Wei, F. Li, and X. Jing, “Study on OTTO fueling schemes of the HTR-PM with boron burnable particles,” *Nucl. Eng. Des.*, vol. 329, pp. 198–203, Apr. 2018, doi: 10.1016/j.nucengdes.2017.09.011.
- [34] A. Demirbaş, “Hydrogen and boron as recent alternative motor fuels,” *Energy Sources*, vol. 27, no. 8, pp. 741–748, Jun. 2005, doi: 10.1080/00908310490450836.
- [35] M. Balat, “Boron as an alternate engine fuel,” *Energy Sources, Part A Recover. Util. Environ. Eff.*, vol. 29, no. 1, pp. 79–83, Jan. 2007, doi: 10.1080/009083190934013.
- [36] H. Su, H. Wen, X. Zheng, and J. Su, “Development of a Super High Efficiency Motor with Boron Aluminum Alloy Rotor,” *Procedia Eng.*, vol. 174, pp. 1221–1228, 2017, doi: 10.1016/j.proeng.2017.01.288.
- [37] Y. Kimura, T. Wakabayashi, K. Okada, T. Wada, and H. Nishikawa, “Boron nitride as a lubricant additive,” 1999. doi: 10.1016/S0043-1648(99)00146-5.
- [38] F. Mahvash, E. Paradis, D. Drouin, T. Szkopek, and M. Siaj, “Space-Charge Limited Transport in Large-Area Monolayer Hexagonal Boron Nitride,” *Nano Lett.*, vol. 15, no. 4, pp. 2263–2268, Apr. 2015, doi: 10.1021/nl504197c.
- [39] M. I. H. Chua Abdullah, M. F. Bin Abdollah, N. Tamaldin, H. Amiruddin, and N. R. M. Nuri, “Effect of hexagonal boron nitride nanoparticles as an additive on the extreme pressure properties of engine oil,” *Ind. Lubr. Tribol.*, vol. 68, no. 4, pp. 441–445, Jun. 2016, doi: 10.1108/ILT-10-2015-0157.
- [40] A. Hosokawa, K. Takagi, T. Kuriwa, Y. Inoue, and K. Ozaki, “Severe plastic deformation of Nd-Fe-B nanocomposite magnets at room temperature,” *J. Magn. Magn. Mater.*, vol. 473, pp. 51–60, Mar. 2019, doi: 10.1016/j.jmmm.2018.10.032.
- [41] D. Prosperi *et al.*, “Performance comparison of motors fitted with magnet-to-magnet recycled or conventionally manufactured sintered NdFeB,” *J. Magn. Magn. Mater.*, vol. 460, pp. 448–453, Aug. 2018, doi: 10.1016/j.jmmm.2018.04.034.
- [42] A. Walton *et al.*, “The use of hydrogen to separate and recycle neodymium-iron-boron-type magnets from electronic waste,” *J. Clean. Prod.*, vol. 104, pp. 236–241, Oct. 2015, doi: 10.1016/j.jclepro.2015.05.033.
- [43] H. Jin, B. D. Song, Y. Yih, and J. W. Sutherland, “A bi-objective network design for value recovery of neodymium-iron-boron magnets: A case study

- of the United States,” *J. Clean. Prod.*, vol. 211, pp. 257–269, Feb. 2019, doi: 10.1016/j.jclepro.2018.11.101.
- [44] Z. Xiang, C. Xu, T. Wang, Y. Song, H. Yang, and W. Lu, “Enhanced magnetization and energy product in isotropic nanocrystalline Mn55Al45 alloys with boron doping,” *Intermetallics*, vol. 101, pp. 13–17, Oct. 2018, doi: 10.1016/j.intermet.2018.07.003.
- [45] E. Aradi, S. R. Naidoo, F. Cummings, I. Motochi, and T. E. Derry, “Cross-sectional transmission electron microscopy studies of boron ion implantation in hexagonal boron nitride,” *Diam. Relat. Mater.*, vol. 92, pp. 168–173, Feb. 2019, doi: 10.1016/j.diamond.2018.12.020.
- [46] M. Mehedi, Y. Jiang, B. Ma, and J. P. Wang, “Nitriding and martensitic phase transformation of the copper and boron doped iron nitride magnet,” *Acta Mater.*, vol. 167, pp. 80–88, Apr. 2019, doi: 10.1016/j.actamat.2019.01.034.
- [47] M. Li *et al.*, “Texture and microstructure improvement of hot-deformed magnets with platelet-like nano h-BN addition,” *Scr. Mater.*, vol. 152, pp. 127–131, Jul. 2018, doi: 10.1016/j.scriptamat.2018.04.032.
- [48] A. Nordelöf, E. Grunditz, S. Lundmark, A. M. Tillman, M. Alatalo, and T. Thiringer, “Life cycle assessment of permanent magnet electric traction motors,” *Transp. Res. Part D Transp. Environ.*, vol. 67, pp. 263–274, Feb. 2019, doi: 10.1016/j.trd.2018.11.004.
- [49] D. Wang, J. Zhou, J. Li, X. Jiang, Y. Wang, and F. Gao, “Cobalt-boron nanoparticles anchored on graphene as anode of lithium ion batteries,” *Chem. Eng. J.*, vol. 360, pp. 271–279, Mar. 2019, doi: 10.1016/j.cej.2018.11.238.
- [50] C. Cummings, Brent C. (Lyons, “Radiation shielding for spacecraft components.” US Patent, 1994. [Online]. Available: <https://www.freepatentsonline.com/5324952.pdf>
- [51] C. G. Pope, “X-ray diffraction and the bragg equation,” *J. Chem. Educ.*, vol. 74, no. 1, pp. 129–131, 1997, doi: 10.1021/ed074p129.
- [52] X. G. Chen, G. Dube, and N. Steward, “Neutron absorption effectiveness for boron content aluminum materials,” 2008 [Online]. Available: <https://patents.google.com/patent/US20080050270A1/en>
- [53] Guy M. Decroix, Dominique Gosset, and Bernard Kryger, “Neutron-absorbing material and its production process,” 5590393, 1996 [Online]. Available: <https://patentimages.storage.googleapis.com/79/e/e/7c/3ecaae91b80ee6/US5590393.pdf>
- [54] A. K. Suri, C. Subramanian, J. K. Sonber, and T. S. R. Ch Murthy, “Synthesis and consolidation of boron carbide: A review,” *International Materials Reviews*, vol. 55, no. 1. pp. 4–38, Jan. 2010. doi: 10.1179/095066009X12506721665211.
- [55] D. Simeone, X. Deschanel, P. Cheminant, and P. Herter, “Behaviour of Different Boron Rich Solids as Promising Absorbers for PWR,” in *Control Assemble Materials for water reactors: Experience, performance and perspectives*, 2000, pp. 103–106. [Online]. Available: http://www.iaea.org/inis/collection/NCLCollectionStore/_Public/31/008/31008489.pdf
- [56] B. Rebensdorff and G. Bart, “Material Operating Behaviour of ABB BWR Control Rods,” in *Control Assemble Materials for water reactors: Experience, performance and perspectives*, 2000, pp. 65–76. [Online]. Available: https://inis.iaea.org/collection/NCLCollectionStore/_Public/31/008/31008486.pdf
- [57] A. G. Ruggiero, “Nuclear fusion of protons with ions of boron,” in *Il Nuovo Cimento A*, 1993, vol. 106, no. 12, pp. 1959–1963. doi: 10.1007/BF02780602.
- [58] T. S. R. C. M. C. Subramanian, A. K. Suri, “Development of Boron-based materials for nuclear applications,” in *Technology Development Article*, 2010, no. 313, pp. 14–22.
- [59] J. T. A. Roberts, *Structural Materials in Nuclear Power Systems*, vol. 80, no. 1. Boston, MA: Springer US, 1981. doi: 10.1007/978-1-4684-7194-6.
- [60] G. I. Risovany, V. D., Zakharov, A. V., Klochkov, E. P., Osipenko, A. G., Kosulin, N. S., & Mikhailichenko, “Reprocessing of the irradiated boron carbide enriched by boron-10 isotope and its reuse in the control rods of the fast breeder reactors,” *Int. At. Energy Agency, IAEA-TECDOC--884*, vol. 4, no. June, pp. 47–52, 1996, [Online]. Available: <http://link.springer.com/10.1007/978-1-4684-7194-6>
- [61] V. Troyanov, A. Pomeschikov, V. Sougonjaev, V. Ponomarenko, and A. Scheglov, “High Temperature Study of the Control Rod Behaviour Under Accident Conditions,” *Control Assem. Mater. water React. Exp. Perform. Perspect.*, pp. 245–258, 1998, [Online]. Available: <https://www.ptonline.com/articles/how-to-get-better-mfi-results>
- [62] P. O. K. V. G. DATE, “Status of control assembly materials in Indian water reactors,” *Cycle*, no. December, pp. 40–55, 1993, [Online]. Available: carden, RA. 1997. Metal matrix compositions for neutron shielding applications. Patent 5,700,962.

List of abbreviations and nomenclature

Sodium (Na)

Aluminum (Al)

Calcium (Ca)

Magnesium (Mg)

Iron (Fe)

Lead (Pb)

Hydrochloric acid (HCl)

Nitric acid (HNO₃)

Solid electrolyte interface (SEI)

Ar-Ge, research, and development (R&D)

Gigapascal (GPa)

Kelvin (°K)

Fahrenheit (°F)

A substance formed naturally in the ground and from which metal can be obtained (Ore)

The dust and small pieces of wood (Sawdust)

A solid substance obtained from coal (Coke)

A hard, transparent mineral substance (Quartz)



Journal of Soft Computing and Artificial Intelligence

Journal homepage: <https://dergipark.org.tr/en/pub/jscai>

International
Open Access

Volume 03
Issue 02

December, 2022

Research Article

An Artificial Intelligence Regression Model for Prediction of NO_x Emission from Flame Image

Sedat Golgiyaz¹, Mahmut Daskin², Cem Onat³, M. Fatih Talu⁴

¹Department of Computer Engineering, Bingol University, Bingol, Turkey

²Department of Mechanical Engineering, Inonu University, Malatya, Turkey

³Department of Air-frame and Power Plant, Firat University, Elazig, Turkey

⁴Department of Computer Engineering, Inonu University, Malatya, Turkey

ARTICLE INFO

Article history:

Received December 2, 2022

Revised December 24, 2022

Accepted December 27, 2022

Keywords:

NO_x,

Regression model

Coal

Emission prediction

Flame Image processing

Combustion control

ABSTRACT

In this study, NO_x emission has been estimated by processing the flame image of visible wavelength and its experimental verification has been presented. The experimental study has been performed by using a domestic coal boiler with a capacity of 85000 Kcal / h. The real NO_x value has been measured from a flue gas analyzer device. The flame image has been taken by CCD camera from the observation hole on the side of the burner. The data set which is related to instantaneous combustion performance and flame images was recorded simultaneously on the same computer with time stamps once a second. The color flame image has been transformed into a gray scale. Features have been extracted from the gray image of flame. The features are extracted by using the cumulative projection vectors of row and column matrices. ANN regression model has been used as the learning model. The relationship between flame image and NO_x emission has been obtained with the accuracy of R = 0.9522. Highly accurate measurement results show that the proposed NO_x prediction model can be used in combustion monitor and control systems.

1. Introduction

As a reliable and low-cost fossil fuel, coal is a strategic energy source in terms of energy security for the very country. Coal stands out as being the safest fossil fuel in terms of obtaining, storing, transporting and using. For this reason, coal is widely used both in domestic areas and industrial areas such as thermal power plants, glass, steel and cement industries. On the other hand, emission values of coal combustion systems are constantly being discussed due to environmental concerns. According to the World Energy Outlook 2017 [1] report published by IEA, it is stated that in 2016, 9.5 billion tons of CO₂ (carbon

dioxide) was emitted from coal-fired thermal power plants to the atmosphere. This rate corresponds to approximately 70% of the emission released from the conversion sector [2]. When we use coal in power plants, sulfur dioxide (SO₂), particulate matter and nitrogen oxides (NO_x) are released into the atmosphere. Therefore, measurement and control of the emission values stand out as an important and daily issue in order to increase efficiency in coal burning systems and to reduce their negative effects on the environment.

¹ Corresponding author

e-mail: sedatg@bingol.edu.tr

DOI: 10.55195/jscai.1213863

1.1. Motivation

In practice, emission values are traditionally made by flue gas analysis devices[3]. Recently, as an alternative method, measurement systems containing artificial intelligence based on flame image have been used [4]–[8]. Measurement mechanisms that make emission estimation by processing flame images are both cheaper systems and lower operating costs compared to their counterparts. In addition, dead time in control systems makes the controller design process extremely difficult [9]–[11]. Since the system created with flame images quickly reflect the combustion conditions, they constitute an important advantage that greatly minimizes the dead time in closed loop control systems [12], [13]. In particular, this feature provides a significant advantage from the control design perspective. These advantages offered by flame image-based measurement systems motivate engineers to design a more effective, flame image-based emission measurement system with higher accuracy.

1.2. Related Works

Emission estimation via CCD (Charge-Coupled Device) cameras is more advantageous systems compared to flue gas analyzer devices because they are inexpensive systems and do not require consumables. The use of computer vision systems in the industry is increasing day by day [14]–[18]. In general, there are three types of application performed by processing the flame image. The first is monitoring and controlling of the combustion process in burners [19]–[23], the second is estimation of the emission resulting from the combustion [24]–[27] and the last one is estimation of the temperature of the combustion chamber [28]–[30]. In addition to these types of applications, there are different studies. For example, coal type can be classified with the image of the flame [28]. In NO_x emission prediction system performed with CCD cameras, available in some studies with color space of HSI (Hue, Saturation, Intensity) [25] as well as in color space of RGB (Red Green Blue) [24]. In a combustion process, there are many factors affecting NO_x emissions. These factors have different effects on NO_x emissions. To find the appropriate formula or mathematical model to predict the NO_x emission from the coal boiler is very difficult. But, it is possible to estimate NO_x emission using image

processing techniques and ANN regression model [24]. Because ANNs are very good at modeling the complex phenomena. It has been reported in [25] that there is a relationship between 30–65 bars and the emission level of NO_x in the tone level histogram in the HSI color space. In studies which uses CCD cameras, radial energy emitted from the flame was used frequently to extract features from the image of flame [27], [31], [32]. In these studies, the Radial Energy Signal (RES) is calculated with the gray image of flame. A good study on combustor control with flame image is given in [31]. Here, NO_x emission and thermal efficiency are optimized with the radiant energy signal obtained from the flame image [31]. [19] and [33] have made a nice contribution to those studying flame characterization by digital image processing on industrial scale burners. In the studies which are performed with colored flame images, the image is generally converted to gray level in order to reduce the dimension (to reduce the calculation load) and the feature is obtained from the gray level image [19], [20], [22], [31]. Similarly, there are studies with only one color (blue) channel [34] or only the tone component of the color image [25]. Flue gas analyzer is used in flue gas emission studies [35] and there are studies in which the concentration of radicals formed as a result of combustion is determined by spectroscopic imaging [26], [27], [36], [37][27], [36]. CCD cameras are preferred in emission estimation because they are both common and cheap [24], [25], [38]. When the studies mentioned above are subjected to a general evaluation, it is concluded that the subject of estimating the combustion emission values from the flame image is a current-trend field of study. The methods used in studies [22], [25], which came to the fore especially in NO_x estimation, have been a significant result of the literature search.

1.3. Contribution

There are some challenging problems with studies of imaging the combustion chamber. Some of these are the large data size of the flame images and the problems of determining the meaningful features expressing the burning from these images. The operations to solve these problems increase the computational complexity. In addition, optimizing the appropriate modeling technique to reveal the relationship between the features obtained from the

flame image and the combustion process is another dimension of the problem. In this study, a new regression model is presented that reveals the relationship between flame image and NO_x emission. The proposed model includes image processing techniques and artificial neural network elements. For emission estimation, the features are extracted out by using the flame image converted to gray level. Position dependent feature vectors are used to express the burning process better. For this purpose, cumulative projection vectors of row and column matrices are used to obtain the features. These simple and effective features are ideal for evaluating the flame in terms of brightness and volume. Using position dependent features also provides information about the homogeneity of the flame. The study performed in comparison with the NO_x emission estimation methods [22], [25] that stand out in the literature, reveals the efficiency of the proposed estimation model.

1.4. Outline of the Paper

In the next Section, data collection process is explained. In Section 3, feature extraction from flame images is explained. In the Section 4, ANN model is designed. In Section 5, experimental results are presented in comparison with the methods mentioned in the literature. Eventually, the final section discusses experimental results. Also, clues about future studies have been given.

2. Data Collection

The experimental study has been carried out with a domestic burner system with a capacity of 85,000 kcal/h. Nut coal has been used as fuel in the experimental study. The schematic representation of the system is given in Figure 1. The system is constructed with a 10 cm diameter circular viewing window on the side of the burner. Combustion has been monitored by a CCD camera placed behind this window.

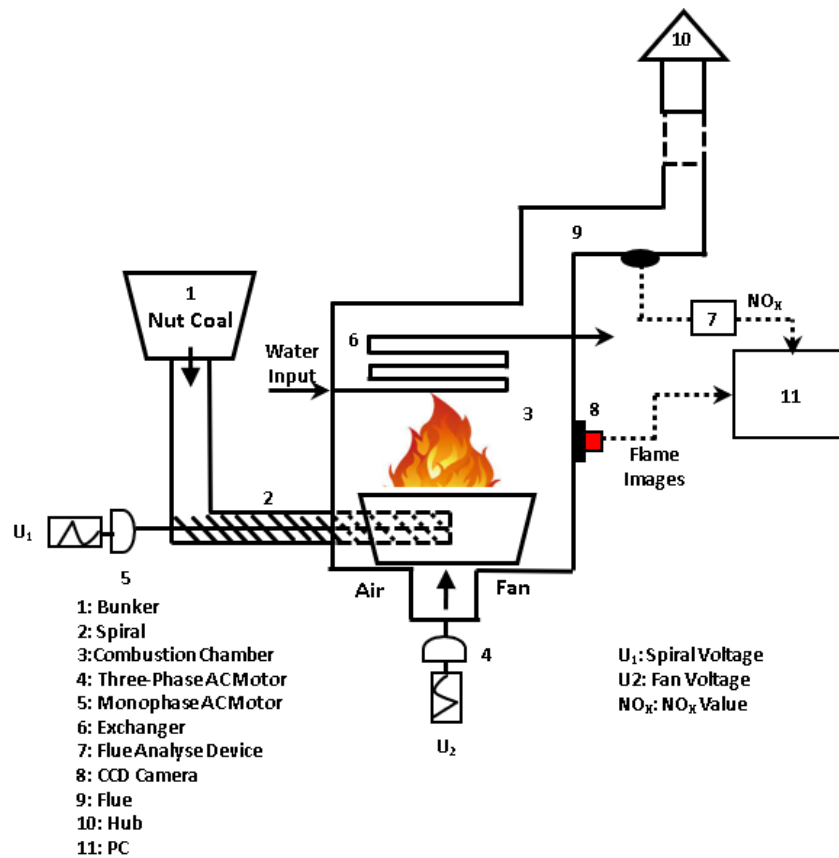


Figure 1 Schema of the burner system

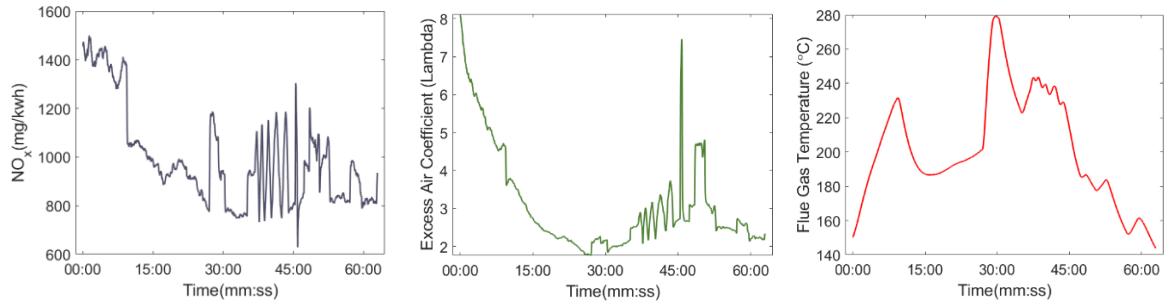


Figure 2 Combustion conditions; (a) NO_x emissions; (b) excess air coefficient; (c) flue gas temperature

The combustion conditions at the time of obtaining experimental data are given in Figure 2. In order to illustrate all possible combustion conditions in the experimental composition, the combustion conditions have been adjusted to be in a wide range.

Different forms of expressions of a colored flame image obtained from the combustion chamber are given in Figure 3.

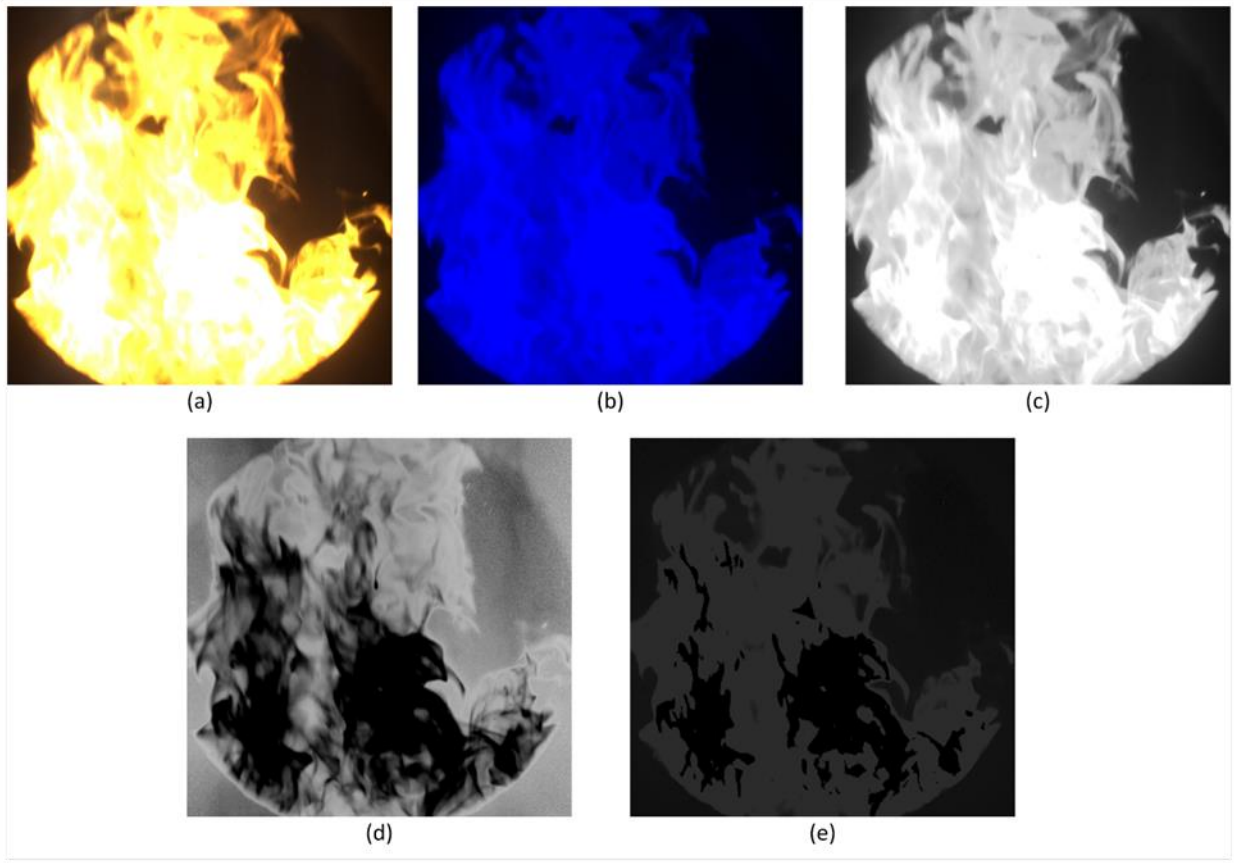


Figure 3 A flame image; (a) RGB and (b) HSI color spaces, (c) intensity (I), (d) saturation(S) and (e) hue (H) components

In this study, the gray level of the flame image in RGB color space has been used. The burning process has been monitored for 63 minutes by recording a single image per second at 1200×1200 resolution via a CCD camera. In addition, the NO_x measurement value per second has been taken from the flue gas emission device synchronously with the flame images. The region of interest has been chosen so that the flame image is 1160×1160 pixels in

size. The flame image obtained from the camera and the NO_x value obtained from the flue gas analyzer have been recorded on the same computer with time labels. In this way, 3780 NO_x measurement values and flame images have been collected simultaneously during the experiment.

In cases when it was not possible to obtain data from the camera or analyzer, the relevant data acquired at his time period have not been taken into consideration. The NO_x

emission data obtained from the flue gas analyzer have been used as reference data in the training and testing stages of the model.

3. Feature Extraction

The main factors affecting NOx emissions in coal combustor systems are given below [39].

- Average temperature in the combustion chamber.
- Homogeneity of temperature in the combustion chamber.
- Gas residence time in high temperature zone.
- Air excess coefficient and property of coal.

There is a relationship between the flame image and the factors affecting NOx emissions [17], [24], [27]. Therefore, the relationship between flame image and NOx emission can be revealed by image processing and machine learning techniques. In this study, cumulative horizontal and vertical projection vectors are used to extract attributes from the flame image.

3.1. Horizontal-Vertical Projection Vectors

Cumulative horizontal and vertical projection vectors can be calculated as in Equation 1-2. Here $I_{m \times n}$ is the gray level image of the flame.

$$X_{csum}^k = \sum_{j=1}^k \sum_{i=1}^n I_{ij}, 1 \leq k \leq m \quad (1)$$

$$Y_{csum}^t = \sum_{i=1}^t \sum_{j=1}^m I_{ij}, 1 \leq t \leq n \quad (2)$$

X_{csum}^k and Y_{csum}^t have been used together for training of the proposed system. Features and density information of the flame image were obtained depending on the location. Not only does density information represent the flame characteristic, but also includes positional information, expressing the combustion process better.

3.2. Relationship Between Hue Level and Combustion

Color HSI image consists of three components such as brightness, hue, and saturation. The conversion process from RGB color space to HSI color space is expressed using Equation 3-4.

$$r = \frac{R}{R+G+B}, g = \frac{G}{R+G+B}, b = \frac{B}{R+G+B} \quad (3)$$

$$h = \cos^{-1} \left(\frac{0.5 * ((r-g) + (r-b))}{((r-g)^2 + (r-b) + (g-b))^{1/2}} \right) \quad (4)$$

Here, if $b \leq g$ then $h \in [0, \pi]$

$$h = 2\pi - \cos^{-1} \left(\frac{0.5 * ((r-g) + (r-b))}{\sqrt{(r-g)^2 + (r-b) + (g-b)}} \right) \quad (5)$$

Here, if $b > g$ then $h \in [\pi, 2\pi]$,

$$s = 1 - 3 * \min(r, g, b); s \in [0, 1] \quad (6)$$

$$I = \frac{R+G+B}{3 * 255}; I \in [0, 1]. \quad (7)$$

In [25], it has been reported that with the tone level of the flame, the light field can represent the dominant wavelength. Also, with regard to a luminous substance, it has been stated that there is a relationship between wavelength and tone level [40]. This relationship can be expressed as in Equation 8.

$$W = \frac{W_{max} - W_{min}}{2^d} Hue + W_{min} \quad (8)$$

In this equation, W is the wavelength and d is the bit depth of the image. Wmax and Wmin values are 700nm and 400nm respectively. For normal images d = 8. Light undergoes radical luminescence with substances such as OH, CH, CO₂, NO₂, CO and H₂O.

4. Artificial Neural Networks

ANNs are mathematical machine learning models inspired by the biological behavior of nerve cells in the human body and the structure of the brain. In this study, a multi-layer perceptron (MLP) approach consisting of at least three layers called input, latent and output layer is used to estimate NOx emission. During the training phase, the features gathered from the flame images constitute the input and the NOx emission measured with the analyzer is used as the desired output. Coefficients of ANN are optimized according to the inputs and the output. A part of the data set is used for verification during the training phase. In the last stage, the rest of the data set is used to test the performance of the model. The rate of the data set used for training, testing and verification is given in Table 1. In the ANN regression model, the number of neurons in the hidden layer was taken as 8.

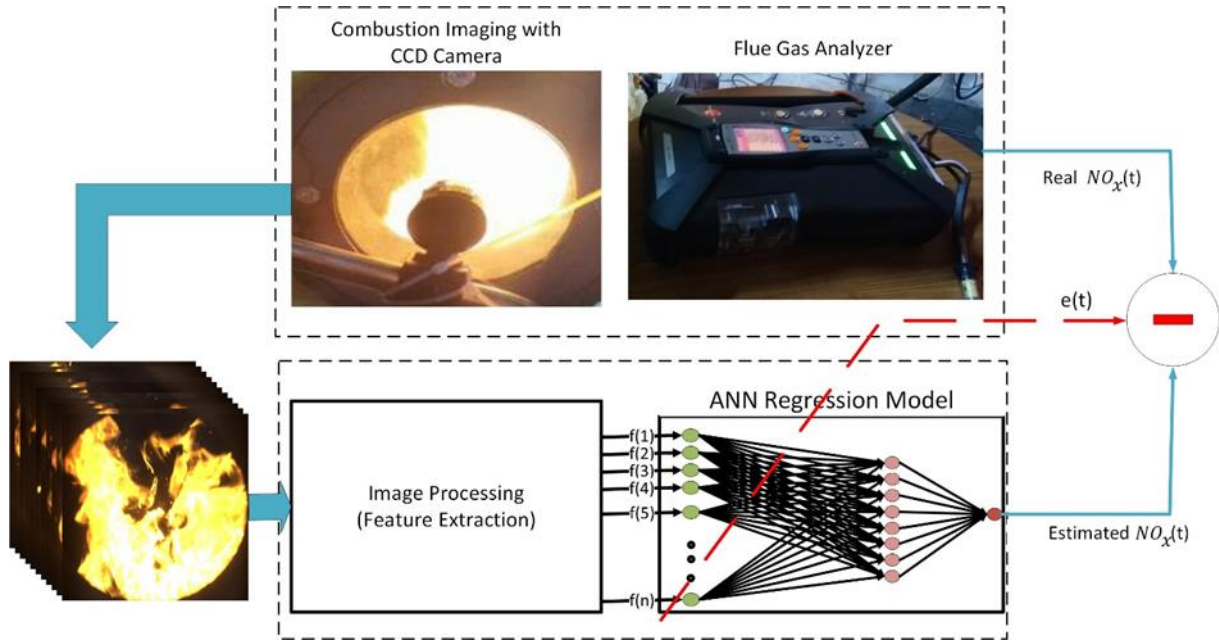


Figure 4. Block diagram of the proposed measurement system

Table 1. Separation of data in percentages for training, testing and validation

	All	Training	Validation	Test
Data Rate	%100	%70	%15	%15
Data number	3780	2646	567	567

In general, the initial weights are randomly selected in ANN and the weights are optimized by minimizing the cost function given in equation 9.

$$J(\theta) = \frac{1}{2N} \sum_{i=1}^N (h_{\theta}(x^{(i)}) - y^{(i)})^2 \quad (9)$$

Many training algorithms for ANN have been reported in the practice. The appropriate training algorithm varies according to many factors. Factors such as the complexity of the problem, the number of data points in the training set, the weight in the network and the number of biases determine the selection of the training algorithm. In the next section, the effects of different learning algorithms on the accuracy of the regression model have been also speculated.

4.1. Performance Metrics for Regression Model

Root mean square error (RMSE) and correlation coefficient (R) criteria were used to reveal the regression performance obtained during the training, validation and testing phases. R and RMSE values are defined by expressions given in Equations 10 and 11, respectively.

$$RMSE = \left[\frac{1}{N} \sum_{i=1}^N (D_i - \tilde{D}_i)^2 \right]^{1/2} \quad (10)$$

$$R = \left[1 - \frac{\sum_{i=1}^N (D_i - \tilde{D}_i)^2}{\sum_{i=1}^N (D_i - \bar{D})^2} \right]^{1/2} \quad (11)$$

Here, D_i and \bar{D} values represent the individual NOx emission value and the average of all D_i values, respectively. In addition, \tilde{D}_i represents the NOx emission value calculated as a result of ANN regression model.

5. Experimental Results

With the designed system, the NOx value measured by the flue gas analyzer has been regressed with the ANN model using the flame image. The NOx value obtained from the flue gas analyzer has been taken as a reference value in the proposed system and used in the training and testing phase.

The results obtained for comparison have been run ten times for all models. The results presented in Table 2 are the average values of these 10 runs. In order to demonstrate the performance of the proposed feature extraction method better, the results of other feature extraction methods presented for NOx emission in the literature with the same data set and the same ANN architecture are comparatively given in Table 2. Training all the proposed methods for the same model and parameters in the same data set provided objective results in terms of comparing the

effectiveness of the methods. Accordingly, the proposed ANN regression model estimated the NO_x emission with at least $R = 0.9522$ accuracy. The results obtained as a result of the experimental study revealed the effectiveness of the proposed feature extraction method.

While comparing the results, the results of four ANN learning models (LM, BFG, CGF and SCG) are given for proposed feature extraction method and other methods. Considering the results obtained, LM (Levenberg-Marquardt) method gave better results despite the high memory requirement. BFG (BFGS Quasi-Newton), CGF (Fletcher-Powell, Conjugate

Gradient) and SCG (Scaled Conjugate Gradient) methods have been performed faster than LM. However, accuracy is not at the desired level in these methods. Although [25] reported a direct relationship between NO_x emission and the tone histogram [30-65] bars, the relation in this study became clear between the bar bars of the histogram [0-85]. 16 cameras have been used in [22] given in Table 2. The feature extraction method presented in [22] is presented for a single camera with the data in this study.

Table 2 Proposed method and other methods' result for same data set and ANN architecture

	Features	Training Algorithm	RMSE	R
Proposed	X_{csum}, Y_{csum}	LM	59,566	0,952
	X_{csum}, Y_{csum}	BFG	99,896	0,863
	X_{csum}, Y_{csum}	CGF	94,072	0,879
	X_{csum}, Y_{csum}	SCG	95,941	0,874
Others	Histogram (0-85) [25]	LM	91,581	0,886
	Histogram (30-65)[25]	LM	121,544	0,789
	Histogram (0-85) [25]	BFG	121,916	0,787
	Histogram (30-65) [25]	BFG	143,506	0,687
	Histogram (0-85) [25]	CGF	120,741	0,789
	Histogram (30-65) [25]	CGF	145,904	0,672
	Histogram (0-85) [25]	SCG	116,810	0,805
	Histogram (30-65) [25]	SCG	142,704	0,691
	μ [22]	LM	176,640	0,451
	μ [22]	BFG	177,876	0,438
	μ [22]	CGF	178,668	0,430
	μ [22]	SCG	178,187	0,435

In Figure 5, the NO_x values produced by using of flame images with the proposed measurement system and the NO_x values obtained from the flue gas analyzer are given. It is seen from this picture that the proposed measurement system is capable of estimating NO_x emissions with at least 95% accuracy in all combustion conditions.

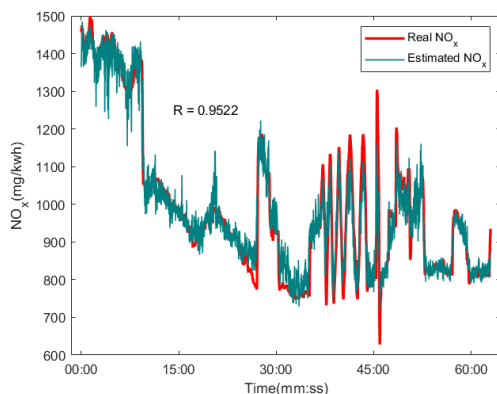


Figure 5 Performance of the proposed model

6. Conclusion

In this study, a new measurement system is proposed for the problem of estimating NO_x emission from the flame image in the coal combustion process. When the obtained results are evaluated, the NO_x estimation system established with the proposed method gives more successful results than other methods reported in the literature. Since CCD cameras are both cheap and common, the measurement structure presented in this study is advantageous in terms of cost. It also provides an option that minimizes the time delay in establishing closed loop combustion control systems. Within the scope of this domestic scale study, the proposed system can be extended for emission estimation in the industry. For future emission estimation studies, both the feature extraction phase and the learning models' phase are open to development.

Acknowledgement

This work was supported by The Scientific and Technological Research Council of Turkey (TUBITAK, Project number: 117M121) and MIMSAN AŞ. We thank to the organizations.

References

- [1] The U.S. Energy Information Administration (EIA), "International Energy Outlook 2017." Accessed: Oct. 22, 2018. [Online]. Available: www.eia.gov/ieo.
- [2] J. Diefenderfer, M. assumptions Vipin Arora, and L. E. Singer, *International Energy Outlook 2016*, vol. 0484, no. May. 2016.
- [3] X. Qiu, L. Duan, Y. Duan, B. Li, D. Lu, and C. Zhao, "Ash deposition during pressurized oxy-fuel combustion of Zhundong coal in a lab-scale fluidized bed," *Fuel Process. Technol.*, vol. 204, p. 106411, Jul. 2020, doi: 10.1016/j.fuproc.2020.106411.
- [4] R. Weber and M. Mancini, "On scaling and mathematical modelling of large scale industrial flames," *J. Energy Inst.*, vol. 93, no. 1, pp. 43–51, Feb. 2020, doi: 10.1016/j.joei.2019.04.010.
- [5] W. Wójcik, B. Suleimenov, M. J.-J. of Ecological ..., and undefined 2017, "Employing Optical Measurements for Monitoring and Diagnostics of Combustion Process in Industrial Conditions," *yadda.icm.edu.pl*, vol. 18, no. 1, pp. 273–283, 2017, doi: 10.12911/22998993/67107.
- [6] C. Onat and M. Daskin, "A basic ANN system for prediction of excess air coefficient on coal burners equipped with a CCD camera," *Math. Stat.*, vol. 7, no. 1, pp. 1–9, 2019, doi: 10.13189/ms.2019.070101.
- [7] C. Onat, M. Daşkin, S. Toraman, S. Golgiyaz, and M. F. Talu, "Prediction of combustion states from flame image in a domestic coal burner," *Meas. Sci. Technol.*, vol. 32, no. 7, p. 075403, Jul. 2021, doi: 10.1088/1361-6501/abe446.
- [8] S. Golgiyaz, M. F. Talu, and C. Onat, "Estimation of Excess Air Coefficient for Automated Feed Coal Burners with Image-Based Gauss Model," in *International Artificial Intelligence and Data Processing Symposium (IDAP'16)*, 2016, pp. 528–531, [Online]. Available: <https://www.researchgate.net/publication/333650492>.
- [9] C. Onat, "A new concept on PI design for time delay systems: weighted geometrical center," *J. Innov. Comput. Inf. Control*, 2013.
- [10] C. Onat, "WGC Based Robust and Gain Scheduling PI Controller Design for Condensing Boilers," 2014, doi: 10.1155/2014/659051.
- [11] C. Onat, "A new design method for PI–PD control of unstable processes with dead time," *ISA Trans.*, vol. 84, pp. 69–81, 2019, doi: 10.1016/j.isatra.2018.08.029.
- [12] C. Katzer, K. Babul, M. Klatt, and H. J. Krautz, "Quantitative and qualitative relationship between swirl burner operating conditions and pulverized coal flame length," *Fuel Process. Technol.*, vol. 156, pp. 138–155, 2017, doi: 10.1016/j.fuproc.2016.10.013.
- [13] S. Taamallah, N. W. Chakroun, H. Watanabe, S. J. Shanbhogue, and A. F. Ghoniem, "On the characteristic flow and flame times for scaling oxy and air flame stabilization modes in premixed swirl combustion," *Proc. Combust. Inst.*, vol. 36, no. 3, pp. 3799–3807, 2017, doi: 10.1016/j.proci.2016.07.022.
- [14] J. Li, M. M. Hossain, J. Sun, Y. Liu, ... B. Z.-A. T., and undefined 2019, "Simultaneous measurement of flame temperature and absorption coefficient through LMBC-NNLS and plenoptic imaging techniques," *Elsevier*.
- [15] T. Lockwood, "Advanced sensors and smart controls for coal-fired power plant controls for coal-fired power plant," no. June, 2015, [Online]. Available: [https://www.usea.org/sites/default/files/media/Advance sensors and smart control for coal fired power plants - ccc251.pdf](https://www.usea.org/sites/default/files/media/Advance%20sensors%20and%20smart%20control%20for%20coal%20fired%20power%20plants%20-%20ccc251.pdf).
- [16] J. Ballester and T. García-Armingol, "Diagnostic techniques for the monitoring and control of practical flames," *Prog. Energy Combust. Sci.*, vol. 36, no. 4, pp. 375–411, 2010, doi: 10.1016/j.peccs.2009.11.005.
- [17] S. Golgiyaz, M. F. Talu, and C. Onat, "Artificial neural network regression model to predict flue gas temperature and emissions with the spectral norm of flame image," *Fuel*, vol. 255, p. 115827, Nov. 2019, doi: 10.1016/j.fuel.2019.115827.
- [18] S. Golgiyaz, M. F. Talu, and C. Onat, "Estimation of Flue Gas Temperature by Image Processing and Machine Learning Methods," *Eur. J. Sci. Technol.*, pp. 283–291, Aug. 2019, doi: 10.31590/ejosat.568348.
- [19] A. González-Cencerrado, B. Peña, and A. Gil, "Coal flame characterization by means of digital image processing in a semi-industrial scale PF swirl burner," *Appl. Energy*, vol. 94, pp. 375–384, 2012, doi: 10.1016/j.apenergy.2012.01.059.
- [20] A. González-Cencerrado, A. Gil, and B. Peña, "Characterization of PF flames under different swirl conditions based on visualization systems," *Fuel*, vol. 113, pp. 798–809, Nov. 2013, doi: 10.1016/j.fuel.2013.05.077.

- [21] Z. Xiangyu, Z. Shu, Z. Huaichun, Z. Bo, W. Huajian, and X. Hongjie, "Simultaneously reconstruction of inhomogeneous temperature and radiative properties by radiation image processing," *Int. J. Therm. Sci.*, vol. 107, pp. 121–130, 2016, doi: 10.1016/j.ijthermalsci.2016.04.003.
- [22] Z. Liu, S. Zheng, Z. Luo, and H. Zhou, "A new method for constructing radiative energy signal in a coal-fired boiler," *Appl. Therm. Eng.*, vol. 101, pp. 446–454, 2016, doi: 10.1016/j.applthermaleng.2016.01.034.
- [23] P. Tóth, A. Garami, and B. Csordás, "Image-based deep neural network prediction of the heat output of a step-grate biomass boiler," *Appl. Energy*, vol. 200, pp. 155–169, Aug. 2017, doi: 10.1016/j.apenergy.2017.05.080.
- [24] F. Wang *et al.*, "The research on the estimation for the NO_xemissive concentration of the pulverized coal boiler by the flame image processing technique," *Fuel*, vol. 81, no. 16, pp. 2113–2120, 2002, doi: 10.1016/S0016-2361(02)00145-X.
- [25] W. B. Baek, S. J. Lee, S. Y. Baeg, and C. H. Cho, "Flame image processing & analysis for optimal coal firing of thermal power plant," *ISIE 2001 IEEE Int. Symp. Ind. Electron. proceedeing, Vols I-III*, p. {928-931}, 2001, doi: 10.1109/ISIE.2001.931596.
- [26] X. Li, D. Sun, G. Lu, J. Krabicka, and Y. Yan, "Prediction of NO_x emissions throughflame radical imaging and neural network based soft computing," *IST 2012 - 2012 IEEE Int. Conf. Imaging Syst. Tech. Proc.*, vol. 44, no. 0, pp. 502–505, 2012, doi: 10.1109/IST.2012.6295594.
- [27] N. Li, G. Lu, X. Li, and Y. Yan, "Prediction of NO_x Emissions from a Biomass Fired Combustion Process Based on Flame Radical Imaging and Deep Learning Techniques," *Combust. Sci. Technol.*, vol. 188, no. 2, pp. 233–246, 2016, doi: 10.1080/00102202.2015.1102905.
- [28] Q. Tang, H. Zhou, G. Lu, Y. Yan, and Y. Li, "Combining flame monitoring techniques and support vector machine for the online identification of coal blends," *J. Zhejiang Univ. A*, pp. 671–689, 2017, doi: 10.1631/jzus.a1600454.
- [29] Z. Xiangyu, L. Xu, Y. yu, Z. Bo, and X. Hongjie, "Temperature measurement of coal fired flame in the cement kiln by raw image processing," *Meas. J. Int. Meas. Confed.*, 2018, doi: 10.1016/j.measurement.2018.07.063.
- [30] T. Li, C. Zhang, Y. Yuan, Y. Shuai, and H. Tan, "Flame temperature estimation from light field image processing," *Appl. Opt.*, vol. 57, no. 25, p. 7259, 2018, doi: 10.1364/ao.57.007259.
- [31] B. Huang, Z. Luo, and H. Zhou, "Optimization of combustion based on introducing radiant energy signal in pulverized coal-fired boiler," *Fuel Process. Technol.*, vol. 91, no. 6, pp. 660–668, Jun. 2010, doi: 10.1016/j.fuproc.2010.01.015.
- [32] Z. Huaichun and C. han, "An Exploratory Investigation of the Computer-Based Control of Utility Coal-Fired Boiler Furnace Combustion," *J. Eng. Therman Enegry Power*, 1994.
- [33] D. Castiñeira, B. C. Rawlings, and T. F. Edgar, "Multivariate image analysis (MIA) for industrial flare combustion control," *Ind. Eng. Chem. Res.*, vol. 51, no. 39, pp. 12642–12652, 2012, doi: 10.1021/ie3003039.
- [34] M. F. Talu, C. Onat, and M. Daskin, "Prediction of Excess Air Factor in Automatic Feed Coal Burners by Processing of Flame Images," *Chinese J. Mech. Eng.*, vol. 30, no. 3, pp. 722–731, May 2017, doi: 10.1007/s10033-017-0095-3.
- [35] C. Moon, Y. Sung, S. Eom, and G. Choi, "NO_x emissions and burnout characteristics of bituminous coal, lignite, and their blends in a pulverized coal-fired furnace," *Exp. Therm. Fluid Sci.*, vol. 62, no. 1, pp. 99–108, 2015, doi: 10.1016/j.expthermflusci.2014.12.005.
- [36] J. Krabicka, G. Lu, and Y. Yan, "A spectroscopic imaging system for flame radical profiling," in *2010 IEEE Instrumentation & Measurement Technology Conference Proceedings*, 2010, pp. 1387–1391, doi: 10.1109/IMTC.2010.5488056.
- [37] N. Li, G. Lu, X. Li, Y. Y.-I. T. on Instrumentation, and undefined 2015, "Prediction of pollutant emissions of biomass flames through digital imaging, contourlet transform, and support vector regression modeling," *ieeexplore.ieee.org*.
- [38] S. Zheng, Z. Luo, Y. Deng, and H. Zhou, "Development of a distributed-parameter model for the evaporation system in a supercritical W-shaped boiler," *Appl. Therm. Eng.*, vol. 62, no. 1, pp. 123–132, 2014, doi: 10.1016/j.applthermaleng.2013.09.029.
- [39] H. C. Zeng, *Combustion and pollution*. Wuhan: Publishing Company of Huazhong University of Science and Technology, 1992.
- [40] J. A. Dean, *Flame photometry*. McGraw-Hill series in advanced chemistry., 1960.